Design and Synthesis of Doxorubicin Conjugated Gold Nanoparticles as Anticancer Drug Delivery System

Long Xia

Thesis submitted to the faculty of the

Virginia Polytechnic Institute and State University

in partial fulfillment of the requirements for the degree of

Master of Science

In

Chemistry

David G. I. Kingston, Committee Chair

Richard D. Gandour

Webster L. Santos

May 4, 2016

Blacksburg, Virginia

Keywords: Doxorubicin, Anticancer, Gold Nanoparticles, Drug Delivery

Design and Synthesis of Doxorubicin Conjugated Gold Nanoparticles as Anticancer Drug Delivery System

Long Xia

Abstract

Doxorubicin is one of the most widely used and effective anticancer agents to treat a wide spectrum of tumors. But its success in cancer therapy is greatly compromised by its cumulative dose-dependent side effects of cardiotoxicity and tumor cell resistance. For the purpose of addressing these side effects, a gold nanoparticles-based anticancer drug delivery system was designed. Five novel thiolated doxorubicin analogs were designed and synthesized and their biological activities have been evaluated. These doxorubicin analogs and the poly(ethylene glycol) (PEG) stabilizing ligands were conjugated to gold nanoparticles via formation of a gold-thiol bond. The systems were evaluated *in vitro* and *in vivo,* and the results show that controlled drug release can be achieved either by acidic conditions or by reducing agents in cancer cells, depending on the design of the thiolated drug construct. The overall drug delivery system should achieve enhanced drug accumulation and retention in cancer cells and favorable drug release kinetics, and should demonstrate therapeutic potential and the ability to address some of the current problems of doxorubicin in cancer therapy.

Acknowledgments

It is my greatest pleasure that I joined Dr. Kingston's group and became his student. Under his guidance, I learned not only a lot of knowledge in chemistry from every aspect, but more importantly, how to do things in the right way. I would like to express my great appreciation and gratitude to Dr. David Kingston for your support, patience and encouragement.

I would like to express my great acknowledgment to my committee, Dr. Richard Gandour, Dr. Webster Santos, and Dr. Harry Gibson. Thank you for providing so many valuable suggestions for my Literature Review and Preliminary Exam, teaching me that "doing" is not the only important component for a successful researcher, and that "thinking" is sometimes even more important. Meanwhile, I greatly appreciate Dr. Gandour's encouragement on my career decision. That really means a lot to me.

I would like to thank Dr. Yumin Dai, who taught me a lot of basic knowledge in synthesis, characterization, etc. He is also a very good friend of mine, and helps me not just in the lab, but also in life without any reservation. I also like to thank all the group members in Dr. Kingston's group, Dr. Harinantenaina Liva, Dr. Yixi Liu, Karen Iannaccone, Peggy Brodie, Dr. Alex Eaton, Chris Presley, Qingxi Su, Amrapali Dengada, Ming Wang, and Yongle Du. Thank you for all the help offered and happy times together.

I want to express my special appreciation to my lovely wife, Ming Wang, for everything, especially for her endless love and support. No matter what difficulties I was facing, no matter what difficult time I had, she would always be there to talk with me, provide support, and help me with everything I want. It is my greatest fortune to have her in my life.

Finally, I would like to express my deepest gratitude to my parents, Bin Xia and Ying Long. They always supported every decision I made and provided anything I needed. I could not go so far without their whole love.

Table of Contents

List of Figures

List of Tables and Schemes

Chapter 1. Introduction to Doxorubicin

1.1 Discovery and History

Doxorubicin (**1.1** in Figure 1.1), also named adriamycin, is an anthracycline antibiotic, and shows excellent bioactivity in experimental systems and against a wide of cancers.[1] It is one of the most active antineoplastic drugs to date[2-4] and is a widely used anticancer agent with clinical activity used against a wide range of human cancers, especially solid tumors.[5]

Its precursor, daunorubicin (**1.2**) was isolated[6] in the 1950's from a strain of *Streptomyces peucetius* by Farmitalia Research Laboratories, an Italian research company, and was found to have good bioactivity against mouse tumors. When using *N*-nitroso-*N*-methyl urethane to mutate a strain of Streptomyces, a new strain was formed and it produced a different red antibiotic. This new compound was originally named adriamycin, because of the Adriatic Sea, but later it was renamed doxorubicin to indicate its relationship to daunorubicin.

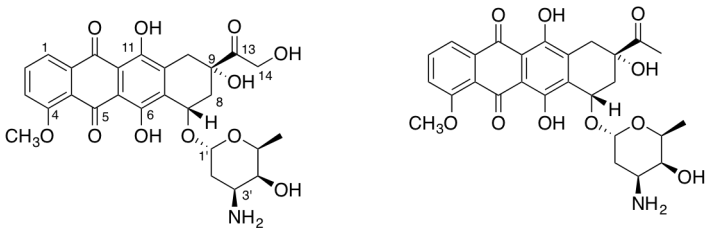

Figure 1.1. Structures of doxorubicin (**1.1**) and daunorubicin (**1.2**)

Doxorubicin was developed into an effective anticancer drug in the 1970's,[2] and it developed into one of the most effective cancer chemotherapeutic agents. Many tumors are highly responsive to it, including acute leukemias, Hodgkin and non-Hodgkin lymphomas, lung microcytomas, breast cancer, and several other cancers.[4]

However, it does have several major limitations, including myelosuppression, vomiting, diarrhea, and life-threatening cardiotoxicity.[4,7] The clinical application of doxorubicin is greatly limited by these side effects. In addition, just like some other systemically administered chemotherapies, it also faces the barrier of elevated tumor interstitial fluid pressure (IFP), which can cause a leaky tumor neovasculature and a collapsed lymphatic system.[8-10] The anti-tumor efficacy is greatly reduced by this inability of chemotherapy to target the cancer cells. As a result, higher doses of toxic drugs are required to achieve meaningful responses.[11]

1.2 Mechanism of Anti-cancer Action of Doxorubicin

The mechanism of anticancer action of doxorubicin has been extensively studied[2] and many mechanisms of action have been proposed, including topoisomerase II inhibition, DNA intercalation, and free radical generation.[12] Although the exact mechanism is still unclear, it is widely accepted that the mechanism for drug activity involves all three actions. Lown reviewed[5] the possible mechanisms, and proposed that topoisomerase II inhibition is likely to be the mechanism most closely associated with its cytotoxicity, although other molecular interactions may play an important role as well. Pommier proposed[13] a detailed topoisomerase II inhibition process. The topoisomerase II DNA complex can be stabilized by doxorubicin when the DNA chain for replication has been broken. The reason for this stabilization is that the electron-deficient quinone chromophore and the electron-rich purines and pyrimidines of DNA have a close contact with each other in a typical electron donor-acceptor complex. As a result, the planar aromatic chromophore part of doxorubicin can intercalate between two base pairs of DNA, and in the meantime the six-membered daunosamine sugar will interact with the base pairs. In this case, there is an extensive overlap between the hydrophobic faces of the base pairs and that

of doxorubicin.[14] Because of this, the DNA double helix cannot be resealed and the replication process will be stopped.[15,16]

1.3 Synthesis Studies

The preclinical and clinical studies of doxorubicin were hindered by supply issues, leading to many synthetic studies being carried out to develop a good solution to the supply problem. To date, however, the most important source for obtaining doxorubicin is still by fermentation. Because the biosynthetic route cannot readily produce structural analogs, several research groups have developed synthetic routes to doxorubicin and its analogs. Since daunorubicin is more abundant than doxorubicin, a semi-synthesis starting from daunorubicin was also developed.[17] The electrophilic bromination of daunorubicin is the key reaction in this route. The route is shown in Scheme 1.1.

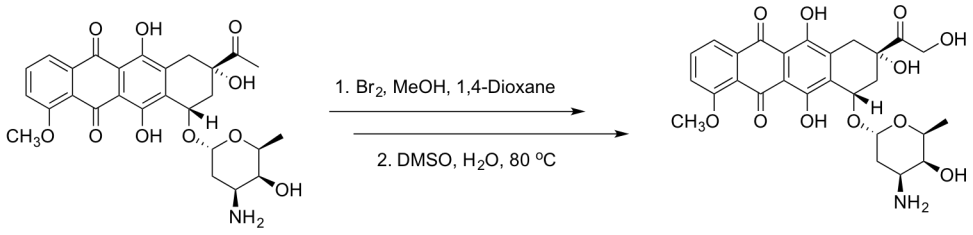

1.2 **1.1**

Scheme 1.1. Synthesis of doxorubicin from daunorubicin

The total synthesis of doxorubicin has also been extensively studied. One synthetic route is to synthesize daunomycinone (**1.3**) first, then use a coupling reaction to obtain daunorubicin, and followed by hydroxylation at the C14 position to obtain doxorubicin.[18] Wong *et al*.

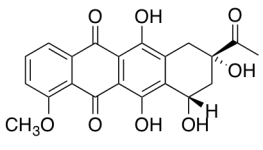

1.3

reported[19] the total synthesis of daunomycinone, and Acton *et al*. reported[20] the second step, the coupling reaction between daunomycinone and the sugar daunosamine to obtain daunorubicin. However, the overall synthetic yield was only around 15%. Although an increased yield was obtained from this route compared with other routes, it is still too low a yield for commercial use, and the many steps required makes this synthesis too complicated. An easier high-yielding route of total synthesis of doxorubicin is still needed.

1.4 Doxorubicin-based Drugs Approved for Clinical Use

Myocet **(Myocet®)** is a liposomal formulation of doxorubicin developed by Elan Corporation[11] and approved by the FDA for clinical use. Compared with doxorubicin, it was found to have a greatly improved therapeutic efficacy. It has less cardiotoxicity and can be better tolerated by patients, while it still demonstrates an equal therapeutic index. Because of these improvements, the clinical options in the overall treatment of breast cancer were extended.[21]

Doxil (**Doxil®**) is another liposome-based doxorubicin formulation. It was approved by the FDA in 1995.[11] It was developed by Schering Plough, and data from its clinical application demonstrated that there is a great improvement with Doxil compared with free doxorubicin in reduction in cardiotoxicity, without reduction in its antitumor efficacy.[22,23]

1.5 Clinical Activity of Doxorubicin and Sides Effects

As mentioned, doxorubicin shows a wide spectrum of antitumor efficacy. When it was administered as a single drug at a dose of 65 mg/m^2 every three weeks, it showed anti-tumor efficacy. However, the most usual administration is to combine doxorubicin with other active drugs.[24] It was reported by Arcamone[2] that until 2005, 113 drug combinations including

doxorubicin were under clinical studies worldwide. Among them, cyclophosphamide was the most frequent component, and the combination with doxorubicin is widely used in the treatment of breast cancer, lung tumors, genital tract tumors, etc. When doxorubicin was administered in the treatment of bronchogenic carcinoma, a 21% response rate was reported. However, when treated with cyclophosphamide combined with doxorubicin, a 46% objective response and longer survival time were observed, indicating the improved effectiveness. Also, the doxorubicin-cyclophosphamide combination is very active in the treatment of breast cancer. With cyclophosphamide combined with doxorubicin, an 80% response rate was observed in patients with breast cancer. Arcamone summarized the clinical studies of doxorubicin in the treatment of various tumors including leukemias, Hodgkin lymphomas, Wilms' tumor, ovarian cancer, etc. in a recent book chapter.[2]

The major side effect of doxorubicin is heart failure caused by a severe cumulative dose-dependence.[20] A total of 59 (1.7%) out of 3461 patients died because of cardiac failure when treated with doxorubicin. Thus, careful control of the cumulative dose of doxorubicin at 450 to 550 mg/m^2 is recommended. This side effect may be a characteristic of anthracycline drugs, since it was also observed with other anthracycline drugs such as daunorubicin. It is hoped that the development of doxorubicin analogs with improved efficacy and reduced side effects will eventually enlarge the clinical usefulness of doxorubicin.

1.6 Medicinal Chemistry and Structure–Activity Relationships (SAR)

1.6.1 Modifications in the Aglycone

Arcamone and Penco reported[25] that positions 6 and 11 have an important influence on doxorubicin's anticancer activity. The C6 and C11 deoxy derivatives were synthesized and results showed that antitumor efficacy was reduced. The reason for this could be that the redox behavior was changed after the substitution of -OH with -H. Capranico *et al*. reported[26] that when the hydroxyl group in position 9 was replaced by a hydrogen atom, a significant decrease of cytotoxicity was observed. They concluded that the C9 hydroxyl group is involved in an interaction with topoisomerase II.

Many further studies were conducted in order to understand how different positions involve in determining doxorubicin's antitumor efficacy. A series of fluorinated analogs were prepared by Arcamone and coworkers[27,28] to explore the effect of fluorination on bioactivity (Figure 1.2). Studies showed that fluorinated idarubicin (**1.4a**) had much lower toxicity than that of its unsubstituted precursor, idarubicin (**1.5**), which implies that position 8 has a significant influence on the bioactivity of doxorubicin. Also, idarubicin derivative (**1.4b**) has activity similar to unsubstituted idarubicin and a higher activity than idarubicin derivative (**1.4a**), which means the relative orientation of the fluorine in position 8 had an effect in determining the antitumor efficacy of anthracyclines. Also, fluorinated doxorubicin (**1.6**) showed comparable activity to its unsubstituted precursor. Position 4 was studied by Arcamone and Penco,[25] who showed that 4 deoxy doxorubicin had similar activity to doxorubicin.

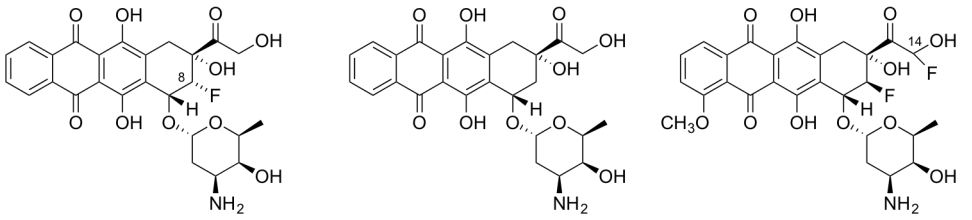

1.4a C8 β
1.4b C8 α

1.5

1.6

Figure 1.2. Fluorinated analogs of idarubicin or doxorubicin

1.6.2 Modifications in the Sugar Moiety

Many studies have been made of modifications to the sugar in doxorubicin. Doxorubicin analogs **1.7** and **1.8** (Figure 1.3) were synthesized by Priebe *et al*.[28] and doxorubicin analog **1.9** was synthesized by Bakker *et al*.[29] The results showed that compounds **1.7** and **1.9** had comparable activity to doxorubicin. Analog **1.8**, however, showed higher potency in cells that were resistant to doxorubicin.

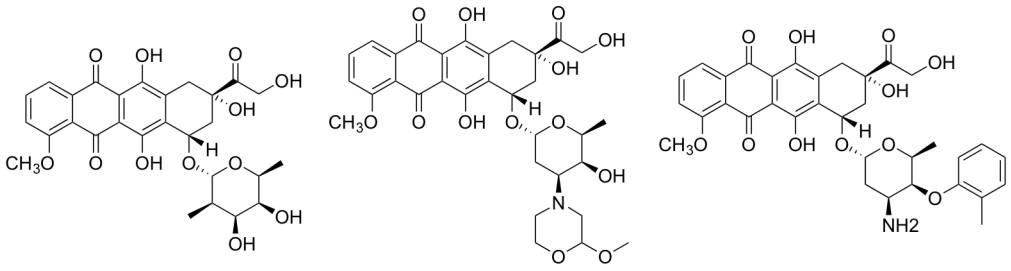

1.7

1.8

1.9

Figure 1.3. Doxorubicin analogs with modification on sugar moiety

Although great efforts have been taken to research the medicinal chemistry of doxorubicin, a more comprehensive and systematic study is still needed to develop a detailed structure-activity relationships. This should be an interesting field for the future development of doxorubicin.

References

1. Minotti, G., Menna, P., Salvatorelli, E., Cairo, G., Gianni, L. Anthracyclines: Molecular Advances and Pharmacologic Developments in Antitumor Activity and Cardiotoxicity. *Pharmacol. Rev.* **2004**, *56,* 185–229.
2. Arcamone, F. Anthracyclines. In *Anticancer Agents from Natural Products*, 2nd Edition; Cragg, G. M.; Kingston, D. G. I.; Newman, D. J., Eds.; CRC Press: Boca Raton, FL, **2012**; pp 383–405.
3. Weiss, R. B. The Anthracyclines: Will We Ever Find a Better Doxorubicin? *Semin. Oncol.* **1992**, *19*, 670–686.
4. Sandy, R.; Chen, C.; Kaur, K. Novel Peptide−Doxorubucin Conjugates for Targeting Breast Cancer Cells Including the Multidrug Resistant Cells. *J. Med. Chem.* **2013**, *56*, 7564−7573.
5. Lown, J. W. Discovery and Development of Anthracycline Antitumour Antibiotics. *Chem. Soc. Rev.* **1993**, *22*, 165–176.
6. Arcamone, F.; Gaetani, M.; Scotti, T.; Dimarco, A. Isolamento ed Attivita Antitumorale di un Antibiotico da Streptomyces sp. *G. Microbiol.* **1961**, *9*, 83–90.
7. Carvalho, F. S.; Burgeiro, A.; Garcia, R.; Moreno, A. J.; Carvalho, R. A.; Oliveira, P. J. Doxorubicin-induced Cardiotoxicity: from Bioenergetic Failure and Cell Death to Cardiomyopathy. *Med. Res. Rev.* **2014,** 34, 106–135.
8. Jain, R. K. Understanding Barriers to Drug Delivery: High Resolution *in vivo* Imaging is Key. *Clin. Cancer Res.* **1999,** 5, 1605–1606.

9. Lejeune, F. J. High Dose Recombinant Tumor Necrosis Factor (rTNFa) Administered by Isolation Perfusion for Advanced Tumors of the Limbs: a Model for Biochemotherapy of Cancer. *Eur. J. Cancer* **1995,** 31, 1009–1016.
10. Paciotti, G. F.; Kingston, D. G. I.; Tamarkin, L. Colloidal Gold Nanoparticles: A Novel Nanoparticle Platform for Developing Multifunctional Tumor-targeting Drug Delivery Vectors. *Drug Dev. Res.* **2006,** 67, 47–54.
11. Peer, D.; Karp, J. M.; Hong, S.; Farokhzad, O. C.; Margalit, R.; Langer, R. Nanocarriers as an Emerging Platform for Cancer Therapy. *Nat. Nanotechnol*. **2007**, *2*, 751–760.
12. Momparler, R. L.; Karon, M.; Siegel, S. E.; Avila, F. Effect of Adriamycin on DNA, RNA, and Protein Synthesis in Cell-free Systems and Intact Cells. *Cancer Res.* **1976**, *36*, 2891−2895.
13. Pommier, Y. *DNA Topoisomerase II Inhibitors, in Cancer Therapeutics, Experimental and Clinical Agents*; Humana Press: Totowa, NJ. , **1997**; pp 153.
14. Frederick, C. A.; Williams, L. D.; Ughetto, G.; Van der Marel, G. A.; Van Boom, J. H.; Rich, A.; Wang, A. H. Structural Comparison of Anticancer Drug-DNA Complexes: Adriamycin and Daunomycin. *Biochemistry* **1990**, *29*, 2538–2549.
15. Pang, B.; Qiao, X.; Janssen, L.; Velds, A.; Groothuis, T.; Kerkhoven, R.; Nieuwland, M.; Ovaa, H.; Rottenberg, S.; van Tellingen, O. Drug-Induced Histone Eviction from Open Chromatin Contributes to the Chemotherapeutic Effects of Doxorubicin. *Nat. Commun*. **2013**, *4*, 1908–1920.
16. Gewirtz, D. A. A Critical Evaluation of the Mechanisms of Action Proposed for the Anti-Tumor Effects of the Anthracycline Antibiotics Adriamycin and Daunorubicin. *Biochem. Pharmacol.* **1999**, *57*, 727–741.

17. Horton, D.; Priebe, W.; Sznaidman, M. Preparative Procedures for Conversion of Daunorubicin into Doxorubicin (Adriamycin) and 14-O-acetyldoxorubicin by Way of 14-bromodaunorubicin. *Carbohydr. Res.* **1988**, *184*, 231–235.
18. Pasqui, F.; Canfarini, F.; Giolitti, A.; Guidi, A.; Pestellini, V.; Arcamone, F. Synthesis of Ring A Fluorinated Anthracyclines. *Tetrahedron* **1996**, *52*, 185–198.
19. Wong, C. M.; Schwenk, R.; Popien, D.; Ho, T. L. The Total Synthesis of Daunomycinone. *Can. J. Chem*. **1973**, *51*, 466–467.
20. Acton, E. M.; Fujiwara, A. N.; Henry, D. W. Total Synthesis of the Antitumor Antibiotic Daunorubicin. Coupling of the Sugar and Aglycone. *J. Med. Chem.* **1974**, *17*, 659–660.
21. Batist, G.; Barton, J.; Chaikin, P.; Swenson, C.; Welles, L. Myocet (Liposome-encapsulated Doxorubicin Citrate): a New Approach in Breast Cancer Therapy. *Expert Opin. Pharmacother*. **2002**, *3*, 1739–1751.
22. Kumar, A.; Zhang, X.; Liang, X. J. Gold Nanoparticles: Emerging Paradigm for Targeted Drug Delivery System. *Biotechnol. Adv*. **2012**, *31*, 593–606.
23. James, N.; Coker, R.; Tomlinson, D.; Harris, J.; Gompels, M.; Pinching, A.; Stewart, J. Liposomal Doxorubicin (Doxil): an Effective New Treatment for Kaposi's Sarcoma in AIDS. *Clin. Oncol*. **1994**, *6*, 294–296.
24. Arcamone, F. In *Doxorubicin: Anticancer Antibiotics*. Academic Press: New York, **1981**; Vol 17, pp 25–32.
25. Arcamone, F.; Penco, S. In *Antitumor Natural Products, Basic and Clinical Research; Gann Monograph on Cancer Research Series*. Taylor & Francis: Florence, Kentucky, **1989**; pp 81–94.
26. Capranico, G.; De Isabella, P.; Penco, S.; Tinelli, S.; Zunino, F. Role of DNA Breakage

in Cytotoxicity of Doxorubicin, 9-Deoxydoxo, and 4-Demethyl-6-Deoxydoxo in Murine Leukemia P388 Cells. *Cancer Res.* **1989**, *49*, 2022–2027.

27. Animati, F.; Arcamone, F.; Bigioni, M.; Capranico, G.; Caserini, C.; De Cesare, M.; Lombardi, P.; Pratesi, G.; Salvatore, C.; Supino, R. Biochemical and Pharmacological Activity of Novel 8-Fluoroanthracyclines: Influence of Stereochemistry and Conformation. *Mol. Pharmacol*. **1996**, *50*, 603–609.
28. Priebe, W.; Skibicki, P.; Varela, O.; Neamati, N.; Sznaidman, M.; Dziewiszek, K.; Grynkiewicz, G.; Horton, D.; Zou, Y.; Ling, Y. H. Non-Cross-Resistant Anthracyclines with Reduced Basicity and Increased Stability of the Glycosidic Bond. *ACS Symp. Ser.* **1995**, *574*, 14–46.
29. Bakker, M.; Droz, J.; Hanauske, A.; Verweij, J.; Van Oosterom, A.; Groen, H.; Pacciarini, M.; Domenigoni, L.; Van Weissenbruch, F.; Pianezzola, E. Broad Phase II and Pharmacokinetic Study of Methoxy-Morpholino Doxorubicin (FCE 23762-MMRDX) in Non-Small-Cell Lung Cancer, Renal Cancer and Other Solid Tumour Patients. *Br. J. Cancer* **1998**, *77*, 139–146.

Chapter 2. Anticancer Drug Delivery Strategies and Gold Nanoparticles Drug Delivery System

2.1 General Principles of Anticancer Drug Delivery

The most common undesirable side effect of traditional anticancer drugs is that they will kill all the cells that are growing rapidly, such as cancer cells, blood cells, hair cells, etc. These effects greatly compromise the anticancer efficacy.[1] A widely used method to deal with these problems and inhibit the growth of tumor cells is to develop an appropriate drug delivery system. Generally speaking, the principles of anticancer drug delivery are to improve the ability to selectively deliver to targeted cancer cells, to accumulate the drug in tumor cells, and to reduce the drug concentration in normal cells. This will reduce side effects, and may increase circulation time, to ensure a high percentage of drug being accumulated in the tumor cells. A short time means the drug will be rapidly cleared by the immune system. The ability to control drug release, how long it needs to be released, and what percentage will be released, are also essential in designing drug delivery systems.[2]

2.2 Nanoparticle Targeting Strategies and Mechanisms in Anticancer Drug Delivery

Before arriving at the target tumor cells, there are a lot of barriers in the anticancer drug delivery procedure, such as mucosal and membrane barriers, etc. So it is necessary to have a fundamental understanding of tumor biology and the tumor microenvironment before discussing drug delivery strategies and their mechanisms. Tumor cells exhibit several characteristic features compared with normal cells, like increased pore sizes, leaky tumor neovasculature and decreased lymphatic drainage. Because of the leaky neovasculature, its permeability to nanoparticles is

enhanced, and combined with poor lymphatic drainage, it is possible to accumulate nanoparticle anticancer drugs into the tumor cells by this enhanced permeability and retention (EPR) effect.[1,3,4]

Based on the principles described above and cancer biology, many efforts have been made on the design and development of various kinds of anticancer drug delivery systems. These systems are mainly based on two major targeting mechanisms, passive targeting and active targeting.

2.2.1 Passive Targeting of Nanoparticle Drug Delivery Systems

Passive targeting means that the combination of the properties of the drug delivery system and the tumor cells' microenvironment work together to determine the location for drug accumulation.[5,6] As described above, cancer cells have certain characteristics in their chemical or physical properties. These characteristics allow the accumulation of a nanoparticle drug carrier of its associated drug load in cancer cells instead of normal cells. For example, the pore size of cancer vasculature is increased compared with normal vasculature, and if the size of nanocarrier can be controlled to a size that is large enough to be excluded by normal vasculature and small enough to get through the tumor vasculature, selective targeting will be achieved.[7-9]

However, it is reported by James *et al*.[10] that there are some limitations in its clinical application. First, since this process is random, it is not always feasible to control it, and some drugs cannot disperse efficiently. Second, selective targeting will not be observed when applying the drug to tumors without enhanced permeability. So selective passive targeting is still a problem in some cases.

2.2.2 Active Targeting of Nanoparticle Drug Delivery Systems

Unlike passive targeting, active targeting is the interaction between a specific agent in the drug carrier and certain receptors on the surface of the cells.[11] To be more specific, certain agents, such as peptides, proteins and other small molecules, can be conjugated onto the surface of the drug carrier.[12] These agents should be designed to be able to interact with specific receptors on the cells, so that the drugs will bind to target cells. When the drug is injected and circulating in the blood, the receptors on the target cells can recognize the targeting agents attached to the drug system,[1] and the drug can be bound to them, and in this way, the drug is actively delivered to targeted cells.

Passive and active targeting can be combined in one drug delivery system to get a heightened delivery performance while reducing problems of each strategy. By controlling the size of the delivery system and improving certain properties, an extended period of time of circulating in the body can be achieved. Then by using ligands that are specific to cancer cells, the chance of getting the drug delivery systems into desired sites will be greatly improved.[13]

2.3 Recently Developed Anticancer Drug Carriers

Peer *et al*. summarized[12] that a lot of materials have been used in the design of anticancer drug delivery systems, including biopolymers, hydrogels, emulsions, nanotechnology, etc. Among these, nanocarriers are the most extensively investigated and developed delivery strategy, at least until now.[9] Currently, three major kinds of nanocarriers, namely liposomes, polymeric nanocarriers, and nanoparticles, are the most widely studied and applied in cancer therapy in the real world.

2.3.1 Liposomal Drug Delivery Systems

Liposomes are frequently applied in the delivery of various anticancer drugs because of their advantages compared with free drug. Liposomes usually are relatively large, and due to the cancer biology mentioned previously, the liposome drug system will not be able to enter healthy cells, and the toxicity caused by nonspecific targeting will be greatly reduced. The drugs attached to liposomes can also be protected from hydrolysis or premature degradation.[12]

Many recent studies are focusing on modifying the liposome by adding certain ligands on its surface to improve the anticancer efficacy, such as targeting ligands, antibodies, peptides and small organic molecules. Molavi *et al*. reported[14] a modification method by adding anti-CD30 (CD30 is a membrane protein which is overexpressed in some types of tumor) monoclonal antibody to Doxil, and by doing this, an enhanced anticancer efficacy was observed; this is the first report of this approach and more research is on the way. Shroff and Kokkoli reported[15] that PEG, which is a water-soluble and hydrophilic polymer, can be introduced to functionalize the surface of liposomes to increase their solubility and ensure a long circulation time, and the results showed that the drug can be encapsulated with high selectivity in targeting and high payloads in the treatment of cancer cells.

2.3.2 Polymeric Drug Delivery Systems

Polymeric nanocarriers have been extensively studied for their applications in construction of anticancer delivery systems for their capability to be incorporated with therapeutics and controlled engineering of the materials.[16] Dendrimers, nanospheres, micelles, polymersomes, etc. all belong to this family and each of them has its own characteristics as a drug carrier.[17] For example, dendrimers are highly branched and normally highly symmetric. It is easy to control

the overall properties of dendrimers by functionalizing them with therapeutics, targeting agents, or other functional groups.[17]

Micelles are also a type of polymeric nanocarrier. They are spherical structures consisting of several hundred block co-polymers and have a diameter between 10 and 200 nm.[18] They are generally amphiphilic molecules, with a hydrophobic core which is densely packed and a hydrophilic surface.[19] Some excellent features are found for polymeric micelles. They are easy to prepare and their size can be easily controlled, they have a high capacity of drug loading, a longer circulation time in blood, the ability to control the drug release kinetics,[20] and improved accumulation in cancer cells through the EPR effect.

Similarly with liposomes, certain ligands and other molecules can be introduced to modify polymeric micelles. Nasongkla *et al*. reported[21] that by conjugating an $\alpha_\gamma\beta_3$ integrin (a protein, which is overexpressed in some tumors) ligand to PEG-poly(ε-caprolactone) polymeric micelles with doxorubicin, the selective targeting effects can be greatly improved. This is because $\alpha_\gamma\beta_3$ integrin is overexpressed in endothelial cells and so targets the drug to the tumor neovasculature can be achieved by a receptor-mediated interaction. Yoo *et al*. prepared[22] doxorubicin-conjugated biodegradable polymers consisting of poly(D,L-lactic-co-glycolic acid) and PEG copolymer. The doxorubicin was conjugated through an acid-cleavable hydrazone bond and doxorubicin was released from the micelles under acidic conditions in a short time. In addition, a higher cytotoxicity was also observed compared with free doxorubicin, and the biodegradable micelles did not cause any side effects.

2.4 Gold Nanoparticle Carrier-based Anticancer Drug Delivery System

2.4.1 Introduction to Gold Nanoparticles

Gold nanoparticles, which belong to the family of nanocarriers, are nanometer-level sized particles of gold. The diameter ranges from 2 to 200 nm.[23] Gold nanoparticles were first introduced to biological studies in the early 1970s, by British chemists Faulk and Taylor.[24] They developed a method, using colloidal gold conjugated antibody, to visualize the surface antigens of *Salmonella* by microscopy. For the past several decades, a great amount of efforts have been made to explore the potential applications of gold nanoparticles by conjugating them with different functional molecules, like drugs, enzymes, antibodies, etc.[25-28] Further, gold nanoparticles are widely used in modern biology, chemistry and medical research, including microbiology, genomics, immunoanalysis, optical bioimaging, biosensors, etc.,[29] and in almost every aspect of the medical area, like diagnostics, prevention, disease therapy, etc.[30]

2.4.2 Metabolism and Excretion of Gold Nanoparticles

A basic requirement for gold nanoparticles in medical applications is that they should be excreted rapidly in order to reduce the potential accumulation toxicity. The metabolism and excretion of gold nanoparticles have been studied. Thakor *et al*.[31] described the general process: although some differences, like the rate and the percentage of excretion, are observed for different patients, the basic mechanism should be the same for all individuals and gold nanoparticles are mainly excreted in the urine and feces. It is reported by Mascarenhas *et al*.[32] that when increased amount of gold nanoparticles are injected, the excreted amounts also increased. However, there was no direct proportional relation between the excretion rate and the amount of gold nanoparticles that was injected. The reason for this phenomenon, the relatively

slow clearance rate of gold nanoparticles, may be the binding capacity between albumin in blood and gold.[33] Nevertheless, although the exact kinetic relationship cannot be determined, it is known that once the gold nanoparticles are injected, certain equilibria will be built up with gold absorbing or excreting between the blood, urine, and feces.

2.4.3 Gold Nanoparticles Anticancer Drug Delivery System

Besides the applications of gold nanoparticles as diagnostic and therapeutic agents, another promising use, which has been extensively studied, is as anticancer drug carriers. This is due to their excellent physical and chemical properties. They are (i) biocompatible[34] and easy to functionalize,[35] (ii) have high surface to volume ratio ensures high functionality and large capacity for drug loading,[12] (iii) drugs can be protected to ensure their overall stability, selective targeting to tumor cells and improved intracellular penetration[8] (iv) have long circulatory half-life.[36] All of these properties make gold nanoparticles highly multifunctional drug carriers.

A large number of gold nanoparticle-based drug delivery systems have been developed to achieve various purposes. Brown *et al*.[9] designed and developed conjugates of platinum-based anticancer drugs like cisplatin with gold nanoparticles as drug carrier. The results of drug uptake and localization studies and cytotoxicity studies showed that compared with free drug, the gold nanoparticle-conjugated drug exhibited enhanced cytotoxicity. As a result, potency was improved and the drug delivery process was simplified. Also, selective accumulation was greatly improved, demonstrating that gold nanoparticles are able to deliver platinum-based drugs to certain cancer cells and release them. The surface modifications of gold nanoparticles have also been applied in improving drug delivery efficiency. Heo *et al*.[37] reported that by surface modifications with various kinds of ligands, certain properties of gold nanoparticles can be

improved. The polymer PEG can be modified by thiol group on one of its end to give methoxy-PEG-thiol, which was widely used in functionalizing surface of gold nanoparticles because of their low toxicity, good protection of nanoparticles from protein adsorption, and ease to be attached to gold nanoparticles.[38,39] PEG has been extensively used in functionalizing drug systems for a long time because of its capability in increasing the blood circulation time for a variety of drugs without causing any side effects.[40] By introducing β-cyclodextrin as a functional ligand, PEGs as a solubility improving agent, biotin as the targeting agent, gold nanoparticles as the drug carrier and paclitaxel as an anticancer drug, a significantly higher efficacy was observed with almost no cytotoxicity to normal cells. This work is meaningful because it demonstrates that certain functional molecules can be introduced to modify gold nanoparticles to improve certain properties and fix existing problems. This should be a useful technique to deal with similar problems in this research.

2.4.4 Mechanism of Specificity of Gold Nanoparticles

As mentioned in Section 2.2, two targeting mechanisms can be applied for anticancer drug delivery. For gold nanoparticles, passive targeting is based on the EPR effect. Tumor cells exhibit characteristic features including increased pore sizes in blood vessels and poor lymphatic drainage. Jain *et al*. reported[41] that the pore size of the blood vessels of tumors can be as large as 400 nm, and Shi *et al*.[17] summarized that if nanocarriers can be controlled within a size range of 20 to 200 nm, they can extravasate and accumulate in tumor cells through these pores. Moreover, because cancer cells lack a well-defined functional lymphatic network, the gold nanoparticles can be retained for a longer time in tumor cells. This is the EPR effect for gold nanoparticles and is the basis for design of gold nanoparticle-based drug carriers.[36]

By modifying the surface of gold nanoparticles with targeting ligands, a specific targeting to cancer cells can be obtained because there is an interaction between the ligands and receptor on the cancer cells. Park *et al*. used[42] herceptin, which is a therapeutic antibody and can bind to one kind of receptor on breast and ovarian tumor cells, to modify gold nanoparticles based drugs. With the antibody–receptor active targeting, the anticancer efficacy was enhanced.

2.4.5 Doxorubicin-gold Nanoparticle Conjugates

As discussed previously, liposomes and polymeric micelles are extensively studied as drug carriers to selective deliver doxorubicin into cancer cells, but there are serious problems with them. For liposomes, the skin toxicity and still severe cardiotoxicity greatly compromise their therapeutic efficacy.[43] Also, the circulation time of several liposome-based doxorubicin drugs is not long enough.[8] For polymeric micelles, they have low selectivity in targeting tumor cells and they would also accumulate in other sites like liver, kidney, etc.[12]

Compared with liposomes and polymeric micelles, functionalized gold nanoparticles generally have many good properties that are desirable for passive targeting of tumor tissue via the EPR effect, and reduced reticuloendothelial system (RES) clearance.[44]

Due to the potential problems of using free doxorubicin in cancer therapy and the obvious advantages of gold nanoparticles, it is reasonable to deduce that by combining the doxorubicin and gold nanoparticles, as well as some necessary modifications, the problems such as side effects may be addressed, at least to some degree. As a result, gold nanoparticle-based anticancer drug delivery systems may be an ideal technique in the therapy of certain cancers.

2.4.6 Current Development of Gold Nanoparticles Conjugated Doxorubicin

Numerous efforts have been made to develop gold nanoparticles conjugated with doxorubicin (gold nanoparticles-doxorubicin), such as modifications of the surface of the gold nanoparticles and size control of gold nanoparticles, modifications of the structures of doxorubicin, etc. A short review of the most recent developments of gold nanoparticle-doxorubicin will be presented below.

Several improvements have been achieved from recent research on such systems. Asadishad *et al*. reported[45] that by using PEG functionalized gold nanoparticles to conjugate doxorubicin, the drug system showed a much higher cytotoxicity than that of free doxorubicin, as well as an increased solubility. Also, from a comparison of cell viability between normal and cancer cells, a reduced side effect was observed. This implies that modification of gold nanoparticles could be a strategy for improving the therapeutic performance of gold nanoparticles-doxorubicin. Besides the modifications on gold nanoparticles, the structure of doxorubicin can also be modified before being conjugated to gold nanoparticles to improve some properties of the drug system like stability, release kinetics, accumulation effects, etc. The doxorubicin prodrugs are designed to achieve selective delivery to tumor cells and thus reduce the toxicity to normal tissues.

Alexander *et al*. prepared[46] a gold nanoparticle-based drug delivery system, which was functionalized by DNA, folic acid (FA), a thermoresponsive polymer, and PEG oligomers onto gold nanoparticles. This study revealed how the cellular uptake and cytotoxicity of the whole drug system was affected by the functional groups attached on the surface of gold nanoparticles. For example, higher cytotoxicity was achieved by carefully controlling the FA coverage to 50%, and higher coverage actually resulted in a decrease of drug efficacy. Also, a thermoresponsive polymer can be introduced to the whole system to further improve the cytotoxicity.

Aryal *et al*. reported[44] that by introducing a pH-sensitive hydrazone bond as linker between doxorubicin and gold nanoparticles, the gold nanoparticles-doxorubicin system showed greatly enhanced solubility and an excellent pH response profile of drug release. The prodrug **2.1** is shown in Figure 2.1.

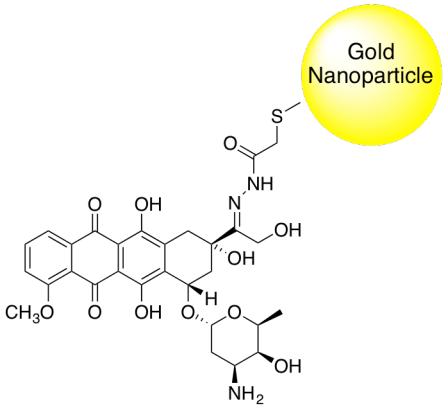

Figure 2.1. Doxorubicin prodrug **2.1**

Wang *et al*.[47] modified doxorubicin by adding PEG to it, and added lipoic acid (LA) as the terminal group using a hydrazone (Hyd) linker. The LA-PEG-Hyd-doxorubicin was obtained and conjugated to gold nanoparticles to construct the modified gold nanoparticles-doxorubicin system. Results showed it had a significant drug efficacy to cancer cells with multidrug resistance. Since multidrug resistance is a major problem in chemotherapy of cancer, the method developed in this paper in dealing with this problem is meaningful for the research of multidrug resistance cancer. The prodrug **2.2** is shown in Figure 2.2.

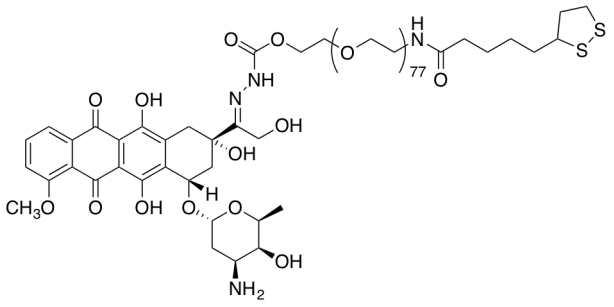

Figure 2.2. Doxorubicin prodrug **2.2**

From the above examples, we can see that we can improve the doxorubicin-gold nanoparticle drug delivery system by either modifying the structure of doxorubicin derivatives or the surface of gold nanoparticles. The doxorubicin conjugated nanoparticle is protected from being cleared by the reticuloendothelial system either by PEG molecules attached to the gold surface or by PEG units built into the drug construct itself. As a result, the circulation time is extended and the accumulation in tumor cells is enhanced. Also, the gold nanoparticle-doxorubicin system showed a higher drug efficacy in treating cancer cells, and side effects were reduced. Furthermore, by specific control of the structure of doxorubicin derivatives, the release of the drug from the system can also be triggered by some chemical stimulus in cancer cells, such as change of pH or temperature, reduction by thiols (glutathione), etc.

2.4.7 Problems in Current Doxorubicin-gold Nanoparticle Systems

However, at this time, there are no gold nanoparticle conjugated doxorubicin systems that have been clinically approved or are under clinical investigation by FDA. Obviously, some problems still exist. First is the slow rate of clearance of the residual nanoparticles, especially for relatively larger particle. Secondly, although the release kinetics of the drug have been improved, they still do not meet clinical requirements, and further work in improving the drug release is

needed. Thirdly, it is difficult to fix all the problems in just a single system, since some problems exist in one system, while other problems exist in other systems. However, unless all the major problems are solved, clinical use of the gold nanoparticle-doxorubicin system will not be possible.

Many techniques have been developed to solve some problems of gold nanoparticle-doxorubicin systems. Although a lot of attention has been paid in developing different doxorubicin analogs, no systematic study has been conducted to study how the overall drug efficacy would be affected by different linkers. This should be a promising way to deal with some existing problems of gold nanoparticle-doxorubicin systems.

The rest of this chapter will focus on the preparation and characterization of gold nanoparticles and modification by PEG. The next chapter will focus on the design and synthesis of different doxorubicin analogs with different types of linkers, position of linkers, etc., so that we can explore how different factors in the linkage of doxorubicin to nanoparticles influence drug efficacy, and further improve the performance of the drug delivery system. We expect that the proposed new delivery method for doxorubicin will improve its delivery and toxicity by targeting delivery to the tumor and minimizing its delivery to non-target organs. It will thus allow the use of higher doses of doxorubicin, reduce side effects, and allow extended use that is not possible with the current delivery methods, thus leading to significantly improved therapeutic outcomes as compared with doxorubicin.

2.5 Synthesis of PEG-tethered Gold Nanoparticles

To obtain PEG-tethered gold nanoparticles (Figure 2.3), we first synthesized monodisperse spherical gold nanoparticles.

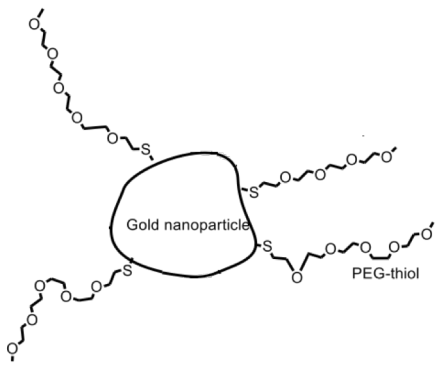

Figure 2.3. PEG-tethered gold nanoparticles

Several successful methods have been developed to prepare gold nanoparticles with different sizes and shapes in aqueous and organic media. But these methods have some problems. For example, the Turkevich method has a broad distribution of size and shape.[48] This will be a serious problem if we use them as drug carriers and apply them in an animal study because it will be difficult to control the selective drug delivery if the size range is too broad and the shape is not quite uniform. To obtain spherical gold nanoparticles which have a relatively narrow size distribution, the method developed by Wang's group was adopted in this research.[49] As discussed in Section 2.4.4, the pore size of the blood vessels of tumors can be as large as 400 nm. Chan *et al*. have reported[50] that cellular uptake is likewise dependent on the size of nanoparticles. In these studies, they found the most efficient cellular uptake was observed with particles ranging from 20 to 50 nm. Apoptosis was also enhanced if the sizes of particles are within a 40–50 nm ranges. Thus, we chose to control the synthesis of gold nanoparticles to obtain a size around 40 nm so that they can extravasate and accumulate in tumors through these pores, and in the meantime, they can be excluded from normal cells to achieve selective delivery.

2.5.1 Synthesis of Gold Nanoparticles

Gold nanoparticles are prepared by the citrate reduction of $HAuCl_4$ in water. The aqueous solution of citrate and $HAuCl_4$ are well mixed at room temperature and then rapidly added to boiling water, and a trace amount of Ag^+ ions are also added. This technique gives good reproducibility and uniformity of the gold nanoparticles size and shape.[26]

2.5.2 Preparation of PEG-tethered Gold Nanoparticles

PEG is very important in stabilizing gold nanoparticles, increasing water solubility, and extending circulation time. It can be conjugated onto gold nanoparticles by using PEG methyl ether thiol (5 kDa), since gold and thiols can form covalent bonds. After conjugation, the water solubility of the gold nanoparticles was greatly improved.

2.5.3 Characterizations of Gold Nanoparticles

UV-Vis Spectroscopy: The gold nanoparticles obtained were characterized by UV-Vis spectroscopy. Figure 2.4 indicates that the gold nanoparticles have a maximum surface plasmon absorption at 523~524 nm, and that naked gold nanoparticles and PEGylated gold nanoparticles had similar surface plasmon absorptions.

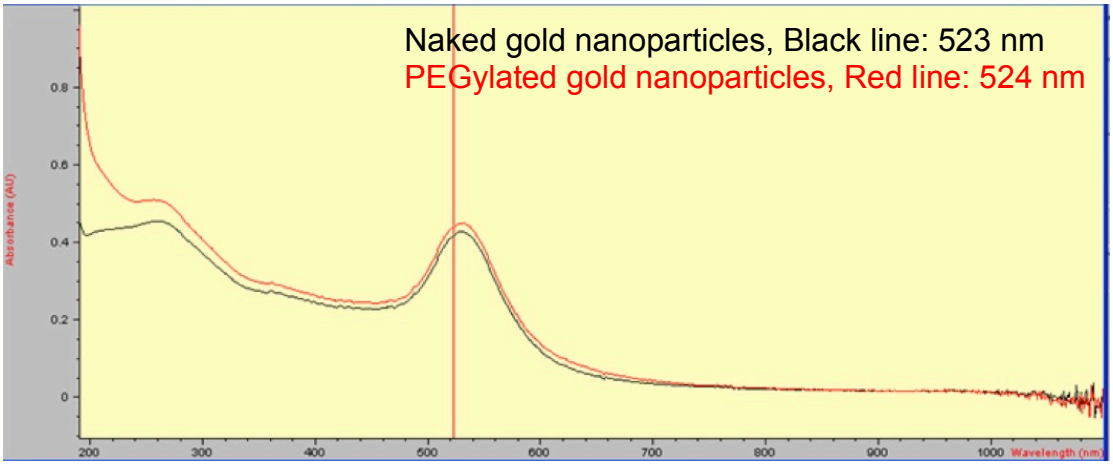

Figure 2.4. UV spectra of naked gold nanoparticles and PEGylated gold nanoparticles

Transmission Electron Microscopy (TEM): The gold nanoparticles obtained were characterized by TEM. Figure 2.5 indicates that the gold nanoparticles before and after attachment of PEG are approximately spherical in shape. TEM imaging demonstrates that the synthesis allows the formation of uniform gold nanoparticles with size 39 ± 3 nm for naked gold nanoparticles, and 42 ± 3 nm for PEGylated gold nanoparticles. The addition of PEG increases the size about 3 nm.

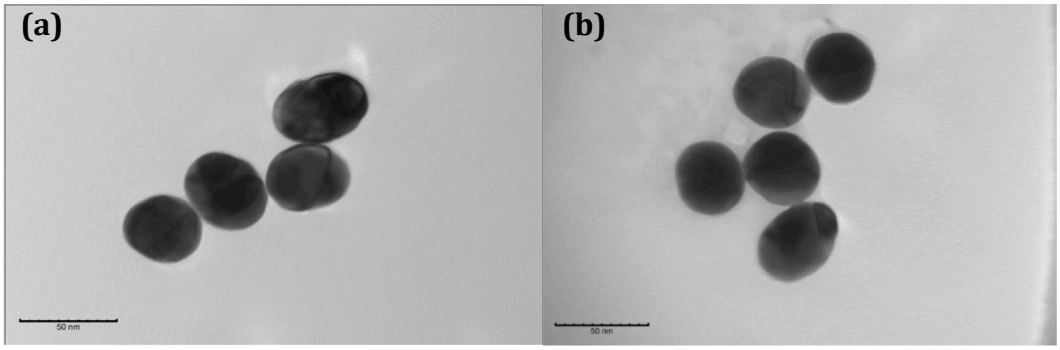

Figure 2.5. TEM images of naked gold nanoparticles (a) and PEGylated gold nanoparticles (b)

Dynamic Light Scattering (DLS): The size distributions of both kinds of gold nanoparticles were analyzed by DLS, and the result (Figure 2.6) shows that gold nanoparticles

before and after attachment of PEG have quite narrow size distributions. Also, from this result, an increase in diameter after addition of PEG can be observed. The difference in results obtained by TEM and DLS can be interpreted by the fact that these two techniques measure two different things. TEM measures the core size, but DLS measures the surfactant and the interaction with solvent molecules is taken into account. This difference causes the results from DLS to be slightly larger than those from TEM.

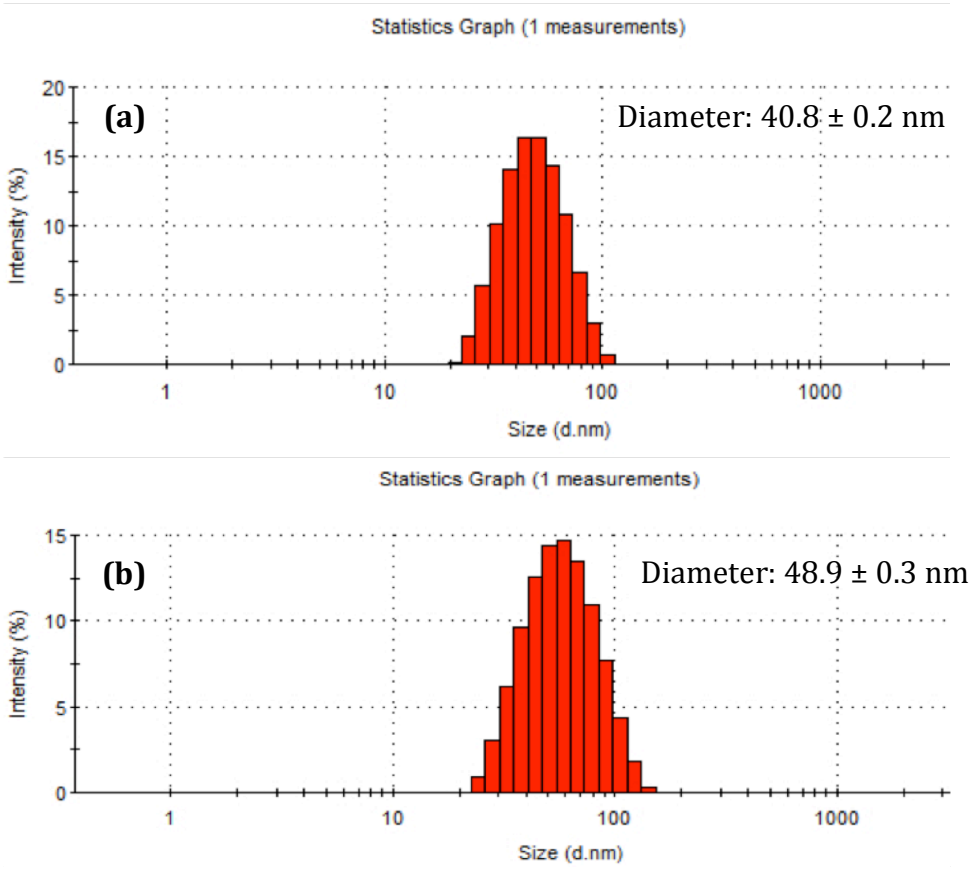

Figure 2.6. DLS analysis of the size distribution of naked gold nanoparticles (a) and PEGylated gold nanoparticles (b)

The surface of gold nanoparticles is one of the most important factors in its drug delivery application.[51] The nanoparticles obtained by our method are negatively charged and parameterized by the Zeta potential. The Zeta potential is defined as the potential difference between a colloidal dispersion and the dispersion medium. This is a crucial parameter because nanoparticles can be cleared by the reticuloendothelial system very quickly if they do not have a strong negative charge. On the other hand, the gold nanoparticles cannot be too negatively charged since this would result in a poor uptake by tissues and/or poor cytotoxicity.[52] The Zeta potentials of both gold nanoparticles were measured by DLS. From Table 2.1, "naked" nanoparticles are in a good negative charge range (less negative than 30 mV) and with the addition of PEG, they became even less negative, due to the replacement of negatively charged citrate ligands by neutral PEG molecules. This is yet another evidence indicating the successful attachment of PEG.

Nanoparticles	Zeta Potential (mV) DLS	Diameter (nm) DLS
"Naked" AuNPs	-26 ± 3	40.8 ± 0.2
PEGylated AuNPs	-16 ± 2	48.9 ± 0.3

Table 2.1. The Zeta potential and average diameters of naked gold nanoparticles and PEGylated gold nanoparticles

2.6 Experimental Section

2.6.1 General Experimental Methods

All chemicals were purchased from Sigma-Aldrich and used as received unless otherwise stated. All reactions were performed in the oven-dried glassware and under protection with nitrogen gas.

Agilent 8453 UV-Vis spectrophotometer was used to record the UV-Vis absorption spectra. TEM images were obtained with a Philips EM420 at 120 kV acceleration voltage. Dynamic light scattering experiments were conducted at room temperature and at a fixed angle of 173^{o} on a Malvern Zetasizer Nano ZS equipped with a 50 mW 533 nm laser.

2.6.2 Synthetic Procedures

Synthesis of Monodisperse Spherical Gold Nanoparticles. A 50 mL round bottom flask was charged with 5 mL sodium citrate aqueous solution (1 wt %) and a magnetic stirring bar. $HAuCl_4$ aqueous solution (10 mL, 0.5 wt %) and $AgNO_3$ aqueous solution (425 μL , 0.1 wt %) were added. H_2O (9.57 mL) was added to bring the volume of the solution to 25 mL. This mixture was incubated for 5 min before addition to hot H_2O prepared below. A 1000 mL two-necked round bottom flask was charged with 475 mL of H_2O, a magnetic stirring bar and condenser, and was heated to boiling. After the H_2O had boiled for 10 minutes, the above solution was quickly injected into the boiling H_2O by pipet under vigorous stirring. The color of the reaction solution changed quickly from colorless, grayish blue, and purple to ruby red within 1 min. The reaction solution was refluxed for 1 h under stirring to warrant formation of uniform quasi-spherical gold nanoparticles.

To remove excess sodium citrate and other small molecules, dialysis was performed. The colloidal gold solution was transferred to dialysis membrane tubing (MW cutoff = 14,000 Da), and the tubing was immersed in 1 L water with vigorous stirring. The water was changed every 2 hours and after 8 hours dialysis, the resulting solution was used for the following steps.

Synthesis of PEG-tethered Gold Nanoparticles. A 500 mL two-necked round bottom flask was charged with 250 mL of solution from the last step, 58 mg PEG methyl ether thiol (MW = 5 kDa, from Creative PEGworks) in 5 mL H_2O, a magnetic stirring bar and condenser. The whole solution was stirring vigorously for 24 hours. To remove unbound PEG methyl ether thiol, the resulting solution was centrifuged at 14000 g for 20 min at room temperature and the pellets containing nanoparticles were redispersed in water. This process was performed three times to ensure complete removal, and the resulting solution was ready for future studies.

2.6.3 Characterization

UV-Vis Spectroscopy*:* Aliquots of 0.1 mL of both solutions (with and without PEG-thiol) were diluted to 1 mL with H_2O and transferred to 2 mL polystyrene cuvettes. The UV-Vis absorbance spectra (200–800 nm) were recorded.

Transmission Electron Microscopy: Aliquots of 0.1 mL of both solutions (with and without PEG-thiol) were deposited on Formvar-coated copper grids (purchased from Ted Pella). After 5 min, excess liquid was wicked away, and the remaining thin solution film was allowed to dry. Grids were imaged using a Philips EM420 with an accelerating voltage of 120 V to enhance the contrast of the electron-dense gold. Enough frames were collected to capture at least 20

particles per replicate. Nanoparticle size (d) was estimated using the formula $d = A / \pi$, where A is the crosssectional area of a particle measured using ImageJ (a software to process TEM images).

Dynamic Light Scattering*:* Aliquots of 0.1 mL of both solutions (with and without PEG-thiol) were diluted to 1 mL with H_2O and transfer to 2 mL polystyrene cuvettes. The Z-average hydrodynamic diameter (HD) and polydispersity index (PDI) were measured using a ZetaSizer Nano ZS. Nanoparticle dilutions that gave an attenuator setting of between 6 and 9 were used for measurement.

References

1. Ghosh, P.; Han, G.; De, M.; Kim, C. K.; Rotello, V. M. Gold Nanoparticles: in Delivery Applications. *Adv. Drug Delivery Rev*. **2008**, *60*, 1307–1315.
2. Kumar, A.; Zhang, X.; Liang, X. J. Gold Nanoparticles: Emerging Paradigm for Targeted Drug Delivery System. *Biotechnol. Adv.* **2013**, *31*, 593–606.
3. Larson, T. A.; Joshi, P. P.; Sokolov, K. Preventing Protein Adsorption and Macrophage Uptake of Gold Nanoparticles via a Hydrophobic Shield. *ACS Nano* **2012**, *6*, 9182–9190.
4. Maeda, H. Macromolecular Therapeutics in Cancer Treatment: The EPR Effect and Beyond. *J. Controlled Release* **2012,** *164*, 138–144.
5. Sagnella, S.; Drummond, C. Drug Delivery: a Nanomedicine Approach. *Aust. Biochem.* **2012**, *43*, 5–8.
6. Gullotti, E.; Yeo, Y. Extracellularly Activated Nanocarriers: a New Paradigm of Tumor Targeted Drug Delivery. *Mol. Pharmaceutics* **2009**, *6*, 1041–1051.
7. Bakker, M.; Droz, J.; Hanauske, A.; Verweij, J.; Van Oosterom, A.; Groen, H.; Pacciarini, M.; Domenigoni, L.; Van Weissenbruch, F.; Pianezzola, E. Broad Phase II and Pharmacokinetic Study of Methoxy-Morpholino Doxorubicin (FCE 23762-MMRDX) in Non-Small-Cell Lung Cancer, Renal Cancer and Other Solid Tumour Patients. *Br. J. Cancer* **1998**, *77*, 139–146.
8. Wang, Y.; Wei, X.; Zhang, C.; Zhang, F.; Liang, W. Nanoparticle Delivery Strategies to Target Doxorubicin to Tumor Cells and Reduce Side Effects. *Ther. Delivery* **2010**, *1*, 273–287.
9. Brown, S. D.; Nativo, P.; Smith, J. A.; Stirling, D.; Edwards, P. R.; Venugopal, B.; Flint, D. J.; Plumb, J. A.; Graham, D.; Wheate, N. J. Gold Nanoparticles for the Improved

Anticancer Drug Delivery of the Active Component of Oxaliplatin. *J. Am. Chem. Soc.* **2010**, *132*, 4678–4684.

10. James, N.; Coker, R.; Tomlinson, D.; Harris, J.; Gompels, M.; Pinching, A.; Stewart, J. Liposomal Doxorubicin (Doxil): an Effective New Treatment for Kaposi's Sarcoma in AIDS. *Clin. Oncol*. **1994**, *6*, 294–296.
11. Galvin, P.; Thompson, D.; Ryan, K. B.; McCarthy, A.; Moore, A. C.; Burke, C. S.; Dyson, M.; MacCraith, B. D.; Gun'ko, Y. K.; Byrne, M. T. Nanoparticle-based Drug Delivery: Case Studies for Cancer and Cardiovascular Applications. *Cell. Mol. Life Sci.* **2012**, *69*, 389–404.
12. Peer, D.; Karp, J. M.; Hong, S.; Farokhzad, O. C.; Margalit, R.; Langer, R. Nanocarriers as an Emerging Platform for Cancer Therapy. *Nat. Nanotechnol*. **2007**, *2*, 751–760.
13. De Jong, W. H.; Borm, P. J. A. Drug Delivery and Nanoparticles: Applications and Hazards. *Int. J. Nanomed.* **2008**, *3*, 133–149.
14. Molavi, O.; Xiong, X.-B.; Douglas, D.; Kneteman, N.; Nagata, S.; Pastan, I.; Chu, Q.; Lavasanifar, A.; Lai, R. Anti-CD30 Antibody Conjugated Liposomal Doxorubicin with Significantly Improved Therapeutic Efficacy Against Anaplastic Large Cell Lymphoma. *Biomaterials* **2013**, *34*, 8718–8725.
15. Shroff, K.; Kokkoli, E. PEGylated Liposomal Doxorubicin Targeted to α5β1-Expressing MDA-MB Breast Cancer Cells. *Langmuir* **2012**, *28*, 4729–4736.
16. Liechty, W. B.; Kryscio, D. R.; Slaughter, B. V.; Peppas, N. A. Polymers for Drug Delivery Systems. *Annu. Rev. Chem. Biomol. Eng.* **2010**, *1*, 149–173.
17. Shi, M.; Lu, J.; Shoichet, M. S. Organic Nanoscale Drug Carriers Coupled with Ligands for Targeted Drug Delivery in Cancer. *J. Mater. Chem*. **2009**, *19*, 5485–5498.

18. Kwon, G. S.; Okano, T. Polymeric Micelles as New Drug Carriers. *Adv. Drug Delivery Rev.* **1996**, *21*,107–116.

19. Mourya, V.; Inamdar, N.; Nawale, R.; Kulthe, S. Polymeric Micelles: General Considerations and Their Applications. *Indian J. Pharmac. Edu. Res.* **2011**, *45*, 128–138.

20. Wang, Y.; Wang, R.; Lu, X.; Lu, W.; Zhang, C.; Liang, W. Pegylated Phospholipids-Based Self-Assembly with Water-Soluble Drugs. *Pharm. Res.* **2010**, *27*, 361–370.

21. Nasongkla, N.; Shuai, X.; Ai, H.; Weinberg, B. D.; Pink, J.; Boothman, D. A.; Gao, J. cRGD-Functionalized Polymer Micelles for Targeted Doxorubicin Delivery. *Angew. Chem., Int. Ed.* **2004**, *46,* 6323–6327.

22. Yoo, H. S.; Lee, E. A.; Park, T. G. Doxorubicin-Conjugated Biodegradable Polymeric Micelles Having Acid-Cleavable Linkages. *J. Controlled Release* **2002**, *82*, 17–27.

23. Zhang, G.; Yang, Z.; Lu, W.; Zhang, R; Huang Q.; Tian, M.; Li, L.; Liang, D.; Li, C. Influence of Anchoring Ligands and Particle Size on the Colloidal Stability and in *vivo* Biodistribution of Polyethylene Glycol-coated Gold Nanoparticles in Tumor-xenografted Mice. *Biomaterials* **2009**, *30*, 1928–1936.

24. De Mey, J.; Moeremans, M.; Geuens, G.; Nuydens, R.; De Brabander, M. High Resolution Light and Electron Microscopic Localization of Tubulin With the IGS (Immuno Gold Staining) Method. *Cell Biol. Int. Rep*. **1981**, *5*, 889–899.

25. Murphy, C. J., Gole, A. M., Stone, J. W., Sisco, P. N., Alkilany, A. M., Goldsmith, E. C., Baxter, S. C. Gold Nanoparticles in Biology: Beyond Toxicity to Cellular Imaging. *Acc. Chem. Res*. **2008**, *41*, 1721−1730.

26. Fadeel, B., Garcia-Bennett, A. E. Better Safe than Sorry: Understanding the Toxicological Properties of Inorganic Nanoparticles Manufactured for Biomedical Applications. *Adv. Drug Delivery Rev*. **2010**, *62*, 362−374.

27. Rana, S., Bajaj, A., Mout, R., Rotello, V. M. Monolayer Coated Gold Nanoparticles for Delivery Applications. *Adv. Drug. Delivery Rev*. **2012**, *64*, 200−216.

28. Giljohnn, D. A., Seferos, D. S., Danial, W. L., Massich, M. D., Patel, P. C., Mirkin, C. A. Gold Nanoparticles for Biology and Medicine. *Angew. Chem., Int. Ed. Engl.* **2010**, *49*, 3280−3294.

29. Dykman, L.; Khlebtsov, N. Gold Nanoparticles in Biology and Medicine: Recent Advances and Prospects. *Acta Naturae* **2011**, *3*, 34–55.

30. Khlebtsov, N. G. Optics and Biophotonics of Nanoparticles with a Plasmon Resonance. *Quantum Electron*. **2008**, *38*, 504–529.

31. Thakor, A. S.; Jokerst, J.; Zavaleta, C.; Massoud, T. F.; Gambhir, S. S. Gold Nanoparticles: a Revival in Precious Metal Administration to Patients. *Nano Lett*. **2011**, *11*, 4029–4036.

32. Mascarenhas, B. R.; Granda, J. L.; Freyberg, R. H. Gold Metabolism in Patients with Rheumatoid Arthritis Treated with Gold Compounds-Reinvestigated. *Arthritis Rheum.* **1972**, *15*, 391–402.

33. Gottlieb, N. Comparative Pharmacokinetics of Parenteral and Oral Gold Compounds. *J. Rheum*. **1982**, *8*, 99–109.

34. Prabaharan, M.; Grailer, J. J.; Pilla, S.; Steeber, D. A.; Gong, S. Amphiphilic Multi-Arm Block Copolymer Based on Hyperbranched Polyester, Poly (L-lactide) and Poly (ethylene glycol) as a Drug Delivery Carrier. *Macromol. Biosci*. **2009**, *9*, 515–524.

35. Prabaharan, M.; Grailer, J. J.; Pilla, S.; Steeber, D. A.; Gong, S. Gold Nanoparticles with a Monolayer of Doxorubicin-Conjugated Amphiphilic Block Copolymer for Tumor Targeted Drug Delivery. *Biomaterials* **2009**, *30*, 6065–6675.

36. Dreaden, E. C.; Mackey, M. A.; Huang, X.; Kang, B.; El-Sayed, M. A. Beating Cancer in Multiple Ways Using Nanogold. *Chem. Soc. Rev.* **2011**, *40*, 3391–3404.

37. Heo, D. N.; Yang, D. H.; Moon, H. J.; Lee, J. B.; Bae, M. S.; Lee, S. C.; Lee, W. J.; Sun, I.-C.; Kwon, I. K. Gold Nanoparticles Surface-Functionalized with Paclitaxel Drug and Biotin Receptor as Theranostic Agents for Cancer Therapy. *Biomaterials* **2012**, *33*, 856–866.

38. Shon, Y.-S.; Mazzitelli, C.; Murray, R. W. Unsymmetrical Disulfides and Thiol Mixtures Produce Different Mixed Monolayer-Protected Gold Clusters. *Langmuir* **2001**, *17*, 7735–7741.

39. Eck, W.; Craig, G.; Sigdel, A.; Ritter, G.; Old, L. J.; Tang, L.; Brennan, M. F.; Allen, P. J.; Mason, M. D. Pegylated Gold Nanoparticles Conjugated to Monoclonal F19 Antibodies as Targeted Labeling Agents for Human Pancreatic Carcinoma Tissue. *ACS Nano* **2008**, *2*, 2263–2272.

40. Knop, K.; Hoogenboom, R.; Fischer, D.; Schubert, U. S. Poly(Ethylene Glycol) in Drug Delivery: Pros and Cons as Well as Potential Alternatives. *Angew. Chem., Int. Ed.* **2010**, *49*, 6288–6308.

41. Yuan, F.; Dellian, M.; Fukumura, D.; Leunig, M.; Berk, D. A.; Torchilin, V. P.; Jain, R. K. Vascular Permeability in a Human Tumor Xenograft: Molecular Size Dependence and Cutoff Size. *Cancer Res.* **1995**, *55*, 3752–3756.

42. Park, J. W.; Hong, K.; Kirpotin, D. B.; Colbern, G.; Shalaby, R.; Baselga, J.; Shao, Y.;

Nielsen, U. B.; Marks, J. D.; Moore, D. Anti-HER2 Immunoliposomes Enhanced Efficacy Attributable to Targeted Delivery. *Clin. Cancer Res*. **2002**, *8*, 1172–1181.

43. Kaminskas, L. M.; McLeod, V. M.; Kelly, B. D.; Cullinane, C.; Sberna, G.; Williamson, M.; Boyd, B. J.; Owen, D. J.; Porter, C. J. Doxorubicin-Conjugated PEGylated Dendrimers Show Similar Tumoricidal Activity but Lower Systemic Toxicity When Compared to PEGylated Liposome and Solution Formulations in Mouse and Rat Tumor Models. *Mol. Pharmacol*. **2012**, *9*, 422–432.
44. Aryal, S.; Grailer, J. J.; Pilla, S.; Steeber, D. A.; Gong, S. Doxorubicin Conjugated Gold Nanoparticles as Water-Soluble and pH-Responsive Anticancer Drug Nanocarriers. *J. Mater. Chem*. **2009**, *19*, 7879–7884.
45. Asadishad, B.; Vossoughi, M.; Alemzadeh, I. Folate-Receptor-Targeted Delivery of Doxorubicin Using Polyethylene Glycol-Functionalized Gold Nanoparticles. *Ind. Eng. Chem. Res.* **2010**, *49*, 1958–1963.
46. Alexander, C. M.; Hamner, K. L.; Maye, M. M.; Dabrowiak, J. C. Multifunctional DNA-Gold Nanoparticles for Targeted Doxorubicin Delivery. *Bioconjugate Chem.* **2014**, *25*, 1261–1271.
47. Wang, F.; Wang, Y.-C.; Dou, S.; Xiong, M.-H.; Sun, T. M.; Wang, J. Doxorubicin-Tethered Responsive Gold Nanoparticles Facilitate Intracellular Drug Delivery for Overcoming Multidrug Resistance in Cancer Cells. *ACS Nano* **2011**, *5*, 3679–3692.
48. Daniel, M. C., Astruc, D. Gold Nanoparticles: Assembly, Supramolecular Chemistry, Quantum-size-related Properties, and Applications Toward Biology, Catalysis, and Nanotechnology. *Chem. Rev.* **2004**, *104*, 293–346.
49. Xia, H.; Bai, S.; Hartmann, J.; Wang, D. Synthesis of Monodisperse Quasi-Spherical

Gold Nanoparticles in Water via Silver (I)-Assisted Citrate Reduction. *Langmuir* **2010**, *26*, 3585–3589.

50. Jiang, W.; KimBetty, Y. S.; Rutka, J. T.; Chan Warren, C. W. Nanoparticle-Mediated Cellular Response is Size-dependent. *Nat. Nanotechnol.* **2008,** *3*, 145–150.
51. Honary, S.; Zahir, F. Effect of Zeta Potential on the Properties of Nano-Drug Delivery Systems - A Review (Part 2). *Trop. J. Pharm. Res.* **2013**, *12*, 265–273.
52. Honary, S.; Zahir, F. Effect of Zeta Potential on the Properties of Nano-Drug Delivery Systems - A Review (Part 1). *Trop. J. Pharm. Res.* **2013**, *12*, 255–264.

Chapter 3. Synthesis of New Thiolated Doxorubicin Analogs for Reactions with Gold Nanoparticles as Drug Delivery System

3.1 Introduction

As discussed in Chapter 2, gold nanoparticles can be modified to achieve selective delivery of drug systems to improve drug efficacy. The size of gold nanoparticles can be controlled so that they can enter the cancer vasculature while being excluded from normal vasculature. This is the passive targeting strategy that was discussed in Chapter 2. However, there are some limitations in applying the passive targeting strategy in the clinical therapy. Firstly, this approach is a random process making it difficult to control and not always possible to achieve ubiquitous targeting. This might cause the cancer cells in patients not be responsive to some anticancer drugs. For this type of cancer cells, one important characteristic is that some proteins that can prevent drugs from entering the cancer cells are overexpressed,[1-3] and the overexpressed proteins will cause a lower concentration of drugs being transported into cancer cells and low therapeutics efficacy eventually. Thus, the resistance formed. On the other hand, the basis of passive targeting is the EPR effect, and the permeability of the vessels is assumed to be enhanced. But in fact, not all the tumors exhibit enhanced permeability effects, that further limits the performance of passive targeting.[4,5]

A good way is to combine passive targeting and active targeting. To be more specific, making modifications to the drug delivery system so that it has the ability to target desired cancer cells by actively binding to them. The gold nanoparticles can be further modified with targeting agents, and the interaction between the specific receptors on the cancer cells and these agents can be applied to further improve the targeting. The receptors which are overexpressed on cancer cells, while minimally expressed on normal cells, are the targets for active binding. How to

modify the drug delivery systems so that they can preferentially recognize these receptors has been studied in the past two decades.[6-9] Paciotti *et al*. reported[10] that TNFα not only serves as the therapeutic agent responsible for the anti-tumor effects, but also serves as a ligand that targets the nanoparticle drug specifically to a solid tumor. It can help target the drug delivery system specifically to the tumor neovasculature without affecting normal blood vessels, where it induces vascular disruption and reduction of tumor IFP.[11-13] In our design, TNFα will be incorporated into the gold nanoparticles to further improve the targeting. Figure 3.1 depicts the overall drug delivery system. Attaching TNFα is a future project after evaluation of the current drug delivery system and the choice of the best formulation for further study has been made. Thus, no work on TNFα will be included in this thesis.

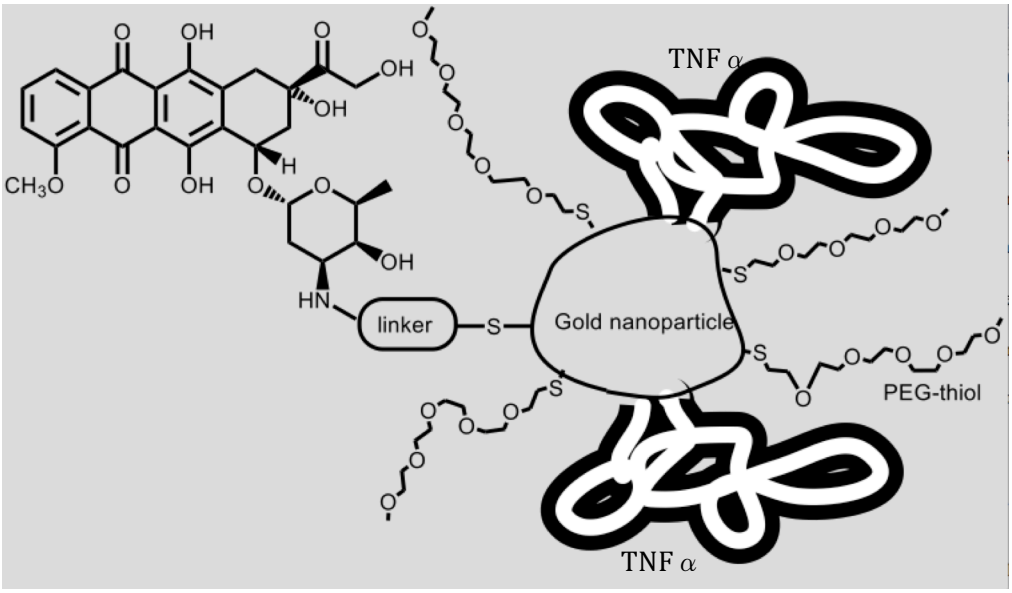

Figure 3.1. Overall doxorubicin-gold nanoparticles drug delivery system design

Modification of gold nanoparticles is a way to improve anticancer drug efficacy, and much attention has been paid to developing various doxorubicin analogs to be conjugated onto gold

nanoparticles. However, to the best of our knowledge, no paper has reported how different factors in the linkage of doxorubicin of nanoparticles influence drug efficacy, including chain lengths, functional groups for hydrolysis, water solubility, and positions for linking. However, these factors can greatly affect the regulation of drug release as well as the selectivity of delivery, both of which are crucial for drug delivery systems.[14] To control the site and rate of release of the anticancer drug, one strategy is to trigger the release by the substances or conditions only found in the target sites while not in other sites.[15-17] Cancer cells have their own characteristics that can be used as external stimuli. Cancer cells contain much higher concentrations of the reducing agent glutathione (1–10 mM) than extracellular fluids (2 μM),[18,19] and the higher concentration of reducing agent can be used as an external stimulus to trigger the drug release from gold nanoparticles by disulfide exchange or place-exchange reactions.[20,21] Also, based on the fact that the pH values of the cancer cells (pH ~ 5) are usually more acidic than plasma and normal cells (pH 7.4),[22] pH-sensitive doxorubicin-gold nanoparticles systems have been developed to achieve selective release. Wang *et al*. developed[23] a hydrazone linker-based doxorubicin-gold nanoparticle drug delivery system and achieved higher intracellular release of doxorubicin, which greatly improved the potency. These stimuli are the basis for designing our target doxorubicin derivatives.

3.2 Synthesis of New Thiolated Doxorubicin Analogs

To develop the prodrugs of doxorubicin, thiol-containing doxorubicin analogs should be designed in order to be attached on the surface of gold nanoparticles. The presence of thiol moieties in the linkers enables the conjugation of analogs with the surface of gold nanoparticles due to the strong covalent bond between gold and sulfur. The prodrugs are designed to achieve

selective delivery of chemotherapeutics to tumor tissues and reduce the toxicity to normal tissues. Thus, the general rule is that the overall drug delivery system is stable and no releasing action should be observed in the blood stream while the drug should be readily cleaved and released upon reaching the cancer cells. Due to the complexity of the *in vivo* environment, it is difficult to judge which type of linker is best. Thus, to seek for doxorubicin analogs with the most suitable linkers, five new thiol-containing doxorubicin analogs (**3.1**–**3.5**) were designed and synthesized. We designed these molecules based on different triggering mechanisms, hydrophilicity and hydrophobicity, positions of modification, and others, to study how different factors affect the properties of the analogs.

Analog **3.1** was designed to achieve drug release responsive to the higher levels of the reducing agent glutathione in cancer cells. Analog **3.2** should undergo cleavage and release of doxorubicin in acidic conditions. Analog **3.3** has a similar structure to **3.2**, but with the addition of PEG, to increase water solubility, which allows us to study how the hydrophilicity and hydrophobicity would affect drug efficacy. The modifications of these three analogs are all in the amine group in the 3` position. To study the influence of the positions of modification, we designed analogs **3.4** and **3.5** with positions of modifications at C13 and C14, respectively. Also, analog **3.4** contains a pH-sensitive hydrazone bond. How the addition of this bond changes the performance can thus be determined.

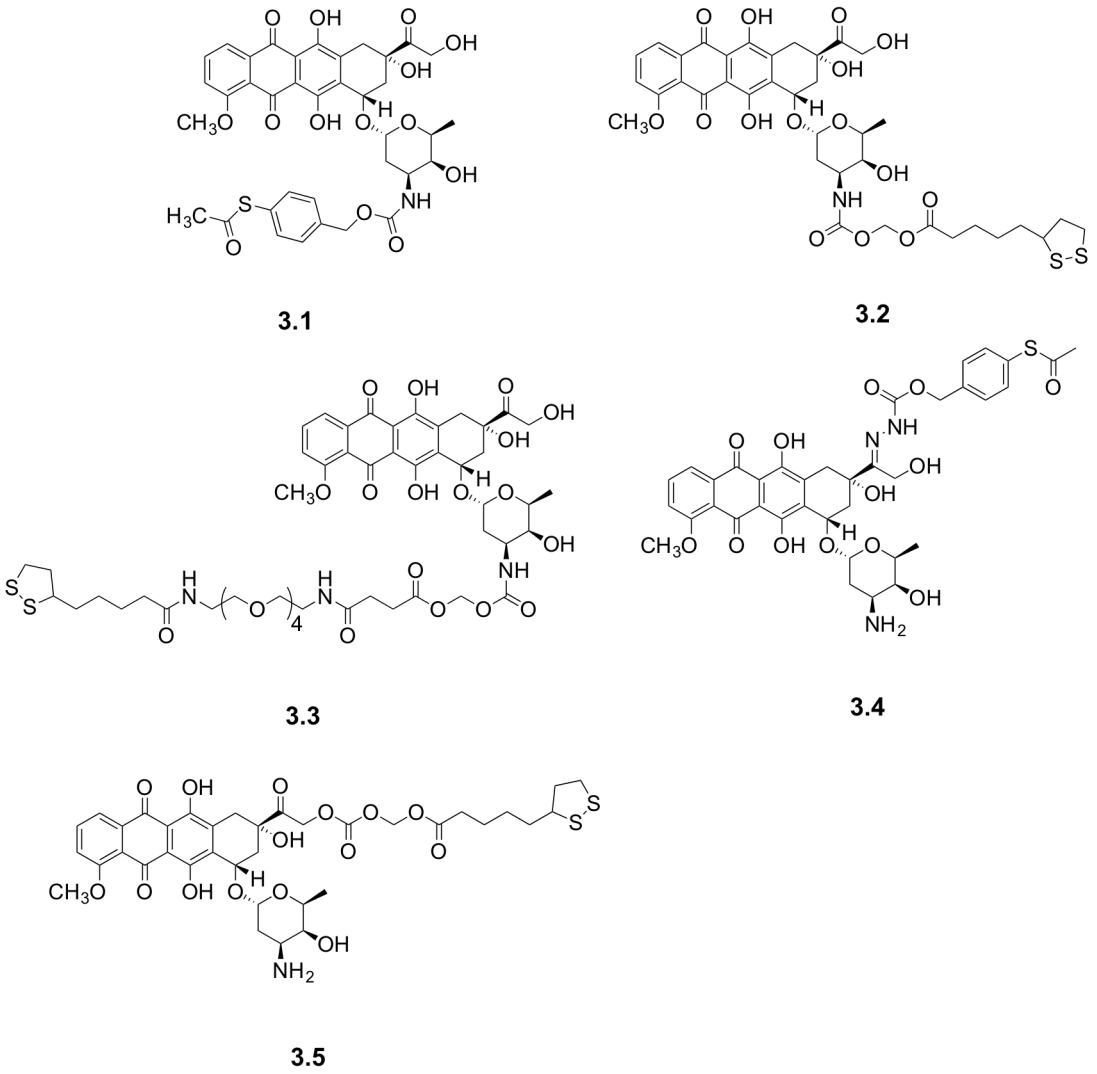

Scheme 3.1. Structure designs of five new doxorubicin analogs

3.2.1 Synthesis of Analog 3.1.

The reaction scheme for the synthesis of analog **3.1** is shown in Scheme 3.2. Commercially available 4-mercaptobenzoic acid (**3.6**) underwent acetylation, reduction and nucleophilic substitution to obtain compound **3.9**, which was then reacted directly with doxorubicin hydrochloride **3.10** to give final product **3.1** with 88% yield.

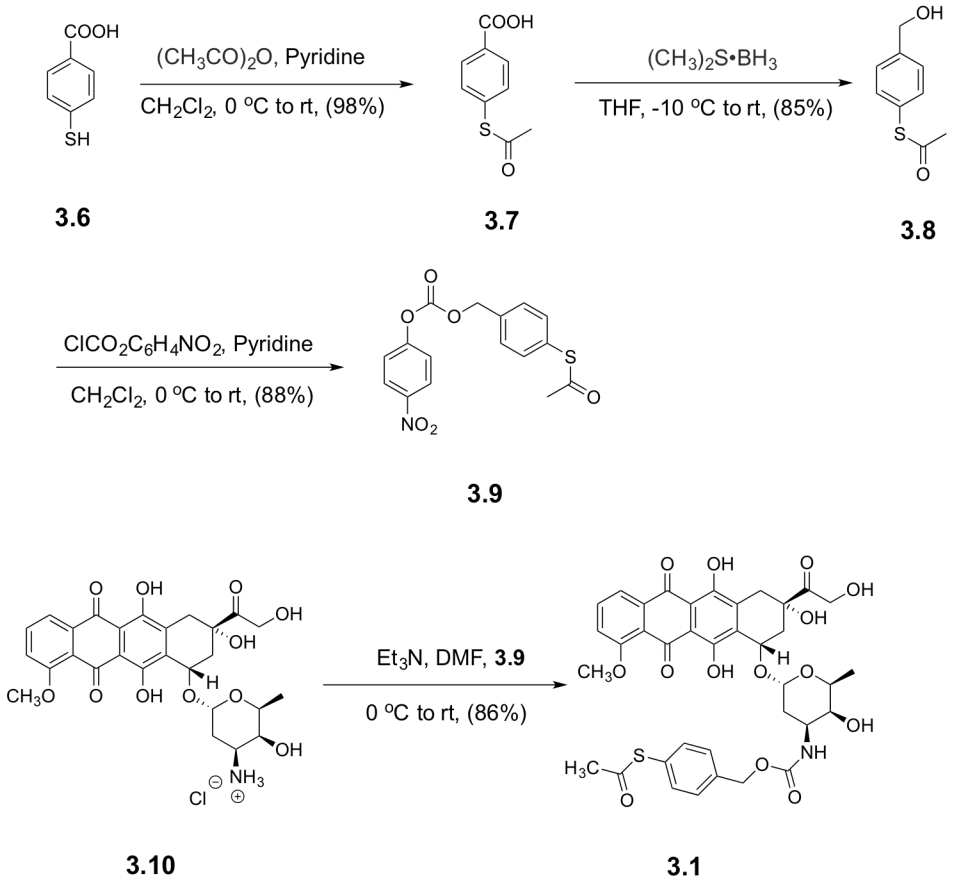

Scheme 3.2 Synthesis of **3.1**

3.2.2 Synthesis of Analog 3.2.

Instead of using the acetylthiol moiety in analog **3.1**, lipoic acid was incorporated into analog **3.2** to provide the sulfur group to conjugate with gold nanoparticles. Lipoic acid is

derived from octanoic acid. It exists in nature and is essential for aerobic metabolism because it is an essential cofactor of many enzyme complexes,[24] so it is a perfect sulfur source for research and clinical studies because of its low cost and non-toxicity.

As shown in Scheme 3.3, analog **3.2** was prepared from 4-nitrophenol by reaction with chloromethyl chloroformate to give compound **3.12**. Then the halogen exchange reaction was performed to exchange the chlorine to iodine to increase the reactivity of the resulting compound **3.13**. Compound **3.13** was then reacted with lipoic acid to give compound **3.14**, which was further reacted with doxorubicin hydrochloride **3.10** to give the final product **3.2**.

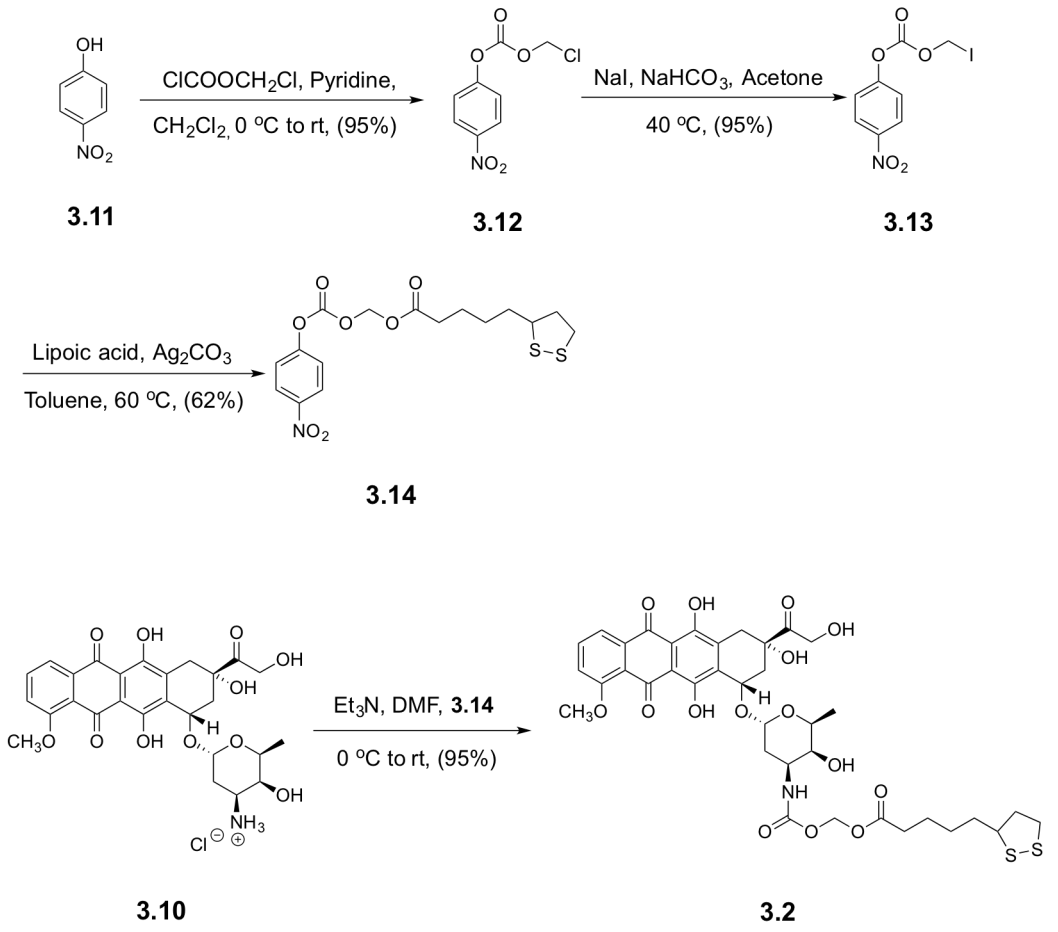

Scheme 3.3 Synthesis of **3.2**

3.2.3 Synthesis of Analog 3.3.

To increase the hydrophilicity of the compound, doxorubicin analog **3.3** was designed. The PEG part in the linker can improve the water solubility of the whole compound so that we can study how the increased hydrophilicity can affect the overall drug delivery system.

Because of the complexity of introduction of the PEG, the synthetic strategy was changed accordingly. As shown in Scheme 3.4, synthesis started from *N*-hydroxysuccinimide (**3.15**), which was condensed with lipoic acid to give compound **3.16**. The succinimide ester then reacted with the amine group of amino-dPEG$_4$-acid to obtain **3.17**, which was further reacted with **3.13** to give **3.18**. Compound **3.18** was then reacted with doxorubicin hydrochloride **3.10** to give the final product **3.3**.

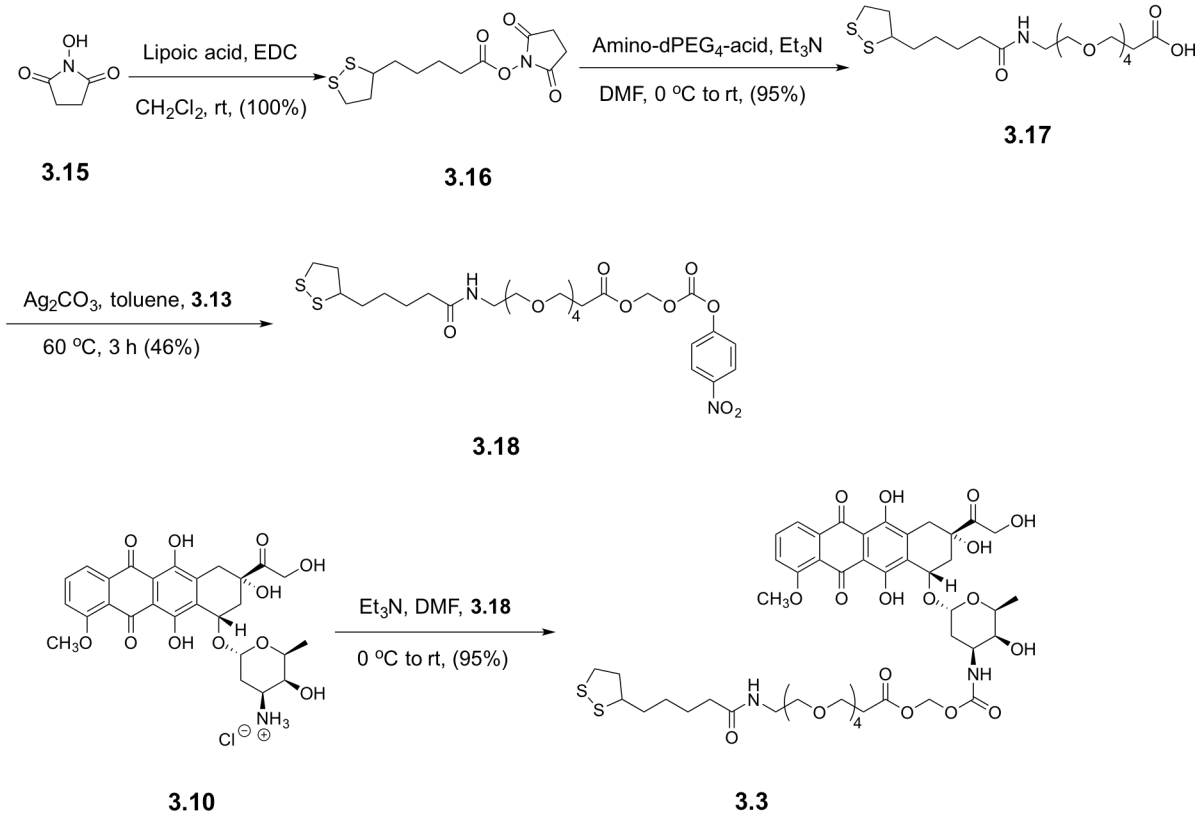

3.15 **3.16** **3.17** **3.18** **3.10** **3.3**

Scheme 3.4 Synthesis of **3.3**

3.2.4 Synthesis of Analog 3.4.

To better compare how different linkers can affect the performance of the overall drug delivery system, the hydrazone analog **3.4** was designed. It is the only analog in these series that possesses a C13 linker. The hydrazone bond can be cleaved under acid condition, such as those in the cancer cell, but it should be quite stable in neutral or basic conditions.

The synthetic path is quite simple and straightforward from compound **3.9**, which is activated by 4-nitrophenyl. Reaction of **3.9** with hydrazine monohydrate, and followed by reaction with doxorubicin hydrochloride **3.10** in the presence of trifluoroacetic acid (TFA) gave the final product **3.4** (Scheme 3.5).

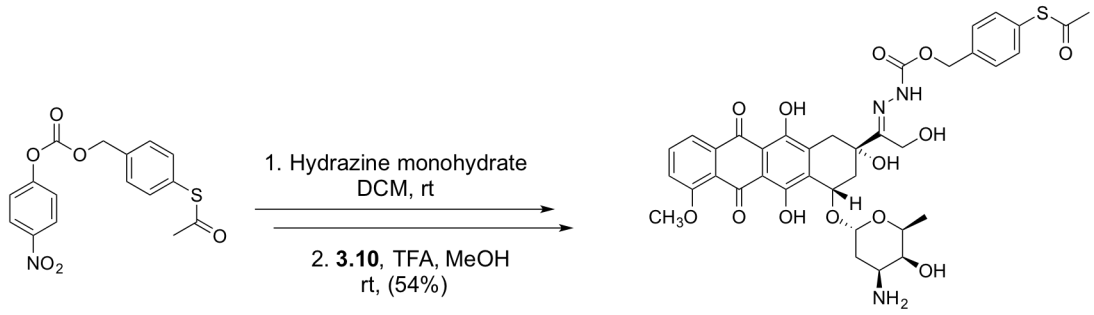

3.9 **3.4**

Scheme 3.5 Synthesis of **3.4**

3.2.5 Synthesis of Analog 3.5.

Another possible position of modification is C14. Thus, we designed a similar compound to analog **3.2** but with a C14 linker. This is to study how the different positions of the linker affect the overall drug performance.

Because of the presence of an amine group in doxorubicin, we needed to protect it before reacting at the C14 hydroxyl group. As shown in Scheme 3.6, synthesis starts from doxorubicin hydrochloride (**3.10**), which was first protected with Fmoc by reacting with Fmoc N-hydroxysuccinimide ester (Fmoc-OSu). The resulting derivative was reacted with compound **3.14**, followed by deprotection to obtain the final product **3.5**.

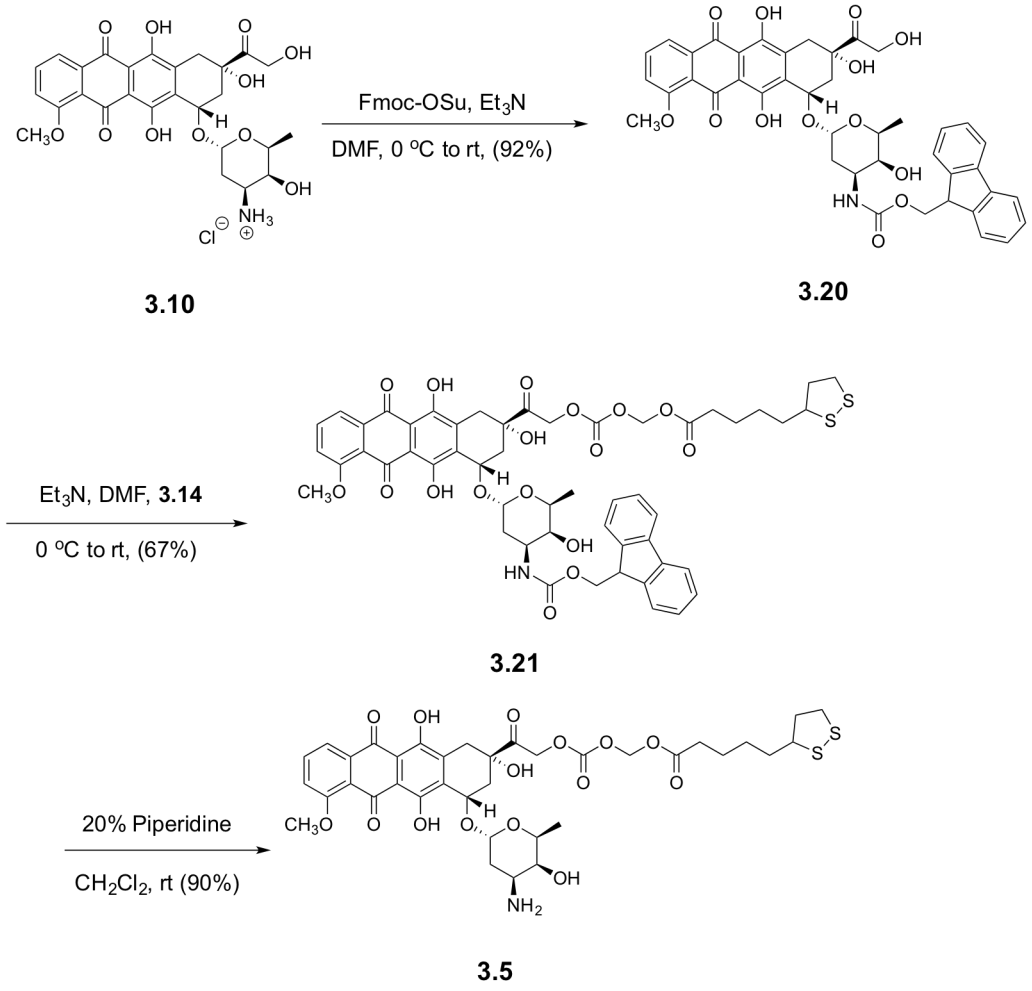

Scheme 3.6 Synthesis of **3.5**

3.3 Biological and Chemical Evaluations of the Native Analogs

3.3.1 Biological Activity

In order to compare the *in vitro* antiproliferative activities of the analogs **3.1**–**3.5** with free doxorubicin, a cytotoxic assay against the A2780 cell line was conducted in the Kingston group. The results are shown in Table 3.1.

Table 3.1. A2780 Human Ovarian Cancer Cell Line

In vitro antiproliferative activities IC_{50} values (nM)					
3.1	**3.2**	**3.3**	**3.4**	**3.5**	Doxorubicin
31 ± 5	10 ± 4	28 ± 3	11 ± 5	11 ± 1	26 ± 3

Note: Assay was repeated three times and each concentration was in triplicate. Data obtained by Peggy Brodie, Qingxi Su and Ming Wang.

The results show that all five derivatives demonstrated comparable or even higher bioactivity than doxorubicin, indicating they are all potential candidates to be conjugated onto gold nanoparticles to obtain drug delivery systems. Analogs **3.1** and **3.2** were evaluated for stability and nanoparticles binding as part of this work.

3.3.2 Stability Studies of the Analogs

The stability of the analogs is a key factor for the gold nanoparticle-based drug delivery systems to achieve selective delivery of doxorubicin to tumors. On one hand, the linkers should be stable enough in the blood circulatory system. If not, doxorubicin will be released prematurely and result in severe side effects. One the other hand, the linkers should be cleaved once the drug systems enter into cancer cells and the therapeutics should be released.

3.3.2.1 Construction of a Calibration Curve

In order to be able to determine the concentration of the doxorubicin and its analogs by HPLC during the stability studies, it was necessary to construct calibration curves for each substance.

As shown in Figure 3.2, the calibration curves for free doxorubicin, analog **3.1** and analog **3.2** were constructed as following. A series of standard concentrations of each substance were prepared by dissolving in DMSO. For example, for analog **3.1**, six different concentration solutions were prepared, including 3.75, 2.50, 1.25, 0.625, 0.313, 0.156 µM. Aliquots (50 µL) of

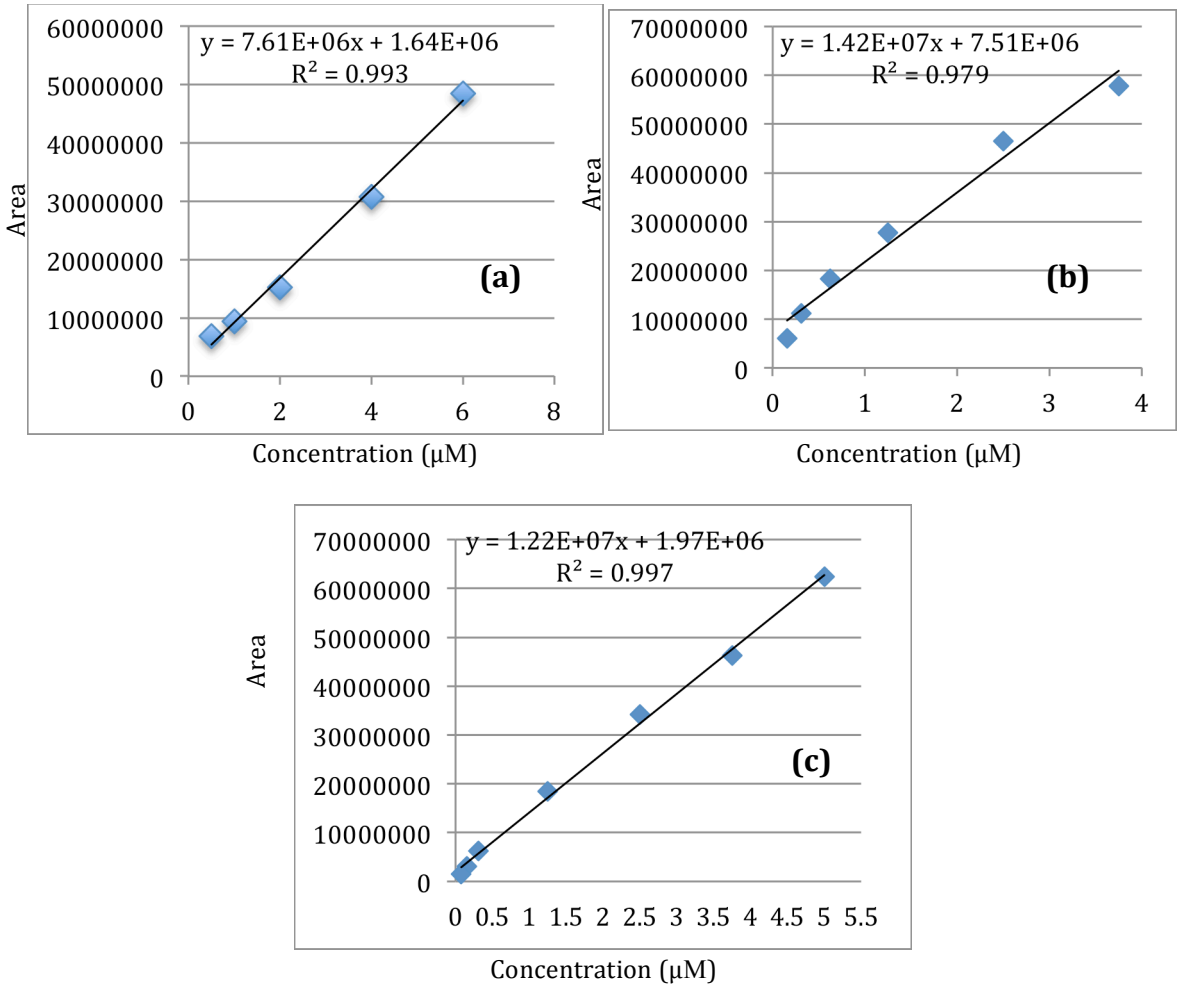

Figure 3.2. Calibration curves for free doxorubicin (a), analog **3.1** (b) and analog **3.2** (c)

each solution were taken and injected onto an HPLC column (purchased from Phenomenex loaded with Luna 5µ C18 (2) 25 x 4.6 mm) for analysis. The gradient solution system was applied in the analysis. Starting with 30% CH_3CN / 70% H_2O at 0 min, the solvent composition changed to 100% CH_3CN / 0% H_2O at 30 min. The UV lamp with wavelength of 253 nm was used to detect the compounds eluted. The HPLC chromatograms were recorded and area of each peak was calculated. A linear regression for each substance was obtained by plotting the concentration of the substance versus the area.

3.3.2.2 Stability of Analogs 3.1 and 3.2

The stabilities of analogs **3.1** and **3.2** in buffer solution at the physiological pH 7.4 and under the acidic conditions of cancer cells at pH 4.6 were evaluated (Scheme 3.7).

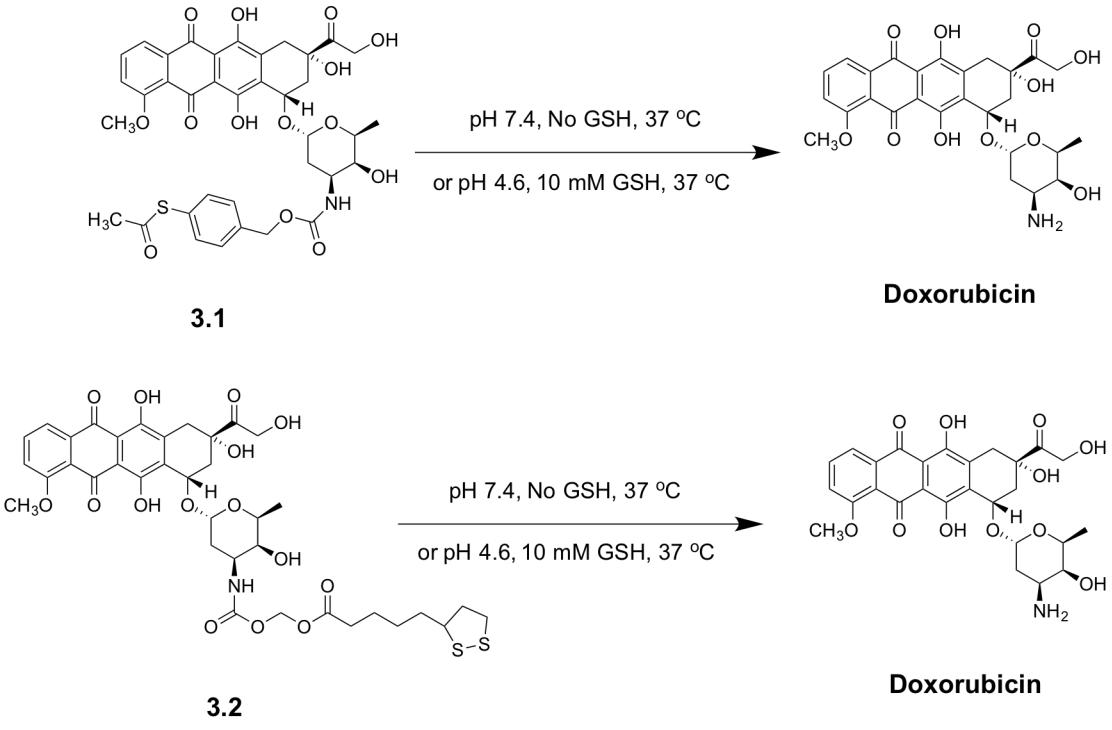

Scheme 3.7. Conversion of analogs **3.1** and **3.2** to doxorubicin

Analogs **3.1** and **3.2** were dissolved in a 1:3 mixture of methanol and PBS buffer (pH 7.4) or sodium acetate buffer (pH 4.6). Methanol was used to increase the solubility of the analog. Both solutions were stirring vigorously at 37 ^{o}C. Aliquots were taken at various time points over a 72 h range, and the concentration of the analogs were determined by quantitative HPLC analyses. Plots of the concentration of analogs versus time gave the results shown in Figure 3.3.

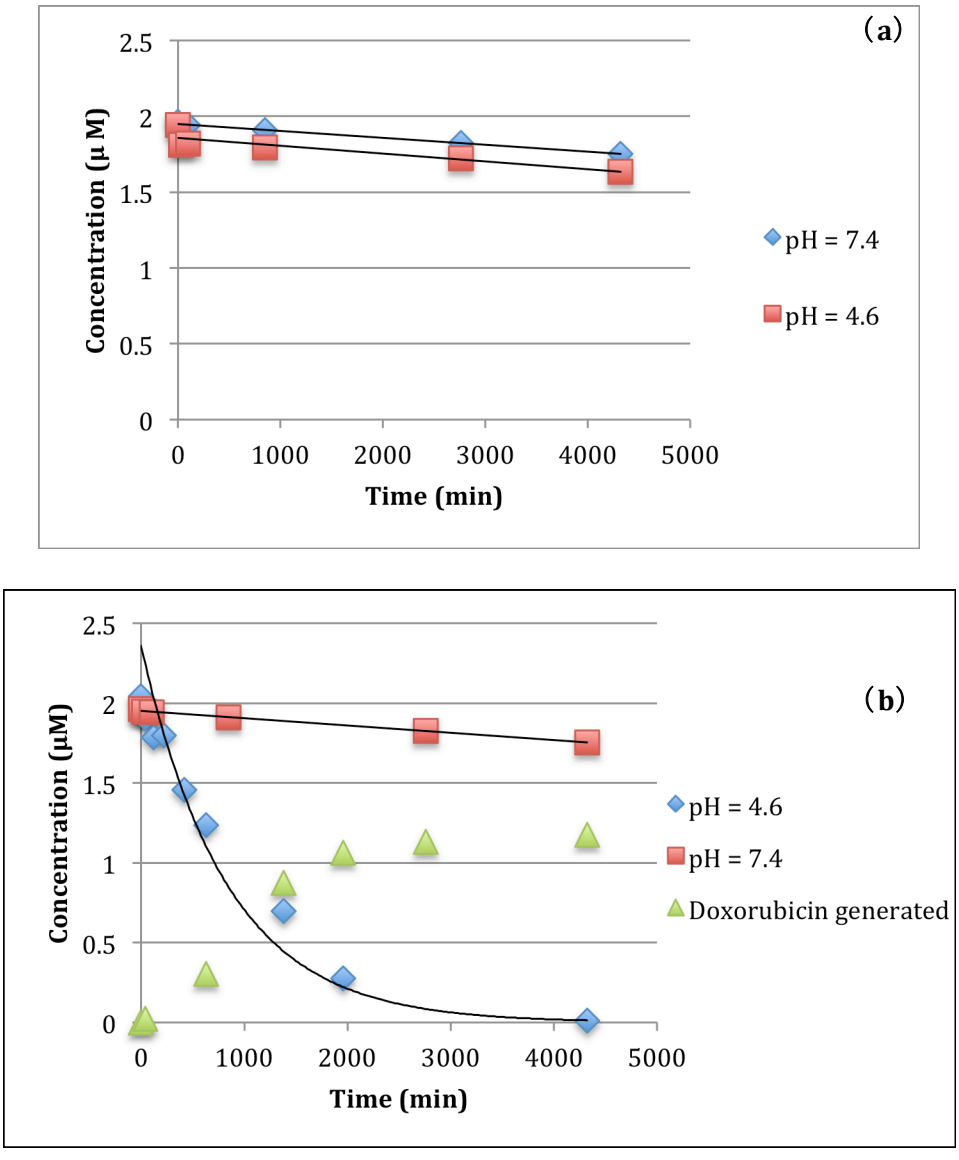

Figure 3.3. Quantitative analyses of the *in vitro* stability of analog **3.1** (a) and analog **3.2** (b) at pH 7.4 or pH 4.6

From the results, analog **3.1** is stable at both pH 7.4 and pH 4.6. The half-life was calculated as following (analog **3.1** in pH 7.4 was shown as an example): a linear regression was obtained by plotting the logarithm of the of analog concentration (**3.1**) versus time (Figure 3.4), indicating pseudo 1st order kinetics. The equation is shown in Figure 3.4. The half-life can be calculated by the following formula, where k_{obs} is the slope of the linear regression.

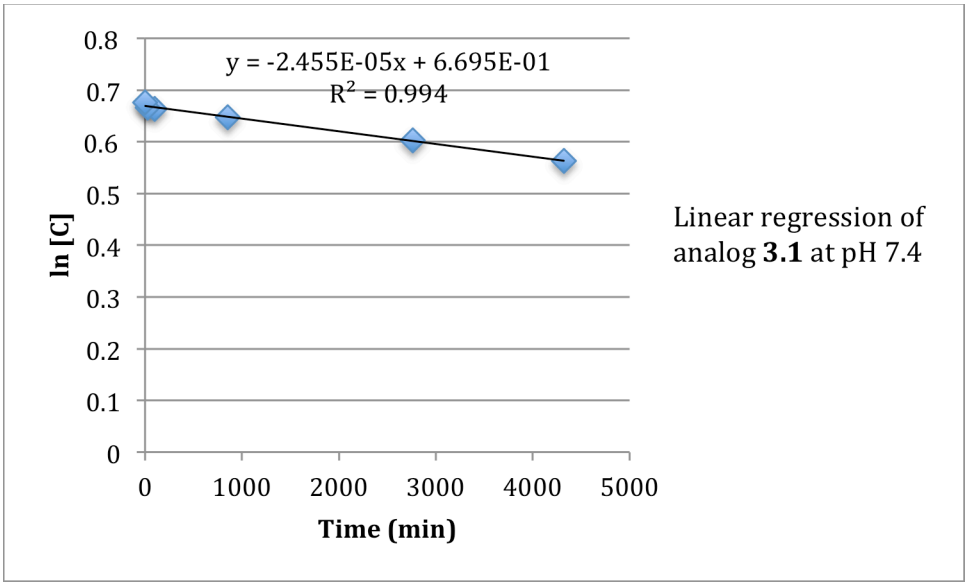

Figure 3.4. Kinetics of drug release of analog **3.1** at pH 7.4

Half-life calculation:

$$\ln C_t = -k_{obs}.t + \ln C_0$$

$$k_{obs} = 2.455\text{E-}5 \text{ min}^{-1}$$

$$T_{1/2} = \ln 2 / k_{obs} = 471 \text{ h}$$

Based on the above calculation, the half-lives of analog **3.1** are 471 h at pH 7.4 and 421 h at pH 4.6 respectively. This is acceptable since the release of doxorubicin was designed to be triggered only by reducing agents when attached to gold nanoparticles.

Analog **3.2**, however, is quite stable at pH 7.4 (half-life: 376 h) while rapid degradation can be observed at pH 4.6 (half-life: 9.6 h). The analog was gradually hydrolyzed within 72 h in the

buffer solution and doxorubicin was generated (the triangle plot in Figure 3.3 (b)). A linear regression was obtained by plotting the logarithm of the concentration of analog **3.2** versus time (Figure 3.5), indicating pseudo 1st order kinetics. The controlled release of doxorubicin triggered by acidic conditions in cancer cells can thus be achieved for analog **3.2**. Both derivatives have demonstrated desired properties and were chosen for conjugation studies with gold nanoparticles.

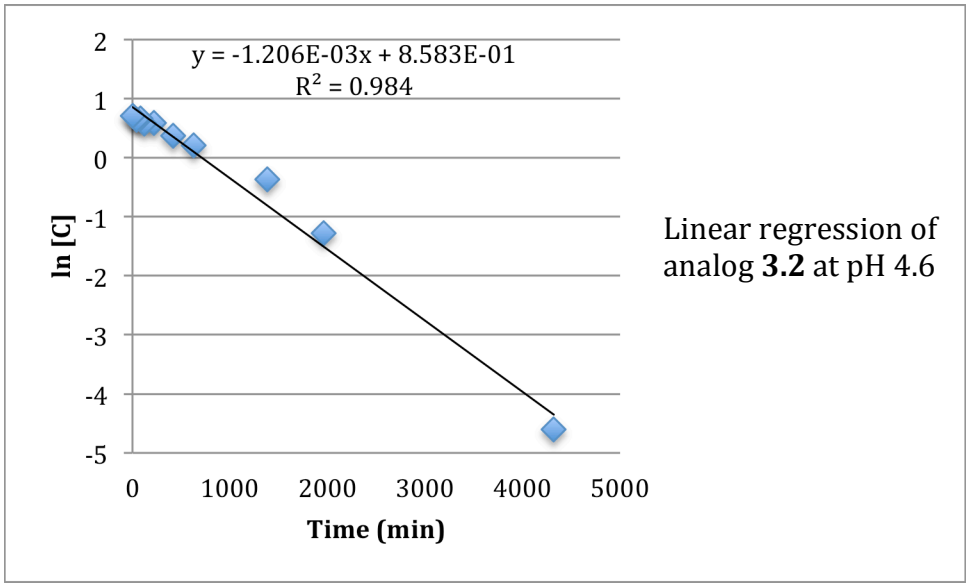

Figure 3.5. Kinetics of drug release of analog **3.2** at pH 4.6

3.4 Manufacture and Evaluation of a Gold Nanoparticle-based Multifunctional Anticancer Drug Delivery System

3.4.1 Functionalization of Gold Nanoparticles

From Chapter 2, monodisperse spherical gold nanoparticles have been prepared and PEG has been successfully attached onto the surface of the nanoparticles to improve water solubility and to stabilize them. The gold nanoparticles now needed to be further functionalized by doxorubicin analogs to construct an anticancer drug delivery system with multi-functionalities (Figure 3.6).

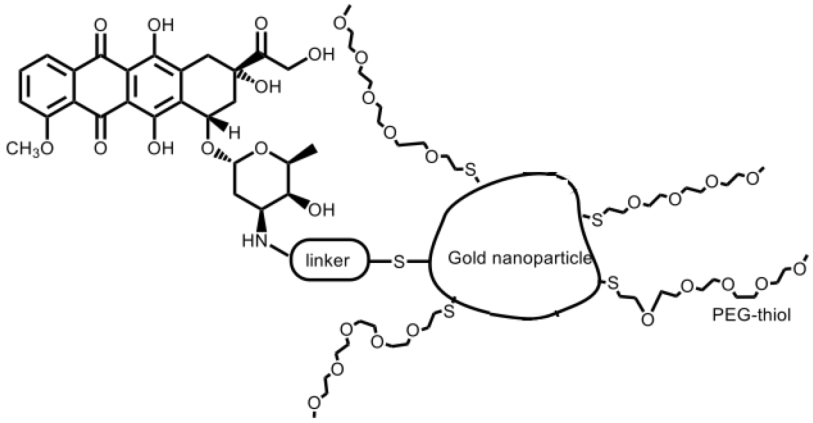

Figure 3.6. Schematic illustration of doxorubicin-PEG-gold nanoparticle multifunctional anticancer drug delivery system

To prepare for the gold nanoparticle-based multifunctional anticancer drug delivery system, a 10 mL aqueous solution of naked gold nanoparticles containing 10 mg gold nanoparticles prepared as described in Chapter 2, a 20 mL solution of 10 mg doxorubicin analog in CH_3OH, and a 3 mL aqueous solution of 30 mg PEG thiol (5 kDa) were mixed and stirred for 48 h at room temperature. To remove unbound drugs and PEG-thiol, as well as to concentrate the nanomedicine, the solution was centrifuged at a speed of 14000 rpm for 20 min at room temperature and the pellets containing nanoparticles were redispersed in water. This process was repeated three times to completely remove the unbound material. The residue was dissolved in 1 mL water for future studies.

3.4.2 Drug Loading Studies

In order to determine the total drug content present in each preparation, we performed a drug release study. The resulting gold nanoparticles solution was incubated under conditions

mimicking those in cancer cells at 37 ^{o}C, which are acidic (pH 4.6) and contain reducing agent GSH (10 mM). Incubation was continued for 72 h to ensure complete drug release. The resulting components were then analyzed by HPLC. This achieved three purposes. First, we can verify that the doxorubicin analogs were actually attached onto the gold nanoparticles. Second, we can determine what compound(s) are formed after the release of the analogs from the gold nanoparticles. Third, we can determine how much of each analog was attached.

The drug loading studies of analogs **3.1** and **3.2** were performed as follows. Each gold nanoparticle solution (0.1 mL) obtained from section 3.4.1 was mixed with 0.9 mL sodium acetate buffer containing 10 mM GSH and the pH was adjusted to 4.6. The solution was stirred vigorously at 37 ^{o}C for 72 h. Then, the solution was centrifuged at a speed of 14000 rpm for 20 min, and aliquots (50 μL) of the supernatant were injected onto an HPLC column and analyzed by quantitative HPLC. The results are shown in Figure 3.7.

From Figure 3.7, doxorubicin analog **3.1** based gold nanoparticle drug delivery system exhibited a single peak which matched with that of doxorubicin. From the area of the peak and based on the calibration curve constructed previously, the actual drug loading of analog **3.1** was determined to be 0.78 mg analog **3.1** per 1 mg gold nanoparticles. However, for analog **3.2**, three peaks were detected. The peak with an elution time of 11.5 min is the analog itself, which indicates the analog was released from the gold, but was not completed hydrolyzed to doxorubicin. The peak with an elution time of 4.0 min is doxorubicin. The peak with an elution time of 2.8 min needs further identification. Its major component is unlikely to contain doxorubicin, however, since it is colorless. It is also unlikely that it comes from synthesized gold nanoparticles, since after incubating naked gold nanoparticles with glutathione, no peak was detected by HPLC. To calculate the drug loading for analog **3.2**, both detected doxorubicin and

analog **3.2** were taken into account, and calculation shows the actual drug loading is 0.22 mg analog **3.2** per 1 mg gold nanoparticles. This loading could however be higher, since this experiment did not detect any drug that remained bound to gold.

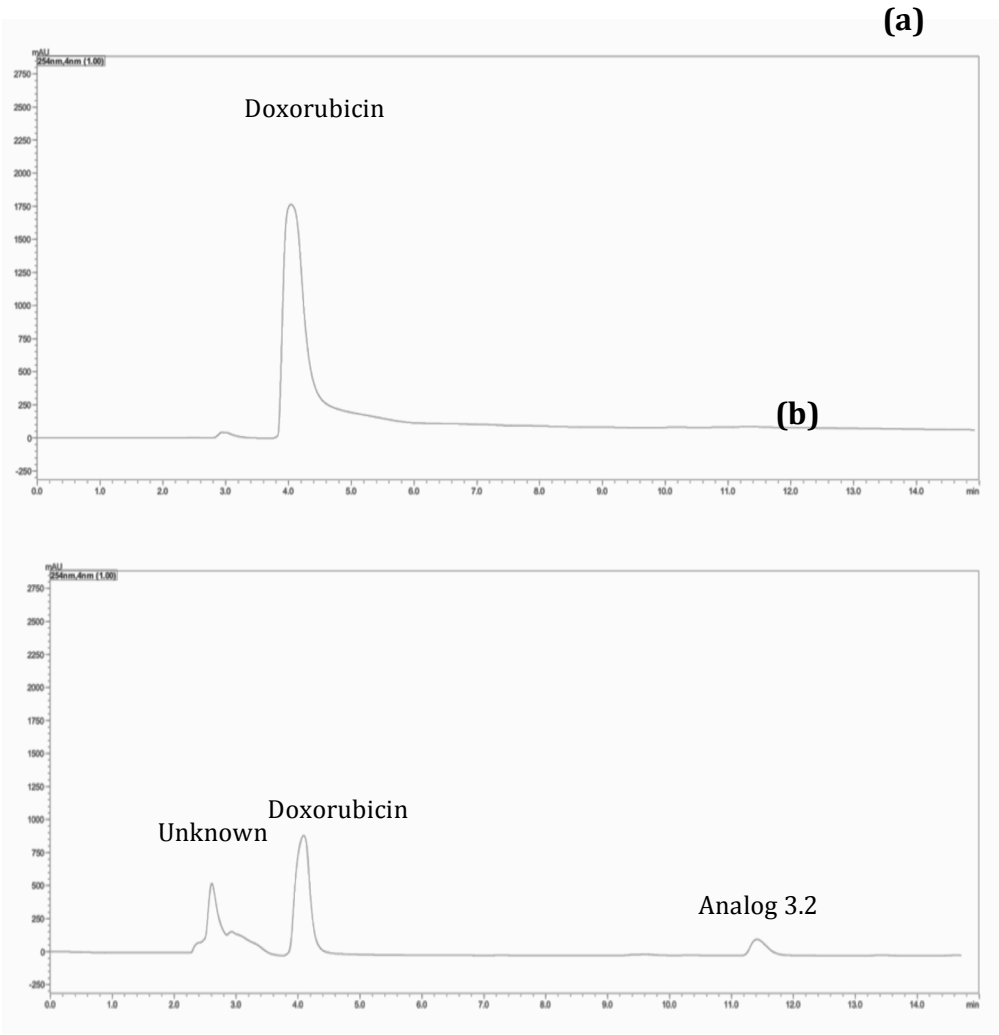

Figure 3.7. Analyses of the supernatant after incubation of doxorubicin analog **3.1**-PEG-gold nanoparticles (a) and doxorubicin analog **3.2**-PEG-gold nanoparticles (b) in pH = 4.6 and presence of 10 mM GSH

From this study, gold nanoparticle drug delivery systems based on analog **3.1** are expected to be better than those based on analog **3.2** for two reasons. First, the drug loading of analog **3.1** is higher which is important to ensure drug efficacy. Second, doxorubicin is the only product

formed after drug release, while analog **3.2** generated an unknown compound. Thus, analog **3.1** based formulations were selected for further studies.

3.4.3 Stability Studies of Analog 3.1 Based Drug Delivery Systems

Although drug delivery systems based on analog **3.1** have favorable drug release properties, their stability under physiological condition is important to avoid premature release in blood. Thus, the stability of analog **3.1** based drug delivery system was studied under physiological conditions (pH 7.4). A gold nanoparticle solution (0.1 mL) obtained as described in section 3.4.1 was mixed with 0.9 mL PBS buffer and the pH was adjusted to 7.4. The solution was stirred vigorously at 37 ^{o}C. Aliquots were taken at different time points over a 72 h range, and the compositions were determined by quantitative HPLC analyses and the previously described calibration curves. However, after 72 h, no doxorubicin was detected, indicating that no drug release occurred. This result demonstrates that the analog **3.1** based drug delivery system is more stable to physiological condition than its native analog.

3.4.4 Determination of *in vitro* Blood Stability

The preliminary stability and drug releasing tests showed the analog **3.1**-loaded gold nanoparticles demonstrated good water solubility, excellent stability in physiological condition, and drug releasing action in the simulated environment of cancer cells, resulting in the formation of doxorubicin from the nanoparticles.

Prior to conducting *in vivo* studies each formulation was tested for stability in a blood *in vivo* model. Briefly, aliquots of the drug solution obtained from section 3.4.1 were spiked into rodent whole blood and incubated at 37 ^{o}C for 0.5, 1, 4, 6, 12, 16 and 24 h. At each interval the sample was extracted with methyl tertiary butyl ether; the top organic layer contained

doxorubicin or analog **3.1** released from the gold nanoparticles by the blood while the aqueous layer consisted of the bound drug. The organic layer was evaporated and analyzed by LC-MS, comparing the sample extracted from blood with that extracted from buffer, using free doxorubicin as an internal standard. The bottom layer with gold nanoparticle-bound doxorubicin was treated with β-mercaptoethanol (BME) to release the drug from the particles, and extracted with methyl tertiary butyl ether to isolate the doxorubicin forcibly released from the particles by BME. This study is now being conducted by Professor Marion Ehrich at the Virginia–Maryland College of Veterinary Medicine.

3.4.5 Determination of *in vivo* Stability in Blood

These studies were done in mice as lower quantities of product are needed. Groups of n = 4 CD-1 outbred mice were dosed with analog **3.1**-loaded gold nanoparticles to be tested, with sacrifice for blood collection at 0.5, 1, 2, 4, 6, 12, 16, 24 and 48 h. The blood samples taken between 0.5 and 48 h were examined for quantity of product and values used to calculate maximal concentration, elimination rate constant, clearance, and half-life. To determine safety, the mice sacrificed at 48 h and additional mice dosed and sacrificed at 4 days and 14 days underwent examination for detrimental effects as determined by clinical pathology and histopathology of liver, heart, lung, gastrointestinal tract, reproductive organs, and spleen. These latter evaluations were compared to vehicle-dosed mice also sacrificed at 48 h, 4 days and 14 days. Physiological endpoints (weight, body temperature) and observational endpoints (general appearance, mobility, nervous system functioning) were compared between vehicle-dosed and test-agent dosed mice. Specific protocols for animal experiments were reviewed and approved

by Virginia Tech's Institutional Animal Care and Use Committee (IACUC). This study is now in progress at the Virginia–Maryland College of Veterinary Medicine.

3.5 Conclusions

For the purpose of development of a gold nanoparticle-based drug delivery system to achieve selective delivery of doxorubicin to target cancer cells, five sulfur containing doxorubicin derivatives **3.1**–**3.5** with different structural properties were designed and synthesized.

These five native analogs **3.1**–**3.5** all demonstrated comparable antiproliferative activities to that of doxorubicin *in vitro*. In the drug stability and releasing study of analog **3.1** and analog **3.2**, analog **3.1** showed excellent stability in both physiological condition (pH 7.4) and acidic condition (pH 4.6). Analog **3.2** also demonstrated great stability at pH 7.4, while the doxorubicin derivative was slowly converted to doxorubicin within 24 h in pH 4.6 buffer solution with a half-life of 9.6 h.

Analogs **3.1** and **3.2** were reacted with gold nanoparticles whose surfaces were decorated with PEG to form the gold bound analogs to study their conjugation with gold nanoparticles. Analog **3.1** based gold nanoparticle drug delivery system had higher drug loading, and only doxorubicin was formed after release from gold in stimulated conditions of cancer cells. In addition, it demonstrated even better stability compared with native analog **3.1** under physiological conditions (pH 7.4).

Based on all these data, the analog **3.1**-based gold nanoparticles drug delivery system was chosen as a lead by us for further development.

3.6 Experimental Section

3.6.1 General Experimental Methods

The following standard conditions apply unless other stated. All chemicals were purchased from Sigma-Aldrich and used as received unless otherwise stated. The anticancer drug doxorubicin hydrochloride was purchased from Wonda Science Inc, USA. All the glassware was oven-dried and all reactions were conducted under the protection of nitrogen. Dichloromethane (CH_2Cl_2) was distilled from $CaCl_2$, tetrahydrofuran (THF) was distilled from CaH_2, anhydrous methanol (MeOH) was purchased directly from Sigma-Aldrich. Thin layer chromatography (TLC) was used to monitor the reaction progress and the TLC plates were coated with silica UV254. Purification was achieved either by column chromatography or preparative thin layer chromatography (PTLC). Silica gel 60 (220–240 mesh) was used to fill in the column eluting solvent systems were indicated in each part. The PTLC plates were using glass-backed plates and coated with silica UV254. HPLC was performed on Shimadzu SCL-10AVP system using a column purchased from Phenomenex (Luna 5μ C18 (2) 25 x 4.6 mm). ^{1}H and ^{13}C NMR spectra were obtained on an Agilent U4-DD2 spectrometers at 400 MHz for ^{1}H and 100 MHz for ^{13}C or a Bruker Avance II spectrometer at 500 MHz for ^{1}H and 125 MHz for ^{13}C. Agilent 6220 accurate-mass TOF LC/MS instrument was used to obtain High-resolution mass spectra. All chemical shifts were referenced to the solvent peaks of $CDCl_3$ (7.26 ppm for ^{1}H and 77.16 ppm for ^{13}C) unless otherwise stated.

3.6.2 Synthetic Procedures and Characterization

Synthesis of 4-acetylthiol benzoic acid (3.7)

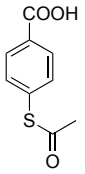

3.7

A 25 mL round bottom flask was oven-dried, cooled to room temperature and charged with a magnetic stirring bar, 4-mercaptobenzoic acid **3.6** (154 mg, 1.0 mmol), and a rubber septum. The flask was evacuated for 5 min and flushed with nitrogen. Dry CH_2Cl_2 (5 mL) was added via syringe to dissolve the solid and followed by adding C_5H_5N (316 mg, 4.0 mmol). Ice bath was used to cool the solution to 0 ^oC, followed by vigorous stirring for 5 min. After the solid was dissolved completely, $(CH_3CO)_2O$ (306 mg, 3.0 mmol) was added over a period of 10 min via syringe. The resulting mixture was warmed to room temperature and stirred for 15 h under nitrogen (balloon). The reaction was diluted with EtOAc (100 mL), washed with 0.6 M HCl solution (2 x 10 mL), saturated $NaHCO_3$ solution (2 x 10 mL), brine (2 x 20 mL), and dried with anhydrous Na_2SO_4. After evaporating the solvent by rotary evaporation (30 ^oC), a white crude product was obtained and then purified by PTLC (eluted with $CHCl_3$: MeOH = 13 : 1) to yield **3.7** (192 mg, 0.98 mmol) as a white powder in a yield of 98%. ^1H NMR (CD_3OD, 500 MHz) δ 8.05 (dd, J = 8.5, 2 Hz, 2H), 7.54 (dd, J = 8.5, 2 Hz, 2H), 2.44 (s, 3H); ^{13}C NMR (126 MHz) δ 194.2, 169.1, 135.2, 135.0, 132.8, 131.2, 30.3; HR-ESI-MS: *m/z* 195.0124 $[M - H]^-$ (calcd for $C_9H_7O_3S$, 195.0121).

Synthesis of *S*-(4-(hydroxymethyl)phenyl) ethanethioate (3.8)

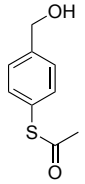

3.8

A 10 mL round bottom flask was oven-dried, cooled to room temperature and charged with a magnetic stirring bar, compound **3.7** (192 mg, 0.98 mmol), and a rubber septum. The flask was evacuated for 5 min and flushed with nitrogen. Dry THF (3 mL) was added to dissolve the solid. Ice bath containing NaCl was used to cool the solution to –10 ^{o}C, followed by vigorous stirring for 5 min. A solution of $(CH_3)_2S{\bullet}BH_3$ in THF (1.5 mL, 3.0 mmol) was added over a period of 15 min via syringe. The resulting mixture was warmed to room temperature and was stirred for 15 h under nitrogen (balloon). H_2O (2 mL) was added into the flask to remove unreacted $(CH_3)_2S{\bullet}BH_3$, the reaction was diluted with EtOAc (100 mL), washed with brine (2 x 20 mL), and dried with anhydrous Na_2SO_4. After evaporating the solvent by rotary evaporation (30 ^{o}C), a liquid crude product was obtained, which was further purified by PTLC (eluted with $CHCl_3$: MeOH = 15 : 1) to yield 3.8 (151 mg, 0.83 mmol) as a colorless liquid in a yield of 85%. ^{1}H NMR (CD_3OD, 500 MHz) δ 7.36 (m, 4H), 4.60 (s, 2H), 2.34 (s, 3H); ^{13}C NMR (126 MHz) δ 194.5, 143.2, 134.2, 127.2, 126.6, 63.2, 28.6; HR-ESI-MS: *m/z* 183.0466 $[M + H]^+$ (calcd for $C_9H_{11}O_2S^+$, 183.0474).

Synthesis of 4-((((4-nitrophenoxy)carbonyl)oxy)methyl)-phenyl ethanethioate (3.9)

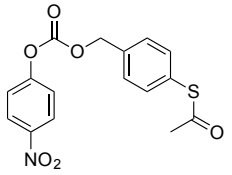

3.9

A 50 mL round bottom flask was oven-dried, cooled to room temperature and charged with a magnetic stirring bar, compound **3.8** (151 mg, 0.83 mmol), and a rubber septum. The flask was evacuated for 5 min and flushed with nitrogen. Dry CH_2Cl_2 (10 mL) was added via syringe to dissolve the liquid followed by adding C_5H_5N (198 mg, 2.5 mmol). Ice bath was used to cool the solution to 0 ^oC, followed by vigorous stirring for 5 min. A solution of $ClCO_2C_6H_4NO_2$ (335 mg, 1.66 mmol) in 5 mL CH_2Cl_2 was added over a period of 20 min via syringe. The resulting mixture was warmed to room temperature and stirred for 5 h under nitrogen (balloon). The reaction was diluted with EtOAc (100 mL), washed with saturated $NaHCO_3$ solution (2 x 10 mL), H_20 (2 x 10 mL) and brine (2 x 10 mL), and dried with anhydrous Na_2SO_4. After evaporating the solvent by rotary evaporation (30 ^oC), a solid crude product was obtained, which was further purified by column chromatography (silica gel, 100 g, eluted with C_6H_{14} : CH_2Cl_2 = 5 : 1) to yield **3.9** (253 mg, 0.73 mmol) as a white powder in a yield of 88%. ^1H NMR ($CDCl_3$, 500 MHz) δ 8.27 (dd, *J* = 9, 2 Hz, 2H), 7.47 (m, 4H), 7.38 (dd, *J* = 9, 2 Hz, 2H), 5.31 (s, 2H), 2.44 (s, 3H); ^{13}C NMR (126 MHz) δ 193.7, 155.5, 152.5, 145.5, 135.6, 134.8, 129.3, 129.0, 125.4, 121.9, 70.2, 30.4; HR-ESI-MS: *m/z* 365.0795 $[M + NH_4]^+$ (calcd for $C_{16}H_{17}N_2O_6S^+$, 365.0807).

Synthesis of 14-doxorubicin acetylthiol benzyl derivative *S*-(4-(((((2*S*,3*S*,4*S*,6*R*)-3-hydroxy-2-methyl-6-(((1*S*,3*S*)-3,5,12-trihydroxy-3-(2-hydroxyacetyl)-10-methoxy-6,11-dioxo-1,2,3,4,6,11-hexahydrotetracen-1-yl)oxy)tetrahydro-2H-pyran-4yl)carbamoyl)oxy) methyl)phenyl) ethanethioate (3.1)

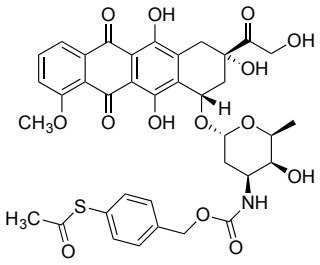

3.1

A 10 mL round bottom flask was oven-dried, cooled to room temperature and charged with a magnetic stirring bar, doxorubicin hydrochloride (20 mg, 0.0345 mmol), compound **3.9** (20 mg, 0.0576 mmol), and a rubber septum. The flask was evacuated for 5 min and flushed with nitrogen. Anhydrous DMF (5 mL) was added by syringe to dissolve the solids. Ice bath was used to cool the solution to 0 ^{o}C, followed by vigorous stirring for 5 min. Then to the solution was added Et_3N (10 mg, 0.0988 mmol) over a period of 5 min via syringe. The resulting mixture was warmed to room temperature and stirred for 2 h under nitrogen (balloon). The reaction was diluted with EtOAc (30 mL), washed with 0.6 M HCl solution (2 x 5 mL), saturated sodium $NaHCO_3$ (2 x 5 mL), brine (2 x 10 mL), and dried with anhydrous Na_2SO_4. After evaporating the solvent by rotary evaporation (30 ^{o}C), a solid crude product was obtained, which was further purified by PTLC (eluted with $CHCl_3$: MeOH = 13 : 1) to yield **3.1** (22.3 mg, 0.0297 mmol) as a red solid in a yield of 86%. ^{1}H NMR ($CDCl_3$, 500 MHz) δ 8.02 (dd, *J* = 10, 1 Hz, 1H), 7.78 (t, *J*

= 8 Hz, 1H), 7.39 (dd, *J* = 10, 1 Hz, 1H), 7.34 (m, 4H), 5.50 (d, *J* = 3 Hz, 1H), 5.27 (s, 1H, -OH), 5.19 (d, *J* = 10.5 Hz, 1H, -OH), 5.04 (s, 2H), 4.75 (m, 2H), 4.53 (s, 1H), 4.13 (q, *J* = 6.5 Hz, 1H), 4.07 (s, 3H), 3.86 (s br, 1H, OH), 3.66 (d, *J* = 6.5 Hz, 1H), 3.25 (dd, *J* = 19, 1.5 Hz, 1H), 3.01 (m, 2H), 2.39 (s, 3H), 2.32 (d, *J* = 15 Hz, 1H), 2.16 (dd, *J* = 15, 4 Hz, 1H), 2.05 (d, *J* = 7.5 Hz, 1H), 1.87 (dd, *J* = 13.5, 4.5 Hz, 1H), 1.25 (d, *J* = 6.5 Hz, 3H); ^{13}C NMR (126 MHz) δ 214.0, 194.0, 187.2, 186.8, 161.2, 156.3, 155.8, 155.5, 138.0, 135.9, 135.6, 134.7, 133.7, 133.6, 128.8, 127.8, 121.0, 120.0, 118.6, 111.7, 111.6, 100.9, 69.8, 69.7, 67.4, 66.2, 65.7, 56.8, 47.2, 35.8, 34.1, 30.4, 30.3 17.0; HR-ESI-MS: *m/z* 774.1840 $[M + Na]^+$ (calcd for $C_{37}H_{37}NO_{14}SNa^+$, 774.1832).

Synthesis of chloromethyl (4-nitrophenyl) carbonate (3.12)

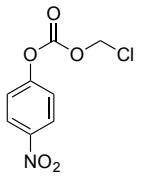

3.12

A 100 mL round bottom flask was oven-dried, cooled to room temperature and charged with a magnetic stirring bar, 4-nitrophenol (2.0 g, 14.4 mmol), and a rubber septum. The flask was evacuated for 5 min and flushed with nitrogen. Anhydrous CH_2Cl_2 (20 mL) and C_5H_5N (2.1 g, 26.6 mmol) were added via syringe to dissolve the solids. Ice bath was used to cool the solution to 0 ^oC, followed by vigorous stirring for 5 min. Then, the solution of $ClCOOCH_2Cl$ in 10 mL CH_2Cl_2 was added into the flask over a period of 30 min via constant pressure funnel. The mixture was warmed to room temperature and was stirred for 2 days under nitrogen (balloon). The reaction was diluted with EtOAc (100 mL), wished with saturated $NaHCO_3$ solution (2 x 20

mL), H_2O (2 x 20 mL), brine (2 x 20 mL), and dried with anhydrous Na_2SO_4. After evaporating the solvent by rotary evaporation (30 ^oC), a solid crude product was obtained, which was purified by column chromatography (silica gel, 300 g, eluted with C_6H_{14} : CH_2Cl_2 = 10 : 1) to yield **3.12** (3.17 g, 13.7 mmol) as a white solid in a yield of 95%. ^1H NMR ($CDCl_3$, 500 MHz) δ 8.31 (dd, *J* = 9, 2 Hz, 2H), 7.43 (dd, *J* = 9, 2 Hz, 2H), 5.85 (s, 2H); ^{13}C NMR (126 MHz) δ 154.9, 151.1, 145.8, 125.5, 121.7, 72.8.

Synthesis of iodomethyl (4-nitrophenyl) carbonate (3.13)

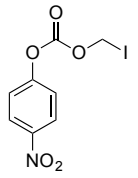

3.13

A 250 mL round bottom flask was oven-dried, cooled to room temperature and charged with a magnetic stirring bar, compound **3.12** (3.17 g, 13.7 mmol), NaI (3.00 g, 20.1 mmol), $NaHCO_3$ (3.45 g, 41.1 mmol) and a rubber septum. The flask was evacuated for 5 min and flushed with nitrogen. Anhydrous CH_3COCH_3 (100 mL) was added to the flask via syringe. The resulting solution was heated to 40 ^oC and stirred vigorously for 16 h under nitrogen (balloon). The reaction was diluted with EtOAc (200 mL), wished with H_2O (3 x 100 mL), brine (2 x 50 mL), and dried with anhydrous Na_2SO_4. After evaporating the solvent by rotary evaporation (30 ^oC), a solid crude product was obtained, which was further purified by column chromatography (silica gel, 300 g, eluted with C_6H_{14} : CH_2Cl_2 = 10 : 1) to yield **3.13** (4.2 g, 13.0 mmol) as a light yellow-brown solid in a yield of 95%. ^1H NMR ($CDCl_3$, 500 MHz) δ 8.32 (dd, *J* = 10.5, 2.5 Hz,

2H), 7.43 (dd, *J* = 10.5, 2.5 Hz, 2H), 6.08 (s, 2H); ^{13}C NMR (126 MHz) δ 155.9, 150.8, 145.7, 125.6, 121.7, 33.5.

Synthesis of (((4-nitrophenoxy)carbonyl)oxy)methyl 5-(1,2-dithiolan-3-yl) pentanoate (3.14)

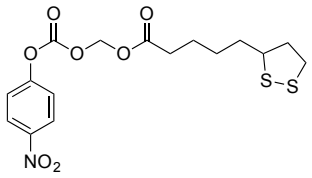

3.14

A 100 mL round bottom flask was oven-dried, cooled to room temperature and charged with a magnetic stirring bar, compound **3.13** (100 mg, 0.31 mmol), lipoic acid (191.6 mg, 0.93 mmol), Ag_2CO_3 (342 mg, 1.24 mmol), and a rubber septum. The flask was evacuated for 5 min and flushed with nitrogen. Anhydrous C_7H_8 (30 mL) was added to the flask via syringe. The resulting solution was heated to 60 ^oC and stirred vigorously for 3 h under nitrogen (balloon). The solution was filtered to remove unreacted Ag_2CO_3 and other insoluble impurities. Then, the solution was diluted with EtOAc (100 mL), wished with saturated $NaHCO_3$ (2 x 100 mL), H_2O (2 x 100 mL), brine (2 x 50 mL), and dried with anhydrous Na_2SO_4. After evaporating the solvent by rotary evaporation (30 ^oC), a solid crude product was obtained, which was purified by column chromatography (silica gel, 100 g, eluted with C_6H_{14} : CH_2Cl_2 = 5 : 1) to yield **3.14** (77.1 mg, 0.192 mmol) as a white powder in a yield of 62%. ^{1}H NMR ($CDCl_3$, 500 MHz) δ 8.30 (dd, *J* = 9.5, 2 Hz, 2H), 7.42 (dd, *J* = 9.5, 2 Hz, 2H), 5.89 (s, 2H), 3.57 (m, 1H), 3.14 (m, 2H), 2.46 (m, 3H), 1.91 (m, 1H), 1.71 (m, 4H), 1.50 (m, 2H); ^{13}C NMR (126 MHz) δ172.0, 155.2, 151.7, 145.9,

125.6, 121.9, 82.7, 56.5, 40.5, 38.7, 34.8, 33.8, 28.8, 24.4; HR-ESI-MS: *m/z* 424.0490 $[M + Na]^+$ (calcd for $C_{16}H_{19}NO_7S_2Na^+$, 424.0501).

Synthesis of lipoic acid doxorubicin derivative ((((2*S*,3*S*,4*S*,6*R*)-3-hydroxy-2-methyl-6-(((1*S*,3*S*)-3,5,12-trihydroxy-3-(2-hydroxyacetyl)-10-methoxy-6,11-dioxo-1,2,3,4,6,11-hexahydrotetracen-1-yl)oxy)tetrahydro-2H-pyran-4-yl)carbamoyl)oxy)methyl 5-(1,2-dithiolan-3-yl) pentanoate (3.2)

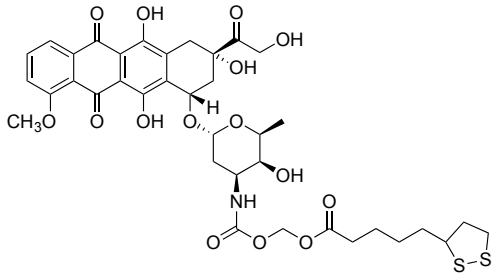

3.2

A 10 mL round bottom flask was oven-dried, cooled to room temperature and charged with a magnetic stirring bar, doxorubicin hydrochloride (20 mg, 0.0345 mmol), compound **3.14** (22 mg, 0.0552 mmol), and a rubber septum. The flask was evacuated for 5 min and flushed with nitrogen. Anhydrous DMF (5 mL) was added via syringe to dissolve the solids. Ice bath was used to cool the solution to 0 ^oC, followed by vigorous stirring for 5 min. Then to the solution was added Et_3N (10 mg, 0.0988 mmol) over a period of 5 min via syringe. The mixture was warmed to room temperature and stirred for 2 h under nitrogen (balloon). The reaction was diluted with EtOAc (30 mL), washed with 0.6 M HCl solution (2 x 5 mL), saturated $NaHCO_3$ solution (2 x 5 mL), brine (2 x 10 mL), and dried with anhydrous Na_2SO_4. After evaporating the

solvent by rotary evaporation (30 ^{o}C), a solid crude product was obtained, which was further purified by PTLC (eluted with $CHCl_3$: MeOH = 13 : 1) to yield **3.2** (26.4 mg, 0.0328 mmol) as a red solid in a yield of 95%. ^{1}H NMR ($CDCl_3$, 500 MHz) δ 8.05 (dd, *J* = 8, 1 Hz, 1H), 7.80 (t, *J* = 8 Hz, 1H), 7.40 (dd, *J* = 8, 1 Hz, 1H), 5.62 (m, 2H), 5.51 (d, *J* = 4 Hz, 1H), 5.30 (m, 1H, -OH), 5.24 (d, *J* = 10.5 Hz, 1H, -OH), 4.76 (m, 2H), 4.50 (s, 1H), 4.13 (q, *J* = 6.5 Hz, 1H), 4.09 (s, 3H), 3.86 (m, br, 1H, -OH), 3.68 (s, 1H), 3.54 (m, 1H), 3.29 (dd, *J* = 19, 1.5 Hz, 1H), 3.11 (m, 2H), 3.01 (s, 1H), 2.44 (m, 1H), 2.33 (s, 3H), 2.18 (dd, *J* = 15, 4 Hz, 1H), 1.88 (m, 3H), 1.78 (m, 1H), 1.65 (m, 4H), 1.43 (m, 2H), 1.29 (d, *J* = 6.5 Hz, 3H); ^{13}C NMR (126 MHz) δ 213.9, 187.4, 186.9, 172.6, 161.3, 156.3, 155.8, 153.9, 136.0, 135.7, 133.7, 133.6, 121.1, 120.0, 118.6, 111.8, 111.7, 100.7, 78.8, 69.9, 69.5, 67.3, 65.7, 56.9, 56.5, 47.2, 40.4, 38.6, 35.8, 34.6, 34.2, 33.9, 30.2, 28.7, 24.4, 17.0; HR-ESI-MS: *m/z* 828.1928 $[M + Na]^+$ (calcd for $C_{37}H_{43}NO_{15}S_2Na^+$, 828.1972).

Synthesis of 2,5-dioxopyrrolidin-1-yl 5-(1,2-dithiolan-3-yl)pentanoate (3.16)

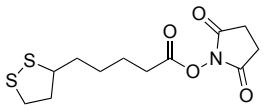

3.16

A 50 mL round bottom flask was oven-dried, cooled to room temperature and charged with a magnetic stirring bar, N-hydroxysuccinimide (345 mg, 3 mmol), lipoic acid (412 mg, 2 mmol), DCC (1.03 g, 5 mmol) and a rubber septum. The flask was evacuated for 5 min and flushed with nitrogen. Anhydrous CH_2Cl_2 (30 mL) was added via syringe to dissolve the solids. The solution was stirred vigorously for 16 h under nitrogen (balloon). The reaction was filtered to remove any

insoluble solids. The resulting solution was diluted with EtOAc (100 mL), wished with saturated $NaHCO_3$ solution (2 x 25 mL), brine (2 x 50 mL), and dried with anhydrous Na_2SO_4. After evaporating the solvent by rotary evaporation (30 ^oC), a solid crude product was obtained, which was further purified by column chromatography (silica gel, 300 g, eluted with C_6H_{14} : CH_2Cl_2 = 10 : 1) to yield **3.16** (557 mg, 1.84 mmol) as a white solid in a yield of 92%. ^1H NMR ($CDCl_3$, 500 MHz) δ 3.57 (m, 1H), 3.14 (m, 2H), 2.83(d, *J* = 4 Hz, 4H), 2.62 (t, *J* = 8 Hz, 2H), 2.46 (m, 1H), 1.92 (m, 1H), 1.73 (m, 4H), 1.58 (m, 2H); ^{13}C NMR (126 MHz) δ 169.2, 168.5, 56.2, 40.3, 38.6, 34.5, 30.9, 28.4, 25.7, 24.5; HR-ESI-MS: *m/z* 303.0615 $[M]^+$ (calcd for $C_{12}H_{17}NO_4S_2^+$, 303.0599).

Synthesis of 1-Amino-3,6,9,12-tetraoxapentadecan-15-oic acid (3.17)

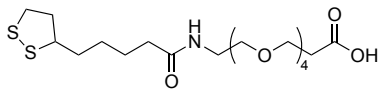

3.17

A 10 mL round bottom flask was oven-dried, cooled to room temperature and charged with a magnetic stirring bar, compound **3.16** (303 mg, 1 mmol), amino-dPEG$_4$-acid (318 mg, 1.2 mmol), and a rubber septum. The flask was evacuated for 5 min and flushed with nitrogen. Anhydrous DMF (5 mL) was added via syringe to dissolve the solids. Ice bath was used to cool the solution to 0 ^oC, followed by vigorous stirring for 5 min. Then to the solution was added Et_3N (303 mg, 3 mmol) over a period of 5 min via syringe. The mixture was warmed to room temperature and stirred for 2 h under nitrogen (balloon). The solvent was evaporated under

vacuum for 3 h and the crude product was purified by column chromatography (silica gel, 100 g, eluted with CH_2Cl_2 : MeOH = 13 : 1) to yield **3.17** (430 mg, 0.95 mmol) as a white solid in a yield of 95%. ^{1}H NMR ($CDCl_3$, 500 MHz) δ 3.76 (t, *J* = 6 Hz, 2H), 3.64 (m, 12H), 3.59 (t, *J* = 4.5 Hz, 2H), 3.55 (m, 1H), 3.45 (q, *J* = 4.5 Hz, 2H), 3.14 (m, 2H), 2.60 (t, *J* = 6.5 Hz, 2H), 2.45 (m, 1H), 2.20 (t, *J* = 7.5 Hz, 2H), 1.90 (m, 1H), 1.67 (m, 4H), 1.45 (m, 2H); ^{13}C NMR (126 MHz) δ 174.4, 173.6, 70.8, 70.7, 70.6, 70.4, 70.3, 70.1, 66.7, 56.6, 40.4, 39.3, 38.6, 36.4, 35.2, 34.8, 29.0, 25.5; HR-ESI-MS: *m/z* 454.1931 $[M + H]^+$ (calcd for $C_{19}H_{36}NO_7S_2^+$, 454.1933).

Synthesis of (((4-nitrophenoxy)carbonyl)oxy)methyl 21-(1,2-dithiolan-3-yl)-17-oxo-4,7,10,13-tetraoxa-16-azahenicosanoate (3.18)

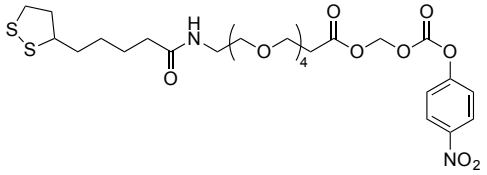

3.18

A 100 mL round bottom flask was oven-dried, cooled to room temperature and charged with a magnetic stirring bar, compound **3.17** (227 mg, 0.5 mmol), compound **3.13** (323 mg, 1 mmol), Ag_2CO_3 (414 mg, 1.5 mmol), and a rubber septum. The flask was evacuated for 5 min and flushed with nitrogen. Anhydrous C_7H_8 (30 mL) was added to the flask via syringe. The solution was heated to 60 ^{o}C and stirred vigorously for 3 h under nitrogen (balloon). The solution was filtered to remove unreacted Ag_2CO_3 and other insoluble impurities. Then, the solvent was evaporated under vacuum and the resulting solid crude product was purified by column

chromatography (silica gel, 100 g, eluted with C_6H_{14} : CH_2Cl_2 = 5 : 1) to yield **3.18** (149 mg, 0.23 mmol) as a white powder in a yield of 46%. ^{1}H NMR ($CDCl_3$, 500 MHz) δ 8.30 (dd, *J* = 9.5, 2 Hz, 2H), 7.42 (dd, *J* = 9.5, 2 Hz, 2H), 6.16 (s, 2H), 3.69 (m, 17H), 3.15 (m, 4H), 2.56 (m, 2H), 2.45 (m, 1H), 2.30 (t, *J* = 6.5 Hz, 2H), 1.88 (m, 1H), 1.66 (m, 4H), 1.49 (m, 2H); ^{13}C NMR (126 MHz); 176.0, 173.9, 156.3, 155.1, 150.9, 125.0, 121.8, 86.5, 70.2, 70.1, 70.0, 69.8, 69.5, 69.2, 66.4, 56.1, 40.6, 39.9, 39.2, 37.9, 34.4, 33.3, 28.4, 24.4 HR-ESI-MS: m/z 671.1915 $[M + Na]^+$ (calcd for $C_{27}H_{40}N_2NaO_{12}S_2$, 671.1920).

Synthesis of ((((2*S*,3*S*,4*S*,6*R*)-3-hydroxy-2-methyl-6-(((1*S*,3*S*)-3,5,12-trihydroxy-3-(2-hydroxyacetyl)-10-methoxy-6,11-dioxo-1,2,3,4,6,11-hexahydrotetracen-1-yl)oxy)tetrahydro-2H-pyran-4-yl)carbamoyl)oxy)methyl 21-(1,2-dithiolan-3-yl)-17-oxo-4,7,10,13-tetraoxa-16-azahenicosanoate (3.3)

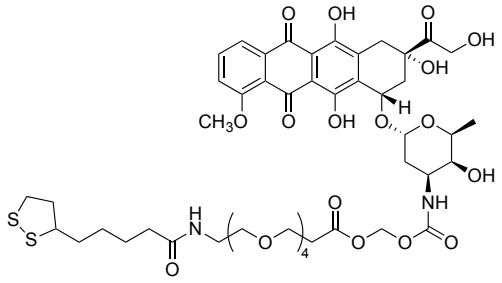

3.3

A 10 mL round bottom flask was oven-dried, cooled to room temperature and charged with a magnetic stirring bar, doxorubicin hydrochloride (20 mg, 0.0345 mmol), compound **3.18** (32.4 mg, 0.05 mmol), and a rubber septum. The flask was evacuated for 5 min and flushed with nitrogen. Anhydrous DMF (5 mL) was added via syringe to dissolve the solids. Ice bath was

used to cool the solution to 0 ^{o}C, followed by vigorous stirring for 5 min. Then to the solution was added Et_3N (10 mg, 0.0988 mmol) over a period of 5 min via syringe. The mixture warmed to room temperature and stirred for 2 h under nitrogen (balloon). Then, the solvent was evaporated under vacuum to give a solid crude product, which was purified by column chromatography (silica gel, 100 g, eluted with $CHCl_3$: MeOH = 18 : 1) to yield **3.3** (30.9 mg, 0.029 mmol) as a red solid in a yield of 85%. ^{1}H NMR ($CDCl_3$, 500 MHz) δ 8.03 (dd, *J* = 8, 1 Hz, 1H), 7.78 (t, *J* = 8 Hz, 1H), 7.38 (dd, *J* = 8, 1 Hz, 1H), 5.62 (m, 2H), 5.51 (d, *J* = 4 Hz, 1H), 4.76 (m, 3H), 4.12 (q, *J* = 6.5 Hz, 1H), 4.09 (s, 3H), 3.65 (m, 21---1H), 3.27 (dd, *J* = 19, 1.5 Hz, 1H), 3.10 (m, 3H), 3.01 (s, 1H), 2.89 (s, 1H), 2.48 (m, 3H), 2.33 (m, 3H), 2.15 (dd, *J* = 15, 4 Hz, 1H), 1.85 (m, 4H), 1.63 (m, 4H), 1.42 (m, 2H), 1.29 (d, *J* = 6.5 Hz, 3H); ^{13}C NMR (126 MHz) δ 213.8, 187.1, 186.7, 172.5, 172.4 161.0, 156.2, 155.6, 153.8, 135.7, 135.6, 135.5, 133.6, 120.9, 119.8, 118.4, 115.9, 111.6, 111.4, 100.7, 79.7, 70.4, 70.1, 70.0, 69.9, 69.7, 69.6, 69.2, 68.7, 67.4, 67.3, 65.5, 56.7, 56.3, 53.4, 47.2, 40.2, 39.7, 38.4, 35.6, 34.5, 34.0, 33.7, 31.4, 30.0, 28.5, 24.2, 16.7; HR-ESI-MS: *m/z* 1053.3593 $[M + H]^+$ (calcd for $C_{48}H_{65}N_2O_{20}S_2$, 1053.3572).

Synthesis of ((5-(1,2-dithiolan-3-yl)pentanoyl)oxy)methyl (E)-2-(1-((2S,4S)-4-(((2R,4S,5S,6S)-4-amino-5-hydroxy-6-methyltetrahydro-2H-pyran-2-yl)oxy)-2,5,12-trihydroxy-7-methoxy-6,11-dioxo-1,2,3,4,6,11-hexahydrotetracen-2-yl)-2-hydroxyethylidene)hydrazine-1-carboxylate (3.4)

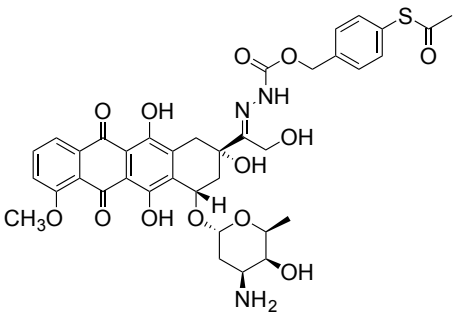

3.4

A 10 mL round bottom flask was oven-dried, cooled to room temperature and charged with a magnetic stirring bar, compound **3.9** (173 mg, 0.5 mmol), and a rubber septum. The flask was evacuated for 5 min and flushed with nitrogen. Anhydrous CH_2Cl_2 (20 mL) was added via syringe to dissolve the solids. Ice bath was used to cool the solution to 0 ^oC, followed by vigorous stirring for 5 min. Then to the solution was added hydrazine monohydrate (160 mg, 5 mmol) over a period of 5 min via syringe. The mixture was warmed to room temperature and stirred for 24 h under nitrogen (balloon). Then, the solvent was evaporated under vacuum. Then doxorubicin hydrochloride **3.10** (80 mg, 0.138 mmol) was added into the flask, followed by adding anhydrous MeOH (20 mL) via syringe to dissolve the solids. The resulting solution was stirred vigorously for 5 min and a drop of TFA was added. The resulting mixture was allowed to be heated to 60 °C for 16 h under nitrogen (balloon). Then, the solvent was evaporated under

vacuum and the resulting crude product was purified by column chromatography (silica gel, 100 g, eluted with $CHCl_3$: MeOH = 3 : 1) to yield **3.4** (57.0 mg, 0.074 mmol,) as a red solid in a yield of 54%. ^{1}H NMR ($CDCl_3$, 500 MHz) δ 8.04 (dd, J = 8, 1 Hz, 1H), 7.78 (t, J = 8 Hz, 1H), 7.38 (m, 5H), 5.51 (d, J = 4 Hz, 1H), 5.30 (s, 1H, -OH), 5.15 (d, J = 10.5 Hz, 1H), 5.00 (m, 2H), 4.76 (m, 2H), 4.54 (s, 1H), 4.12 (q, J = 6.5 Hz, 1H), 4.08 (s, 3H), 3.86 (m, 1H, -OH), 3.66 (s, 1H), 3.26 (dd, J = 19, 1.5 Hz, 1H), 3.01 (s, 1H), 2.40 (s, 3H), 2.32 (m, 1H), 2.18 (dd, J = 15, 4 Hz, 1H), 1.97 (d, *J* = 7.5 Hz, 1H), 1.88 (dd, *J* = 13.5, 4.5 Hz, 1H), 1.60 (s, 2H, -NH_2), 1.28 (d, J = 6.5 Hz, 1H); ^{13}C NMR (126 MHz) δ 193.9, 187.1, 186.7, 161.0, 156.2, 155.6, 155.3, 155.4, 137.9, 135.8, 135.5, 134.5, 133.5, 133.4, 128.7, 127.7, 120.9, 119.8, 118.5, 111.6, 111.4, 100.8, 69.7, 69.5, 67.3, 66.0, 65.6, 56.7, 47.0, 35.6, 34.0, 30.2, 30.1, 16.9; HR-ESI-MS: *m/z* 789.2288 $[M + Na]^+$ (calcd for $C_{37}H_{40}N_3O_{13}SNa$, 789.2280).

Synthesis of (9H-fluoren-9-yl)methyl ((2*S*,3*S*,4*S*,6*R*)-3-hydroxy-2-methyl-6-(((1*S*,3*S*)-3,5,12-trihydroxy-3-(2-hydroxyacetyl)-10-methoxy-6,11-dioxo-1,2,3,4,6,11-hexahydrotetracen-1-yl)oxy)tetrahydro-2H-pyran-4-yl)carbamate (3.19)

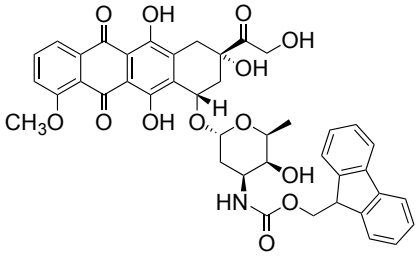

3.19

A 10 mL round bottom flask was oven-dried, cooled to room temperature and charged with a magnetic stirring bar, doxorubicin hydrochloride (80 mg, 0.138 mmol), *N*-(9-

fluorenylmethoxycarbonyloxy) succinimide (93 mg, 0.276 mmol) and a rubber septum. The flask was evacuated for 5 min and flushed with nitrogen. Anhydrous DMF (5 mL) was added via syringe to dissolve the solids. Ice bath was used to cool the solution to 0 ^{o}C, followed by vigorous stirring for 5 min. Then to the solution was added Et_3N (40 mg, 0.395 mmol) over a period of 5 min via syringe. The mixture was warmed to room temperature and was stirred for 2 h under nitrogen (balloon). The reaction was diluted with EtOAc (30 mL), washed with 0.6 M HCl solution (2 x 5 mL), saturated $NaHCO_3$ solution (2 x 5 mL), brine (2 x 10 mL), and dried with anhydrous Na_2SO_4. After evaporating the solvent by rotary evaporation (30 ^{o}C), a solid crude product was obtained, which was further purified by PTLC (eluted with $CHCl_3$: MeOH = 13 : 1) to yield **3.19** (97 mg, 0.127 mmol) as a red solid in a yield of 92%. ^{1}H NMR ($CDCl_3$, 500 MHz) δ 8.05 (dd, *J* = 8, 1 Hz, 1H), 7.65 (m, 2H), 7.48 (d, *J* = 20 Hz, 2H), 7.37 (m, 3H), 7.26 (m, 1H), 7.06 (m, 2H), 5.32 (m, 3H), 4.76 (m, 2H), 4.54 (d, *J* = 21 Hz, 1H), 4.33 (q, *J* = 8.5 Hz, 1H), 4.13 (q, *J* = 6.5 Hz, 1H), 4.05 (s, 3H), 3.86 (m, 1H, -OH), 3.78 (s, 1H), 3.57 (m, 1H), 3.20 (d, *J* = 19, 1H), 3.08 (m, 1H), 2.81 (m, 1H), 2.38 (m, 2H), 2.14 (dd, *J* = 15, 4 Hz, 1H), 1.83 (m, 1H), 1.30 (d, J = 6.0, 3H); ^{13}C NMR (126 MHz) δ 214.0, 187.3, 186.8, 172.6, 161.2, 156.9, 156.3, 155.8, 144.1, 144.0, 141.4, 141.3, 136.0, 135.6, 133.7, 127.8, 127.1, 125.2, 120.1, 120.0, 118.6, 111.7, 111.5, 100.8, 72.5, 69.8, 69.6, 67.4, 66.7, 65.7, 56.8, 53.6, 47.4, 47.1, 35.8, 34.1, 31.1, 30.3, 17.0; HR-ESI-MS: *m/z* 788.2300 $[M + Na]^+$ (calcd for $C_{42}H_{39}NO_{13}Na$, 788.2314).

Synthesis of (((2-((2*S*,4*S*)-4-(((2*R*,4*S*,5*S*,6*S*)-4-((((9H-fluoren-9-yl)methoxy)carbonyl) amino)-5-hydroxy-6-methyltetrahydro-2H-pyran-2-yl)oxy)-2,5,12-trihydroxy-7-methoxy-6,11-dioxo-1,2,3,4,6,11-hexahydrotetracen-2-yl)-2-oxoethoxy)carbonyl) oxy)methyl 5-(1,2-dithiolan-3-yl) pentanoate (3.20)

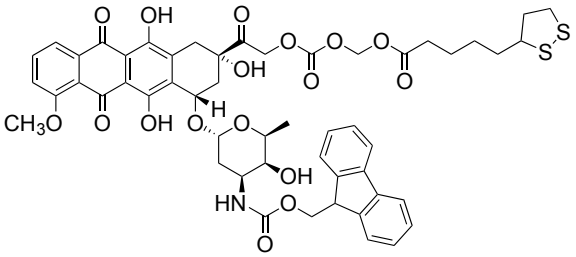

3.20

A 10 mL round bottom flask was oven-dried, cooled to room temperature and charged with a magnetic stirring bar, compound **3.19** (50 mg, 0.0654 mmol), compound **3.14** (40 mg, 0.1 mmol) and a rubber septum. The flask was evacuated for 5 min and flushed with nitrogen. Anhydrous DMF (5 mL) was added via syringe to dissolve the solids. Ice bath was used to cool the solution to 0 ^{o}C, followed by vigorous stirring for 5 min. Then to the solution was added Et_3N (26.5 mg, 0.262 mmol) over a period of 5 min via syringe. The mixture was warmed to room temperature and stirred for 2 days under nitrogen (balloon). The reaction was diluted with EtOAc (30 mL), washed with 0.6 M HCl solution (2 x 5 mL), saturated $NaHCO_3$ solution (2 x 5 mL), brine (2 x 10 mL), and dried with anhydrous Na_2SO_4. After evaporating the solvent by rotary evaporation (30 ^{o}C), a solid crude product was obtained, which was then purified by PTLC (eluted with $CHCl_3$: MeOH = 13 : 1) to yield **3.20** (45 mg, 0.044 mmol) as a red solid in a yield of 67%. ^{1}H NMR ($CDCl_3$, 500 MHz) δ 8.01 (dd, *J* = 8, 1 Hz, 1H), 7.75 (m, 2H), 7.61 (m, 1H), 7.53 (m, 1H), 7.37 (m, 2H), 7.26 (m, 1H), 7.06 (m, 2H), 6.84 (m, 1H), 5.81 (d, J = 24.0 Hz,

2H), 5.46 (m, 1H), 5.21 (m, 2H), 4.76 (m, 2H), 4.60 (s, 1H), 4.32 (q, *J* = 8.5 Hz, 1H), 4.13 (q, *J* = 6.5 Hz, 1H), 4.09 (s, 3H), 3.86 (m, 1H, -OH), 3.78 (s, 1H), 3.65 (m, 1H), 3.56 (m, 1H), 3.15 (m, 3H), 3.08 (m, 1H), 2.81 (m, 1H), 2.62 (s, J = 8 Hz, 2H), 2.45 (m, 1H), 2.34 (m, 2H), 2.14 (dd, J = 15, 4 Hz, 1H), 1.89 (m, 2H), 1.68 (m, 4H), 1.48 (m, 2H); 1.30 (d, J = 6.0, 3H); ^{13}C NMR (126 MHz) δ 214.0, 187.1, 186.7, 178.1, 172.4, 163.2, 156.3, 156.0, 155.8, 155.7, 144.0, 143.9, 141.4, 141.3, 135.9, 135.5, 133.7, 127.8, 127.1, 126.5, 120.0, 119.4, 118.6, 111.7, 111.2, 100.9, 77.4, 72.5, 69.8, 69.6, 67.4, 66.8, 65.7, 56.8, 53.6, 47.4, 47.1, 40.3, 38.6, 36.9, 35.7, 34.7, 33.8, 31.8, 30.2, 28.8, 25.5, 24.6, 17.0; HR-ESI-MS: *m/z* 1050.2661 $[M + Na]^+$ (calcd for $C_{52}H_{53}NO_{17}S_2Na^+$, 1050.2647).

Synthesis of (((2-((2*S*,4*S*)-4-(((2*R*,4*S*,5*S*,6*S*)-4-((((9H-fluoren-9-yl)methoxy)carbonyl) amino)-5-hydroxy-6-methyltetrahydro-2H-pyran-2-yl)oxy)-2,5,12-trihydroxy-7-methoxy-6,11-dioxo-1,2,3,4,6,11-hexahydrotetracen-2-yl)-2-oxoethoxy)carbonyl)oxy) methyl 5-(1,2-dithiolan-3-yl) pentanoate (3.5)

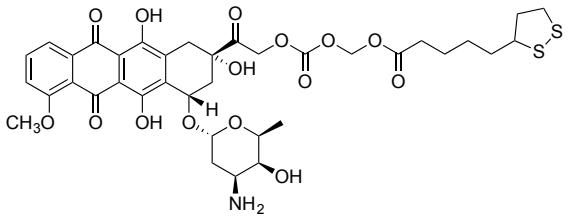

3.5

A 10 mL round bottom flask was oven-dried, cooled to room temperature and charged with a magnetic stirring bar, compound **3.20** (45 mg, 0.044 mmol) and a rubber septum. The flask was evacuated for 5 min and flushed with nitrogen. Anhydrous CH_2Cl_2 (0.4 mL) was added via

syringe to dissolve the solids. The resulting solution was stirred vigorously for 5 min. Then to the solution was added piperidine (112 mg, 1.32 mmol) over a period of 5 min via syringe. The mixture was warmed to room temperature and stirred for 2 h under nitrogen (balloon). The reaction was diluted with EtOAc (30 mL), washed with 0.6 M HCl solution (2 x 5 mL), saturated $NaHCO_3$ solution (2 x 5 mL), brine (2 x 10 mL), and dried with anhydrous Na_2SO_4. After evaporating the solvent by rotary evaporation (30 ^oC), a solid crude product was obtained, which was further purified by PTLC (eluted with $CHCl_3$: MeOH = 13 : 1) to yield **3.5** (31.9 mg, 0.04 mmol) as a red solid in a yield of 90%. ^1H NMR ($CDCl_3$, 500 MHz) δ 8.04 (dd, *J* = 8, 1 Hz, 1H), 7.79 (t, *J* = 8 Hz, 1H), 7.40 (dd, *J* = 8, 1 Hz, 1H), 5.74 (m, 2H), 5.52 (d, *J* = 4 Hz, 1H), 5.31 (m, 2H, -OH), 4.76 (m, 2H), 4.50 (s, 1H), 4.15 (q, *J* = 6.5 Hz, 1H), 4.09 (s, 3H), 3.68 (s, 1H), 3.55 (m, 1H), 3.31 (dd, *J* = 19, 1.5 Hz, 1H), 3.12 (m, 2H), 3.03 (m, 1H), 2.43 (m, 1H), 2.35 (m, 3H), 2.19 (dd, *J* = 15, 4 Hz, 1H), 1.90 (m, 3H), 1.77 (m, 1H), 1.62 (m, 4H), 1.42 (m, 2H), 1.28 (d, *J* = 6.5 Hz, 3H); ^{13}C NMR (126 MHz) δ 213.7, 187.2, 186.8, 172.4, 161.1, 156.1, 155.7, 153.7, 135.8, 135.5, 133.5, 133.4, 120.9, 119.9, 118.4, 111.7, 111.5, 100.6, 80.2, 69.7, 69.4, 67.1, 65.5, 56.7, 56.3, 47.0, 40.2, 38.4, 35.7, 34.5, 34.0, 33.7, 30.0, 28.5, 24.3, 16.8; HR-ESI-MS: *m/z* 804.1920 $[M + Na]^+$ (calcd for $C_{37}H_{42}NO_{15}S_2$, 804.1996).

References

1. Ferrari, M. Cancer Nanotechnology: Opportunities and Challenges. *Nat. Rev. Cancer* **2005**, *5*, 161–171.
2. Gottesman, M. M.; Fojo, T.; Bates, S. E. Multidrug Resistance in Cancer: Role of ATP-Dependent Transporters. *Nat. Rev. Cancer* **2002**, *2*, 48–58.
3. Peer, D.; Margalit, R. Fluoxetine and Reversal of Multidrug Resistance. *Cancer Lett.* **2006**, *237*, 180–187.
4. Jain, R. K. Barriers to Drug-delivery in Solid Tumors. *Sci. Am*. **1994**, *271*, 58–65.
5. de Menezes, D. E. L.; Pilarski, L. M.; Allen, T. M. *In vitro* and *in vivo* Targeting of Immunoliposomal Doxorubicin to Human B-cell Lymphoma. *Cancer Res*. **1998**, *58*, 3320–3330.
6. Sandy, R.; Chen, C.; Kaur, K. Novel Peptide−Doxorubucin Conjugates for Targeting Breast Cancer Cells Including the Multidrug Resistant Cells. *J. Med. Chem.* **2013**, *56*, 7564−7573.
7. van Hensbergen, Y.; Broxterman, H. J.; Elderkamp, Y. W.; Lankelma, J.; Beers, J. C. C.; Heijn, M.; Boven, E.; Hoekman, K.; Pinedo, H. M. A Doxorubicin−CNGRC-peptide Conjugate with Prodrug Properties. *Biochem. Pharmacol*. **2002**, *63*, 897−908.
8. Lee, G. Y.; Song, J.-h.; Kim, S. Y.; Park, K.; Byun, Y. Peptide-doxorubicin Conjugates Specifically Degraded by Matrix Metalloproteinases Expressed from Tumor. *Drug Dev. Res.* **2006**, *67*, 438−447.
9. Inoh, K.; Muramatsu, H.; Torii, S.; Ikematsu, S.; Oda, M.; Kumai, H.; Sakuma, S.; Inui, T.; Kimura, T.; Muramatsu, T. Doxorubicin-conjugated Anti-midkine Monoclonal Antibody as a Potential Anti-tumor Drug. *Jpn. J. Clin. Oncol*. **2006**, *36*, 207−211.

10. Paciotti, G. F.; Kingston, D. G. I.; Tamarki , L. Colloidal Gold Nanoparticles: A Novel Nanoparticle Platform for Developing Multifunctional Tumor-Targeted Drug Delivery Vectors. *Drug Dev. Res.* **2006**, *67*, 47–54.
11. Lejeune, F. J. High Dose Recombinant Tumor Necrosis Factor (rTNFα) Administered by Isolation Perfusion for Advanced Tumors of the Limbs: a Model for Biochemotherapy of Cancer. *Eur. J. Cancer* **1995**, *31*, 1009–1016.
12. Kristensen, C. A.; Nozue, M.; Boucher, Y.; Jain, R. K. Reduction of Interstitial Fluid Pressure after TNF-α Areatment of Three Human Melanoma Xenografts. *Br. J. Cancer* **1996,** *74*, 533–536.
13. Alexander, H. R.; Bartlett, D. L.; Libutti, S. K.; Fraker, D. L.; Moser, T.; Rosenberg, S. A. Isolated Hepatic Perfusion with Tumor Necrosis Factor and Melphalan for Unresectable Cancers Confined to the Liver. *J. Clin. Oncol.* **1998**, *16*, 1479–1489.
14. Peer, D.; Karp, J. M.; Hong, S.; Farokhzad, O. C.; Margalit, R.; Langer, R. Nanocarriers as an Emerging Platform for Cancer Therapy. *Nat. Nanotechnol*. **2007**, *2*, 751–760.
15. Kim, H. J.; Matsuda, H.; Zhou, H.; Honma, I. Ultrasound-triggered Smart Drug Release from a Poly(dimethylsiloxane)-mesoporous Silica Composite. *Adv. Mater.* **2006**, *18*, 3083–3088.
16. Giri, S.; Trewyn, B. G.; Stellmaker, M. P.; Lin V. S. Stimuli-responsive Controlled Release Delivery System Based on Mesoporous Silica Nanorods Capped with Magneticic Nanoparticles. *Angew. Chem., Int. Ed.* **2005**, *44*, 5038–5044.
17. Kam, N. S.; Liu, Z.; Dai, H. Functionalization of Carbon Nanotubes via Cleavable disulfide Bonds for Efficient Intracellular Delivery of siRNA and Potent Gene Silencing. *J. Am. Chem. Soc.* **2005**, *127*, 12492–12493.

18. Jones, D. P.; Carlson, J. L.; Samiec, P. S.; Sternberg, P.; Mody, V. C.; Reed, R. L.; Brown, L. S. Glutathione Measurement in Human Plasma: Evaluation of Sample Collection, Storage and Derivatization Conditions for Analysis of Dansyl Derivatives by HPLC. *Clin. Chim. Acta.* **1998**, *275*, 175–184.
19. Larson, T. A.; Joshi, P. P.; Sokolov, K. Preventing Protein Adsorption and Macrophage Uptake of Gold Nanoparticles via a Hydrophobic Shield. *Acs Nano* **2012**, *6*, 9182–9190.
20. Verma, A.; Simard, J. M.; Worrall, J. E.; Rotello, V. M. Tunable Reactivation of Nanoparticle-inhibited β-galactosidase by Glutathione at Intracellular Concentrations. *J. Am. Chem. Soc.* **2004**, *126*, 13987–13991.
21. Ghosh, P.; Han, G.; De, M.; Kim, C. K.; Rotello, V. M. Gold Nanoparticles in Delivery Applications. *Adv. Drug Delivery Rev.* **2008**, *60*, 1307–1315.
22. Wang, Y.; Wei, X.; Zhang, C.; Zhang, F.; Liang, W. Nanoparticle Delivery Strategies to Target Doxorubicin to Tumor Cells and Reduce Side Effects. *Ther. Delivery* **2010**, *1*, 273–287.
23. Wang, F.; Wang, Y. C.; Dou, S.; Xiong, M. H.; Sun, T. M.; Wang, J. Doxorubicin-Tethered Responsive AuNPs Facilitate Intracellular Drug Delivery for Overcoming Multidrug Resistance in Cancer Cells. *ACS Nano* **2011**, *5*, 3679–3692.
24. Raddatz, G; Bisswanger, H. Receptor Site and Stereospecifity of Dihydrolipoamide Dehydrogenase for R- and S-lipoamide: A Molecular Modeling Study. *J. Biotechnol.* **1997**, *58*, 89–100.

Appendix: NMR Spectra

^{1}H NMR spectrum of **3.7** in CD_3OD (500 MHz)

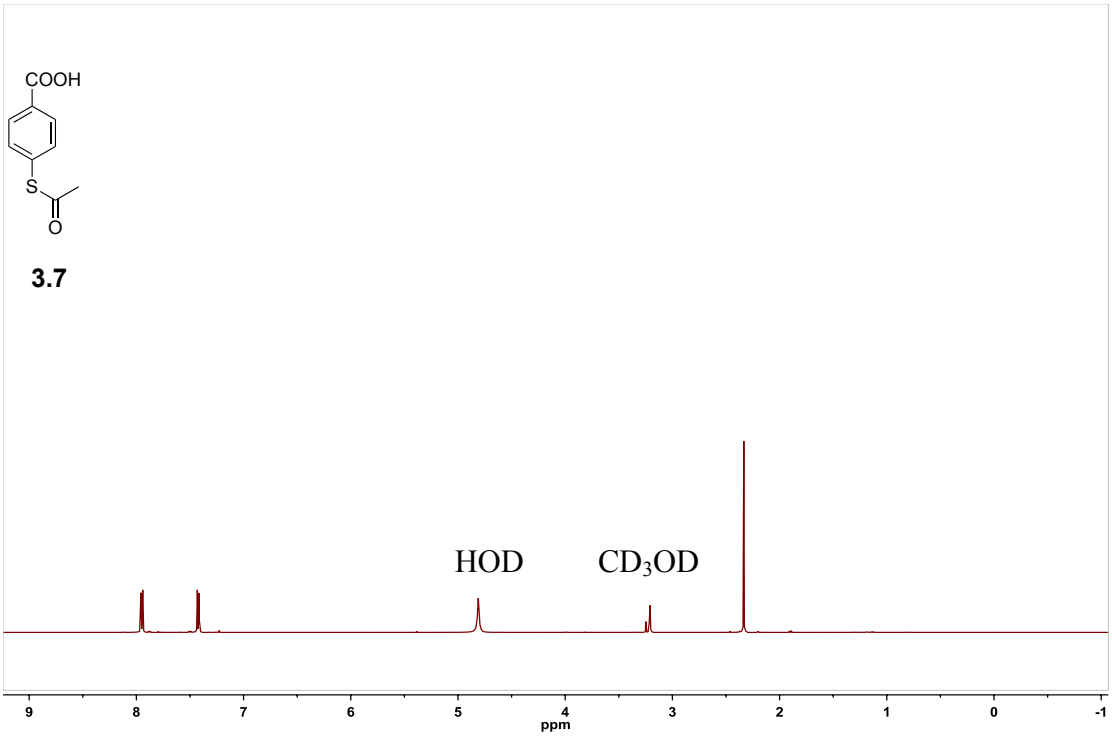

^{13}C NMR spectrum of **3.7** in CD_3OD (125 MHz)

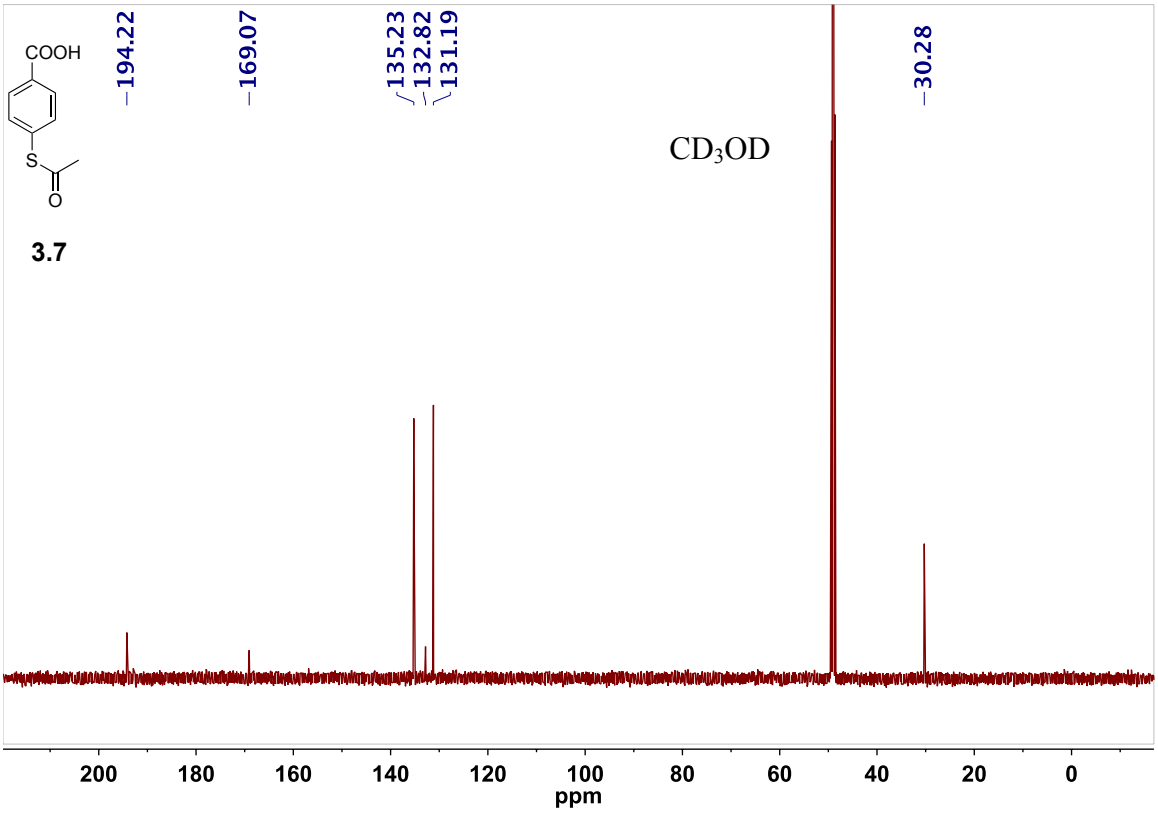

^{1}H NMR spectrum of **3.8** in CD_3OD (500 MHz)

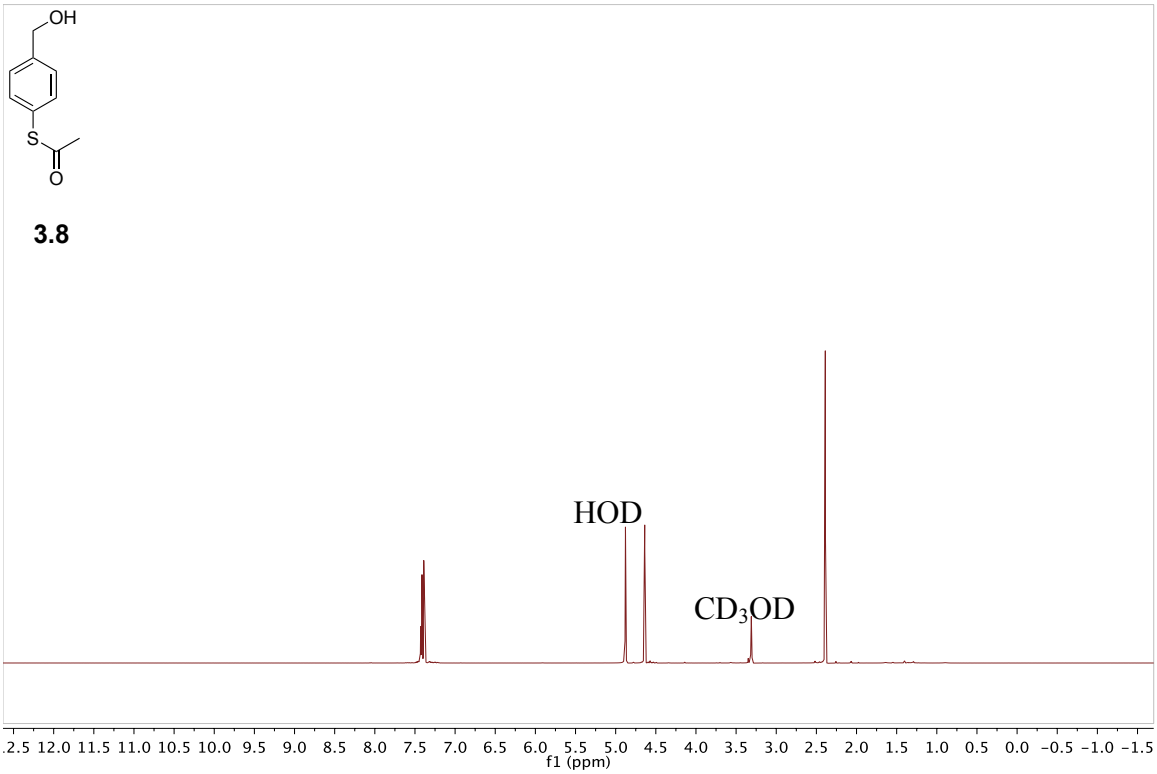

^{13}C NMR spectrum of **3.8** in CD_3OD (125 MHz)

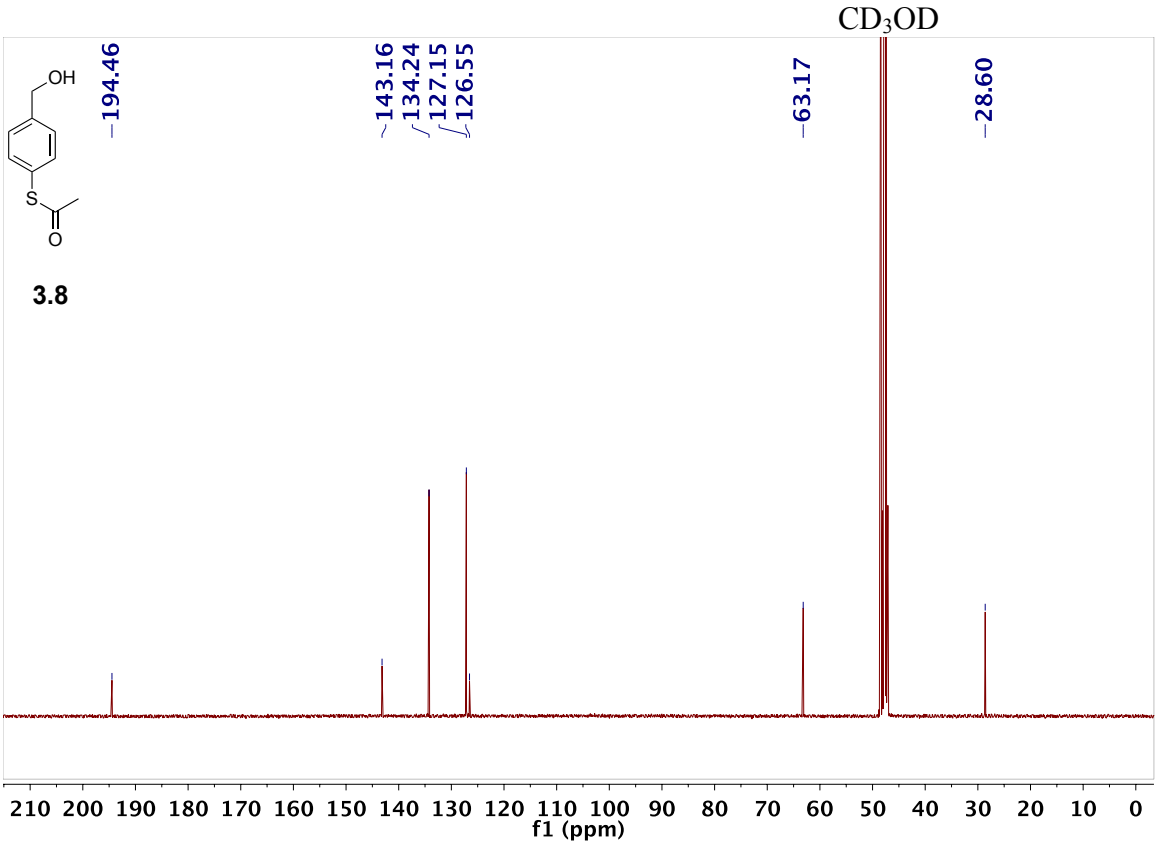

^{1}H NMR spectrum of **3.9** in $CDCl_3$ (500 MHz)

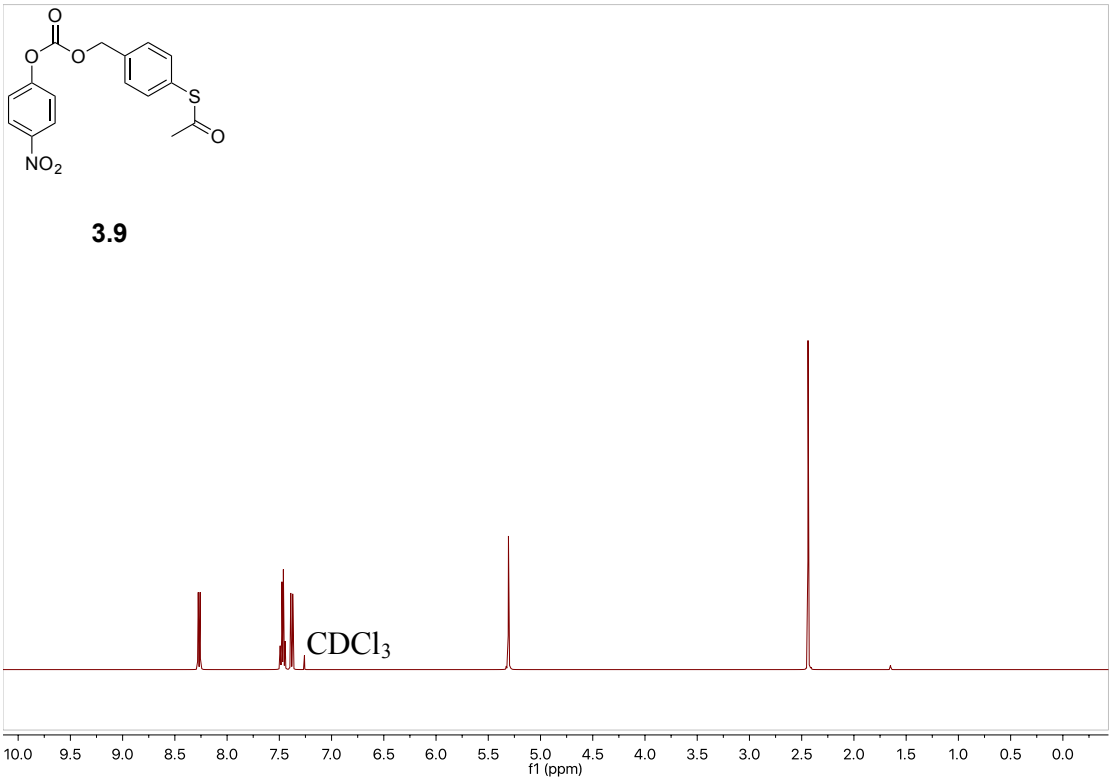

^{13}C NMR spectrum of **3.9** in $CDCl_3$ (125 MHz)

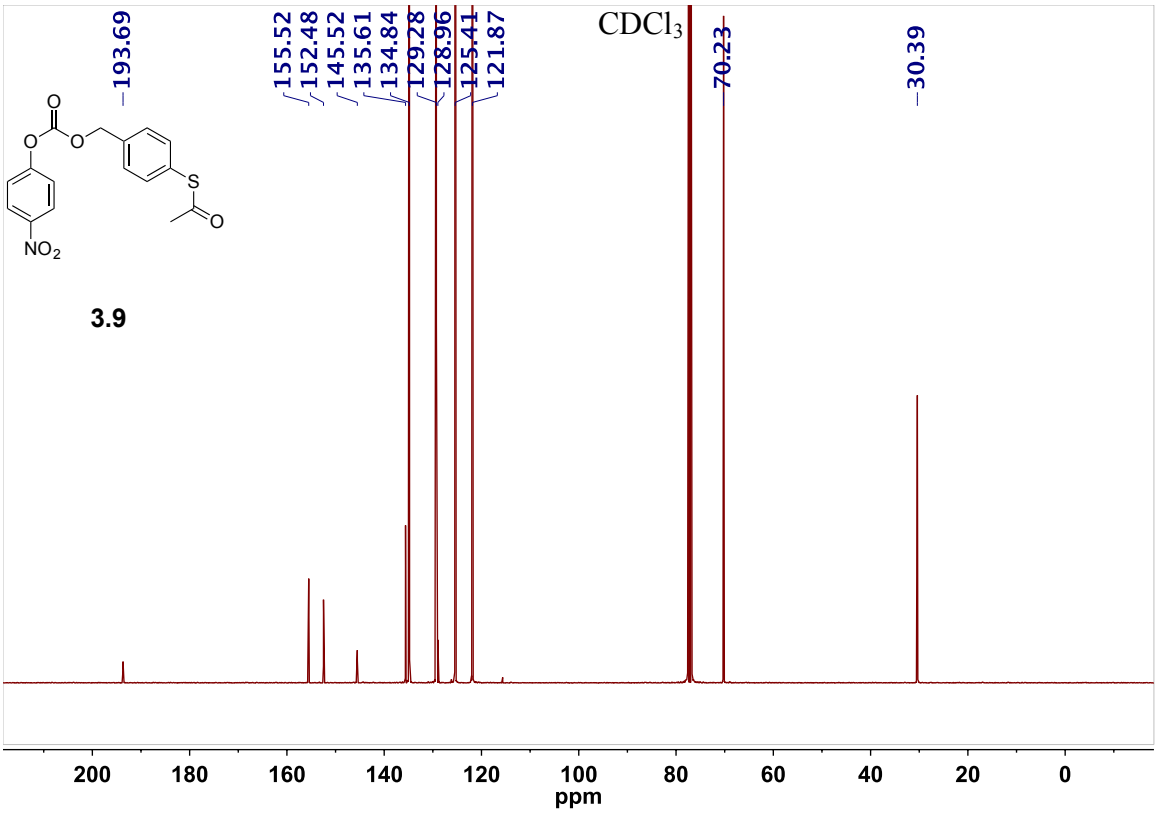

^{1}H NMR spectrum of **3.1** in $CDCl_3$ (500 MHz)

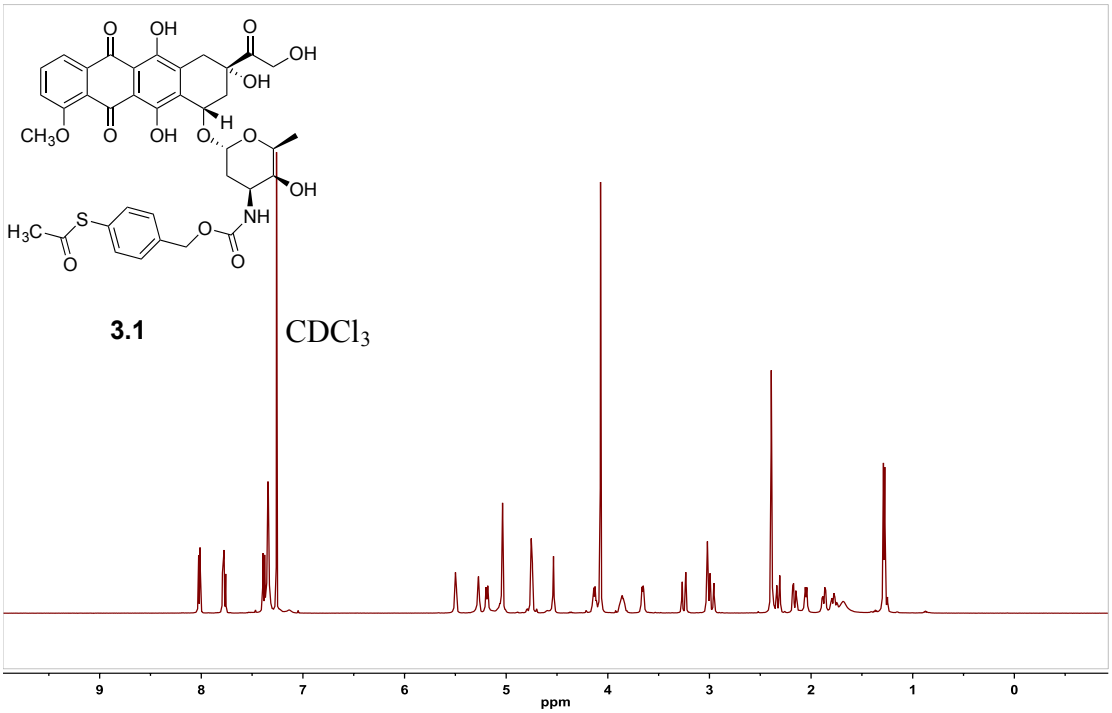

^{13}C NMR spectrum of **3.1** in $CDCl_3$ (125 MHz)

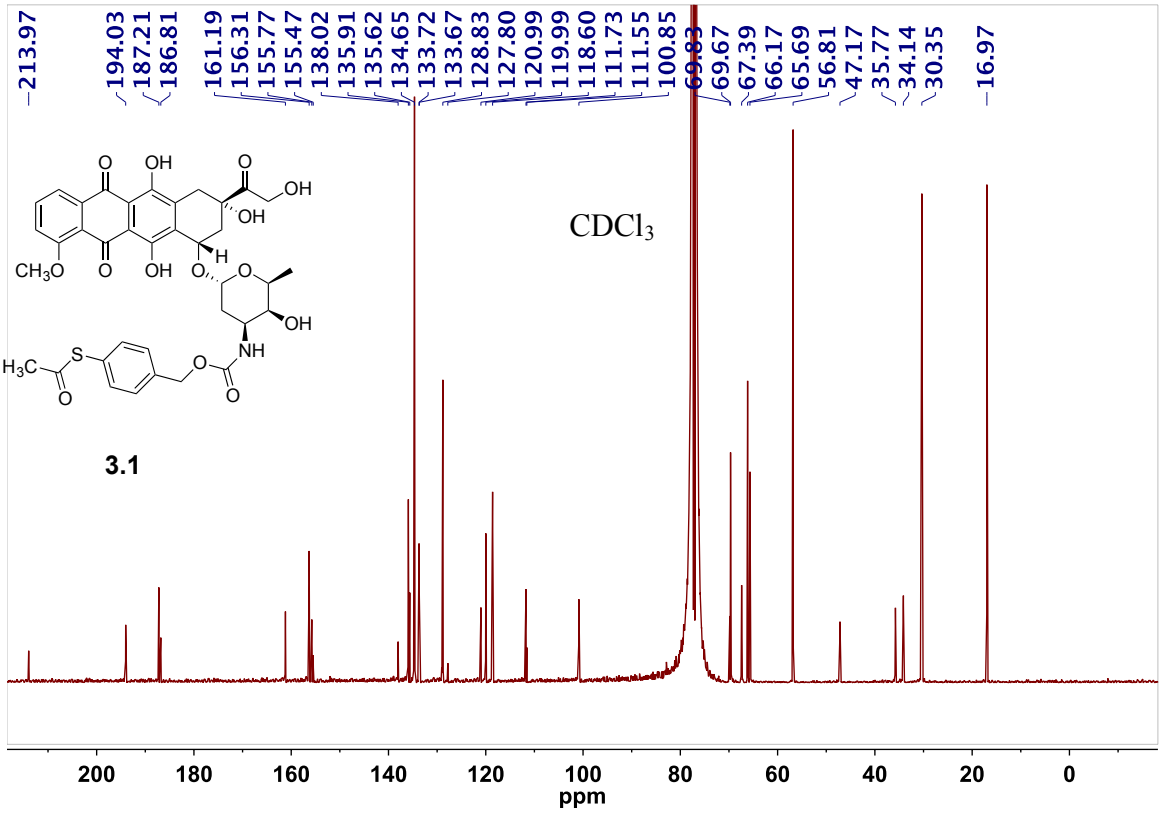

^{1}H NMR spectrum of **3.12** in $CDCl_3$ (500 MHz)

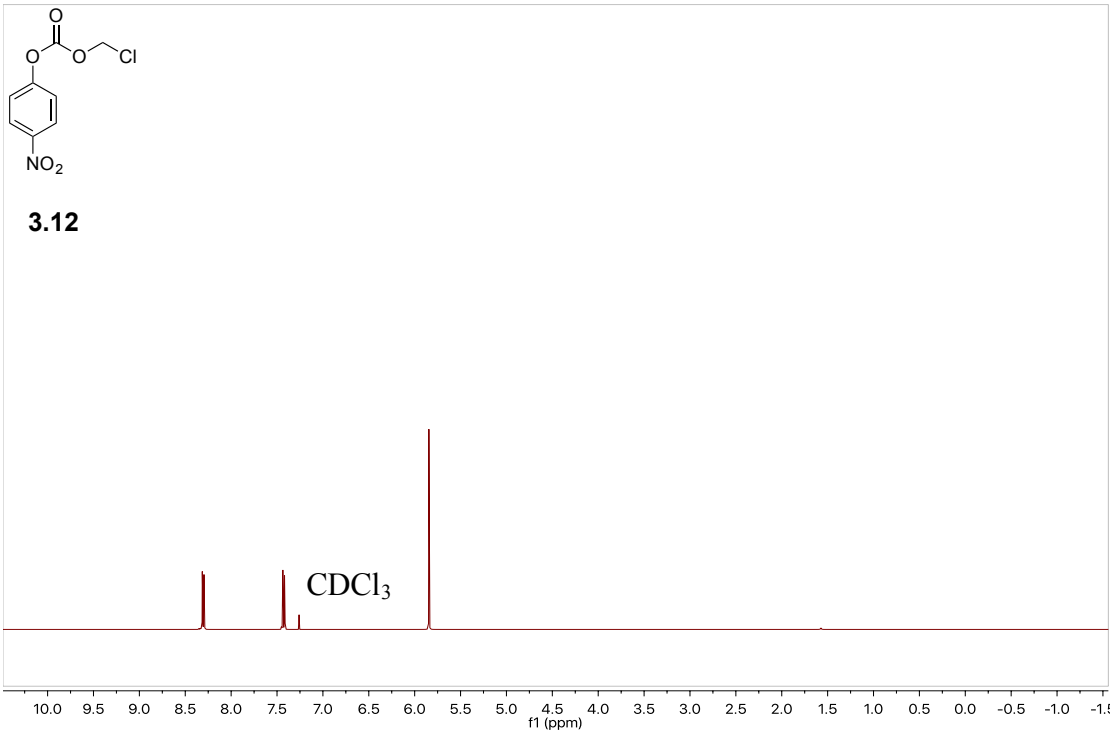

^{13}C NMR spectrum of **3.12** in $CDCl_3$ (125 MHz)

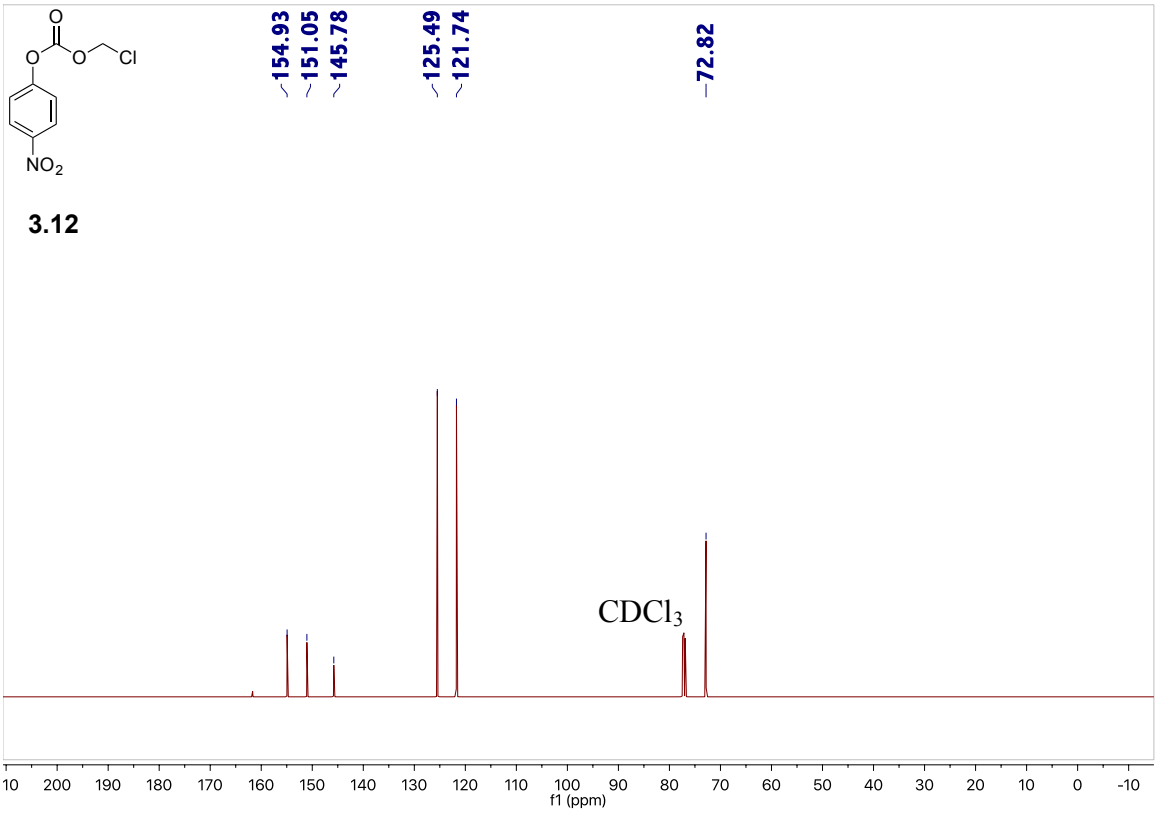

^{1}H NMR spectrum of **3.13** in $CDCl_3$ (500 MHz)

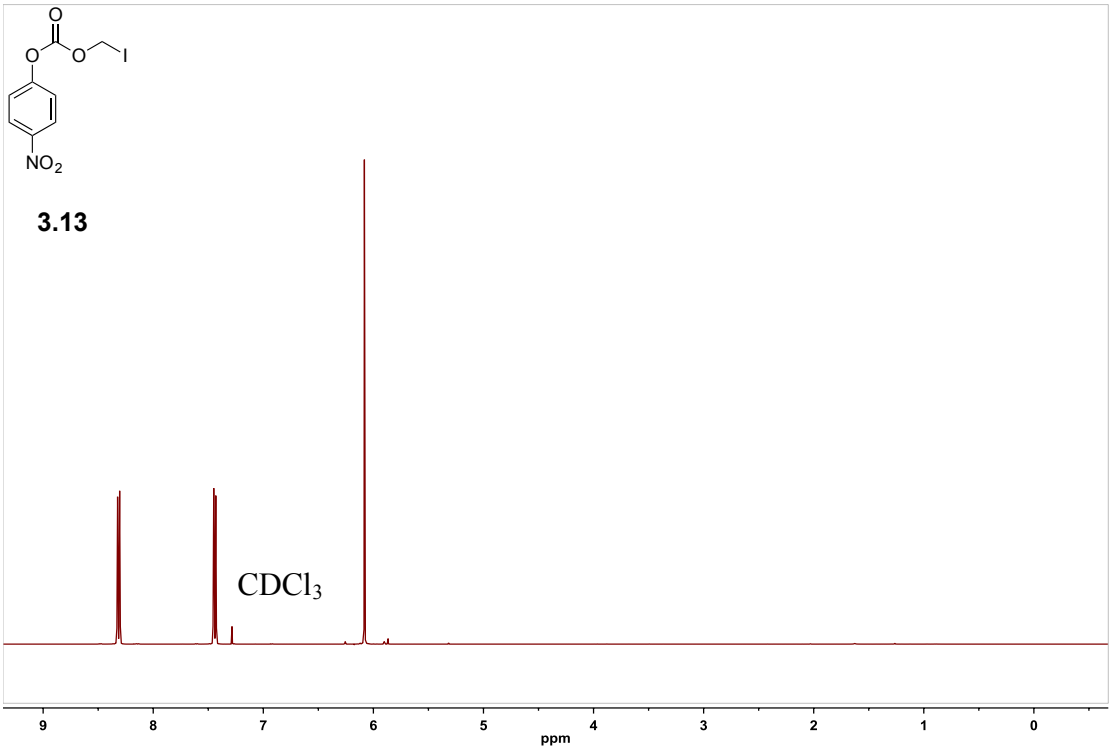

^{13}C NMR spectrum of **3.13** in $CDCl_3$ (125 MHz)

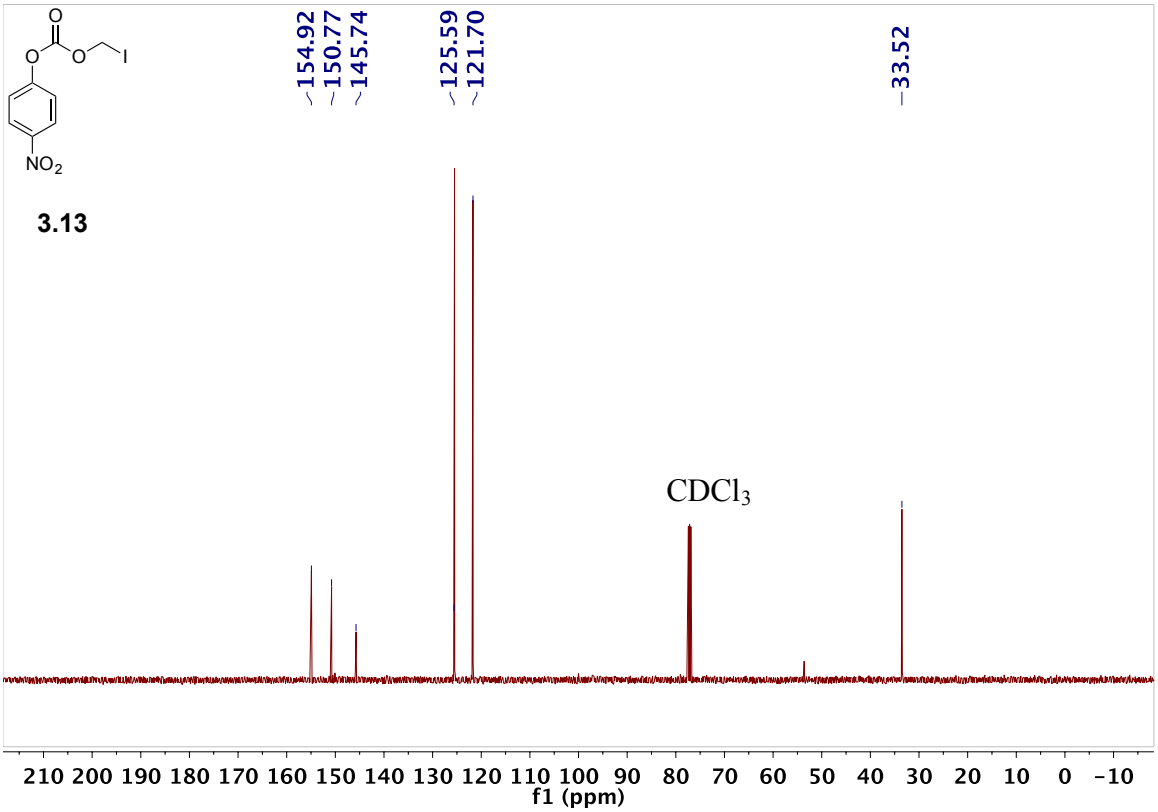

^{1}H NMR spectrum of **3.14** in $CDCl_3$ (500 MHz)

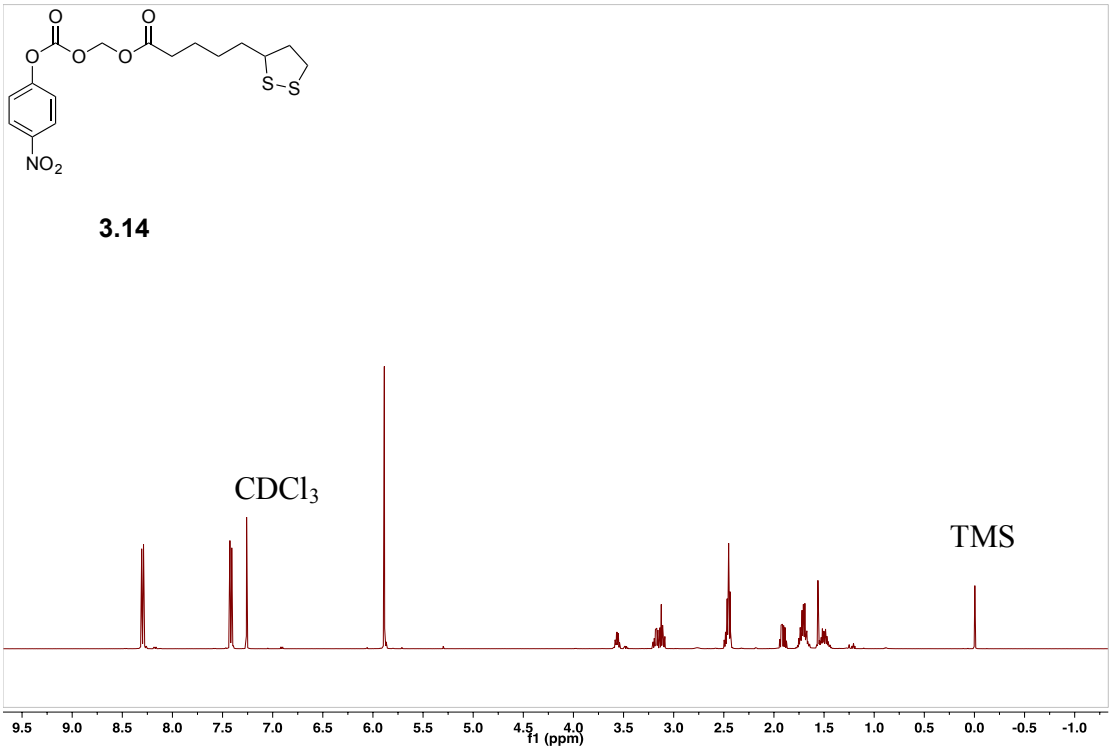

^{13}C NMR spectrum of **3.14** in $CDCl_3$ (125 MHz)

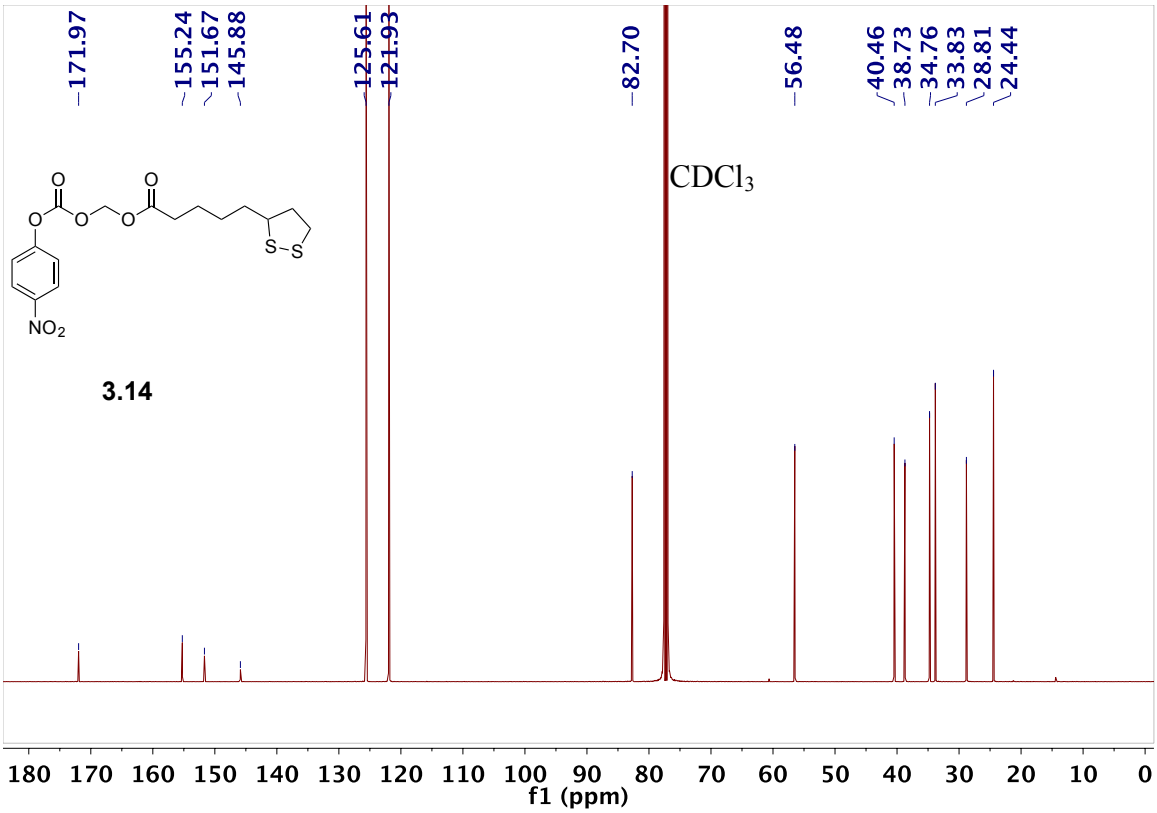

^{1}H NMR spectrum of **3.2** in $CDCl_3$ (500 MHz)

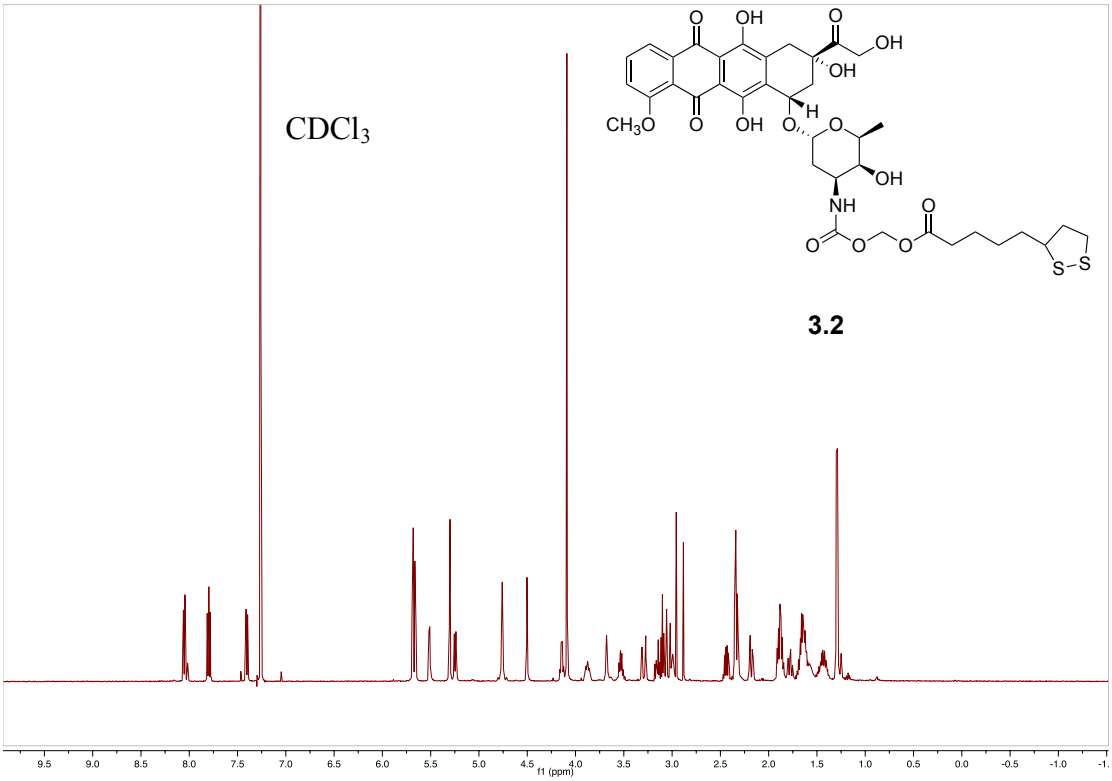

^{13}C NMR spectrum of **3.2** in $CDCl_3$ (125 MHz)

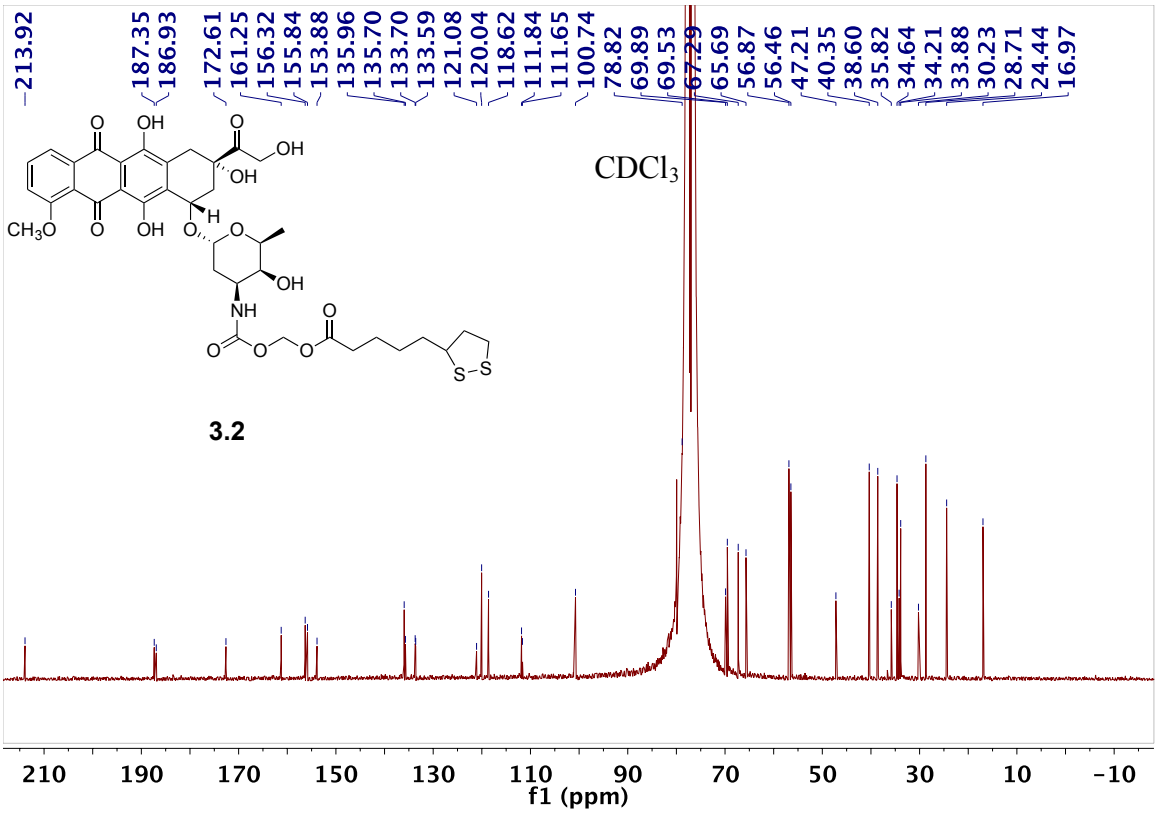

^{1}H NMR spectrum of **3.16** in $CDCl_3$ (500 MHz)

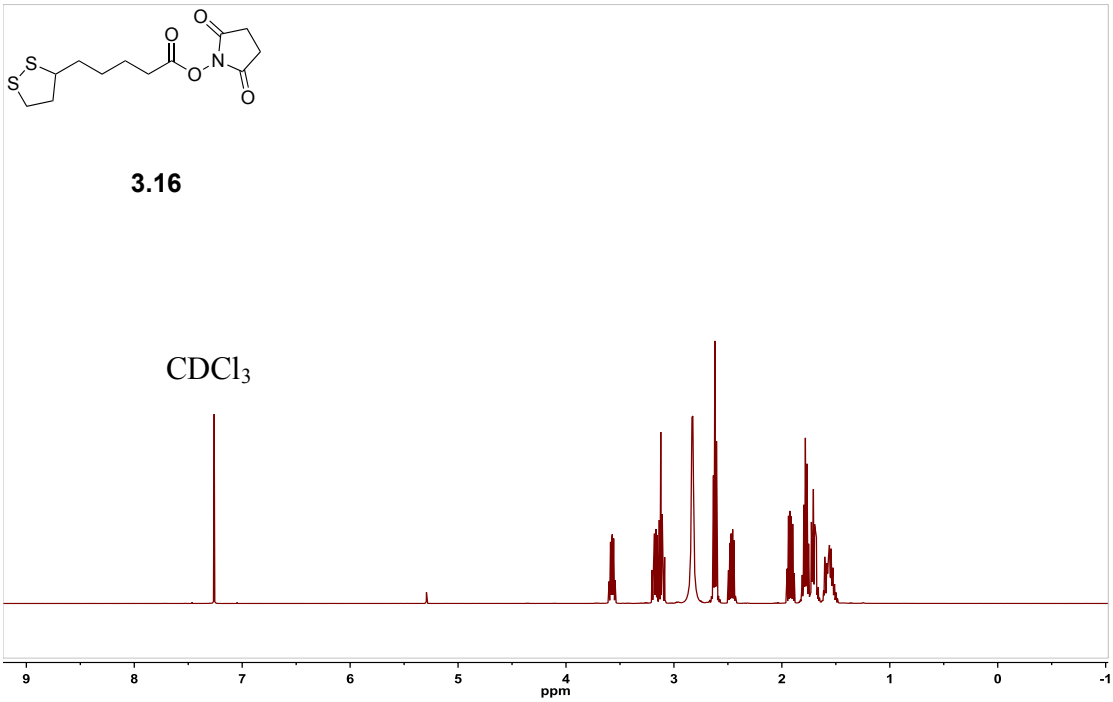

^{13}C NMR spectrum of **3.16** in $CDCl_3$ (125 MHz)

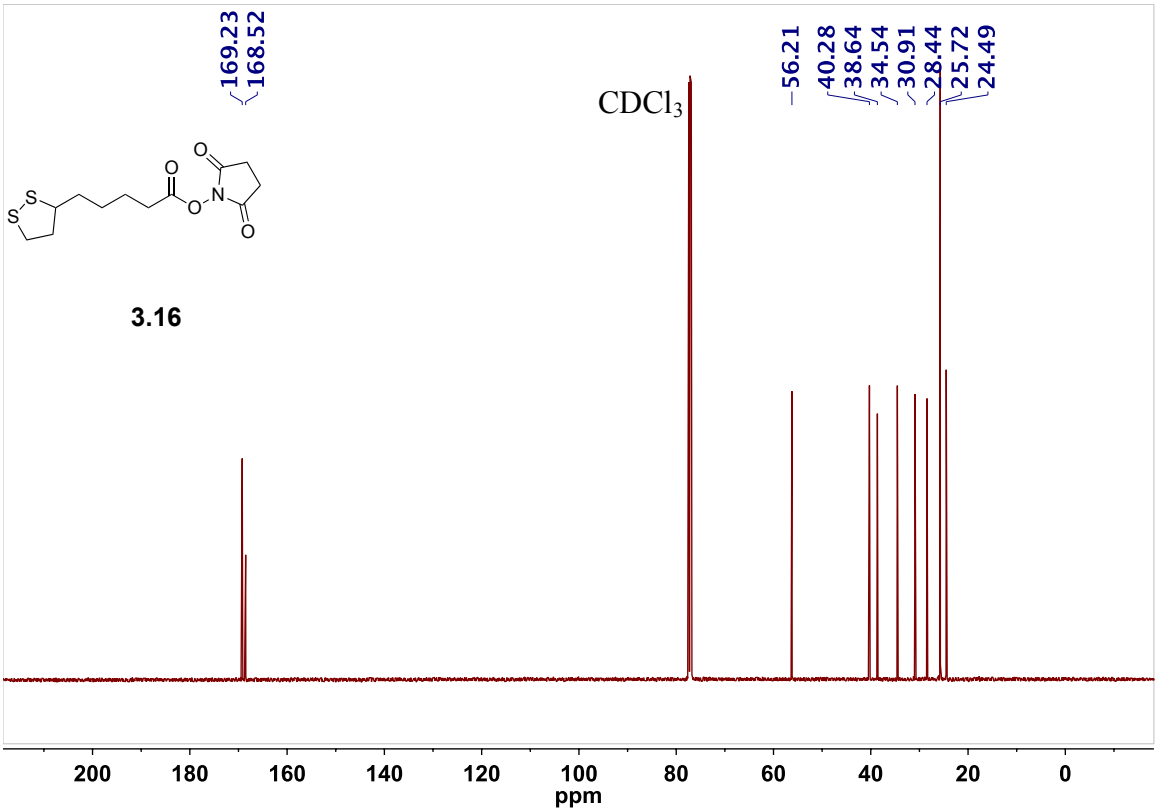

^{1}H NMR spectrum of **3.17** in $CDCl_3$ (500 MHz)

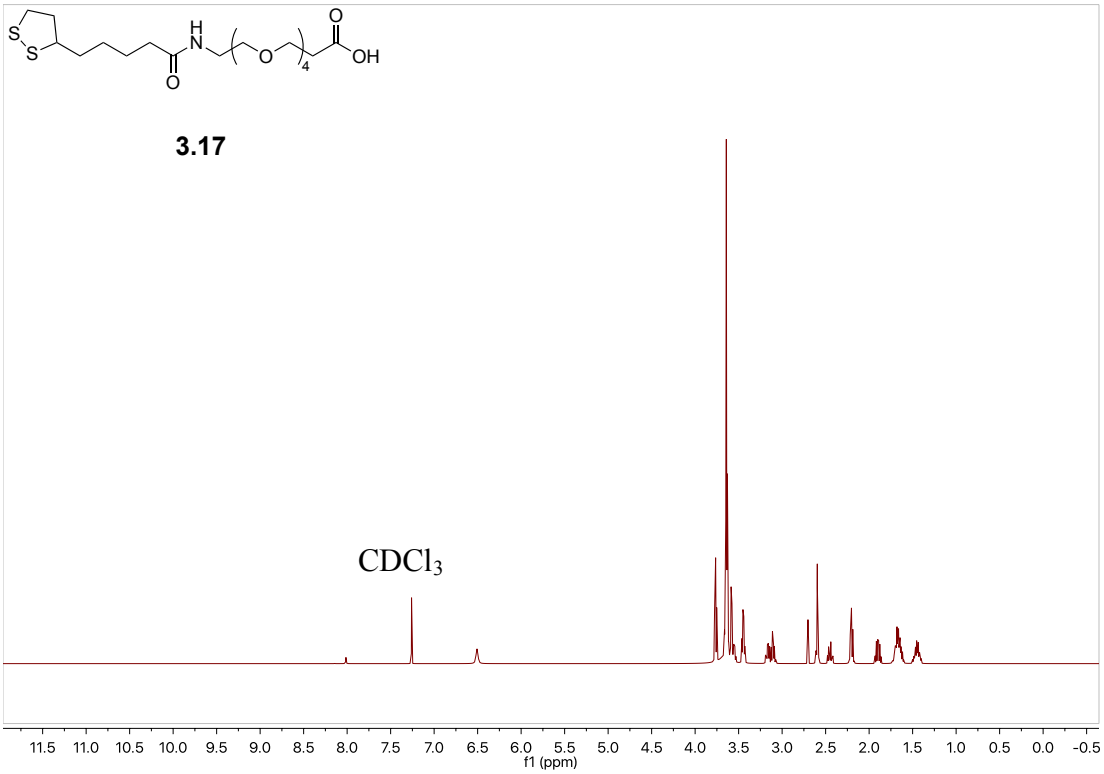

^{13}C NMR spectrum of **3.17** in $CDCl_3$ (125 MHz)

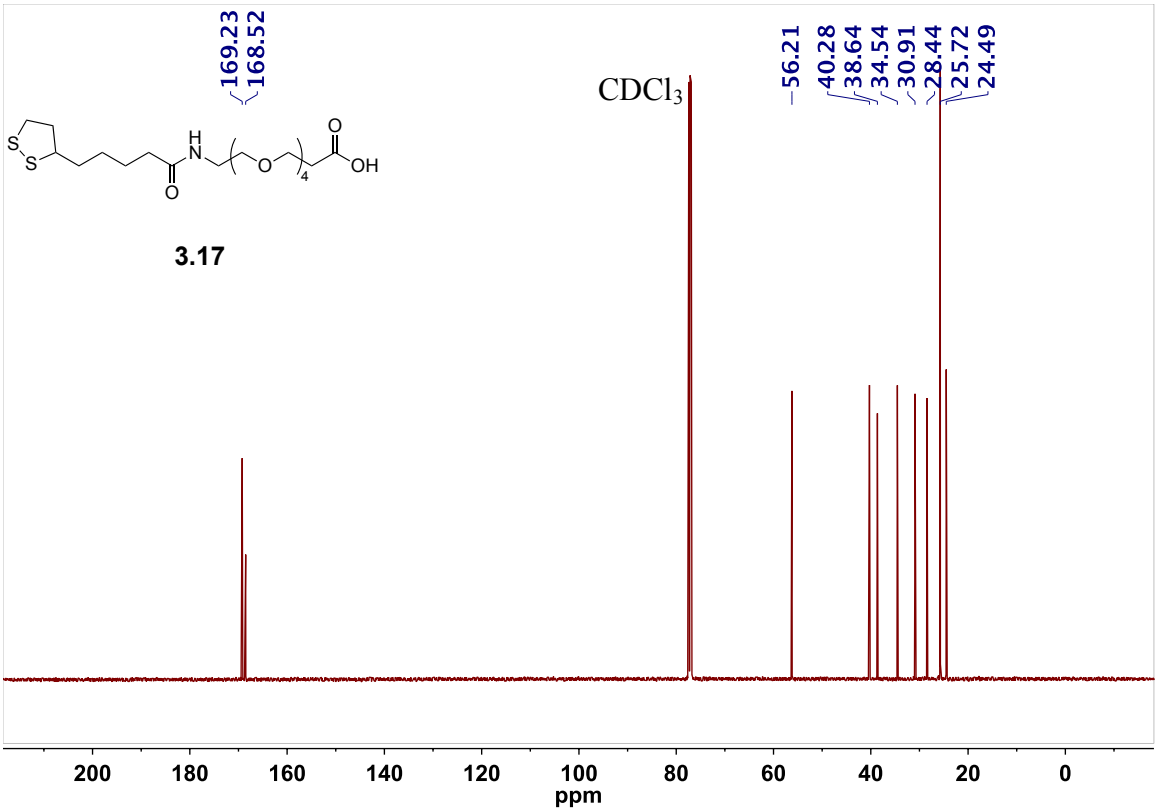

^{1}H NMR spectrum of **3.18** in CD_3OD (500 MHz)

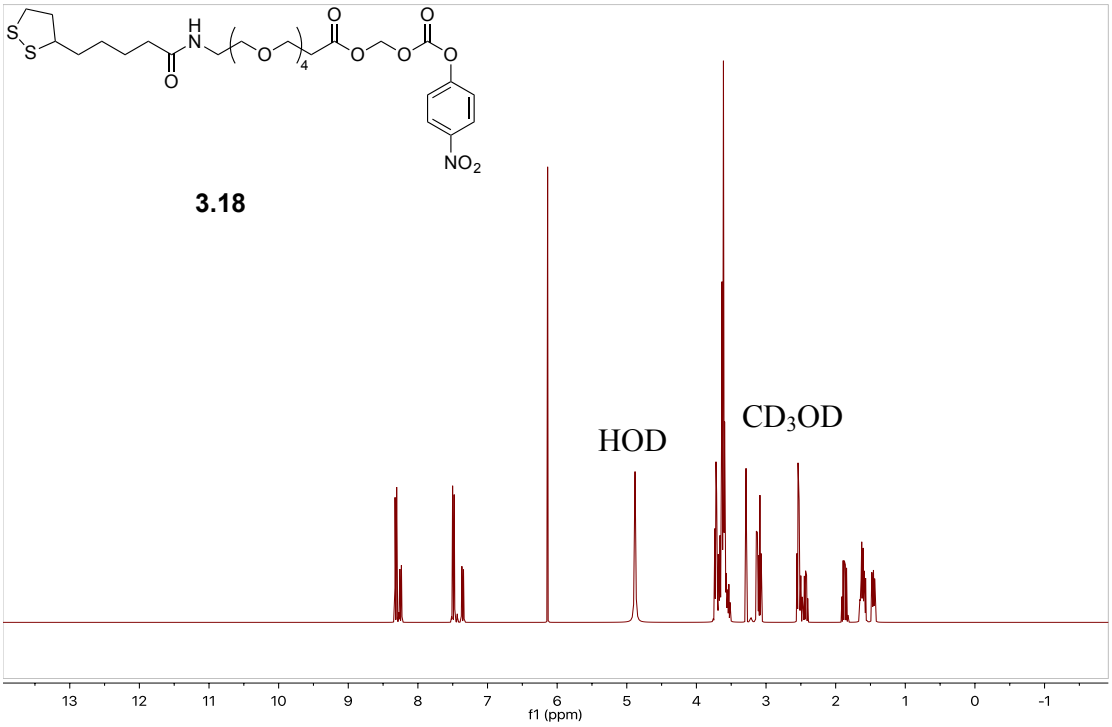

^{13}C NMR spectrum of **3.18** in CD_3OD (125 MHz)

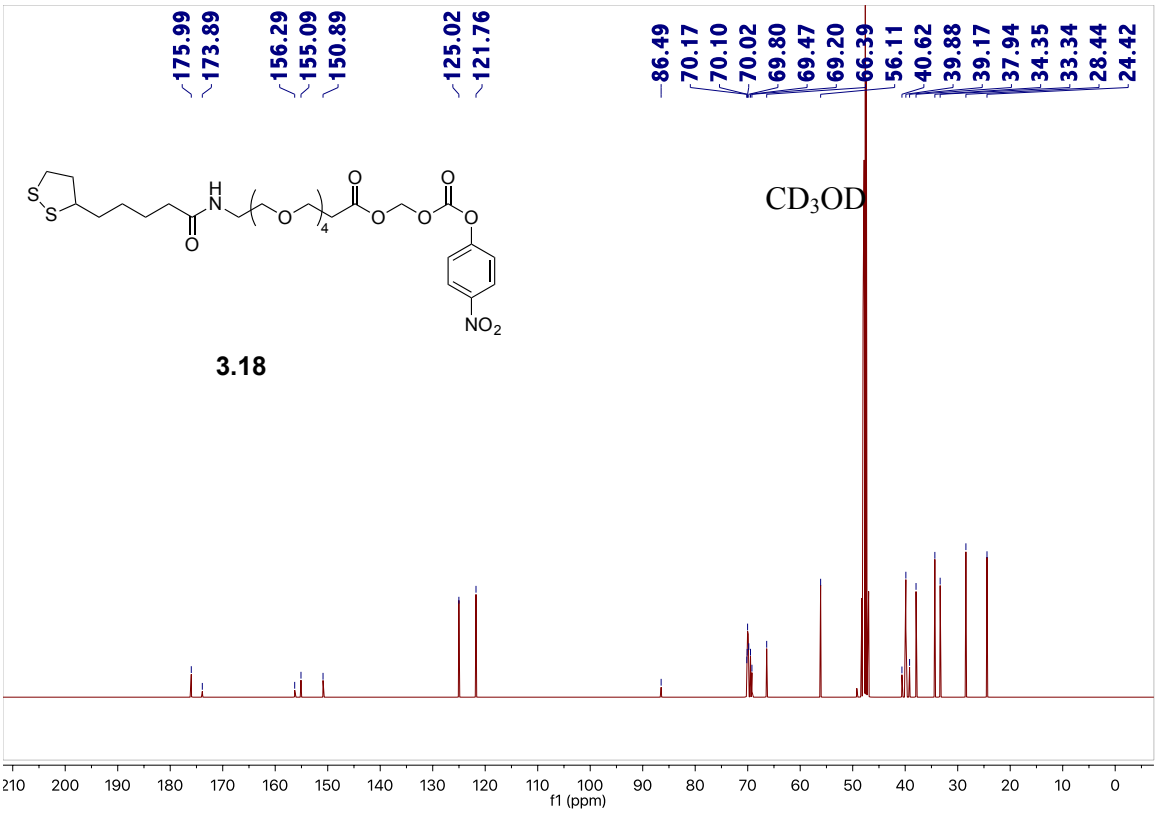

^{1}H NMR spectrum of **3.3** in $CDCl_3$ (500 MHz)

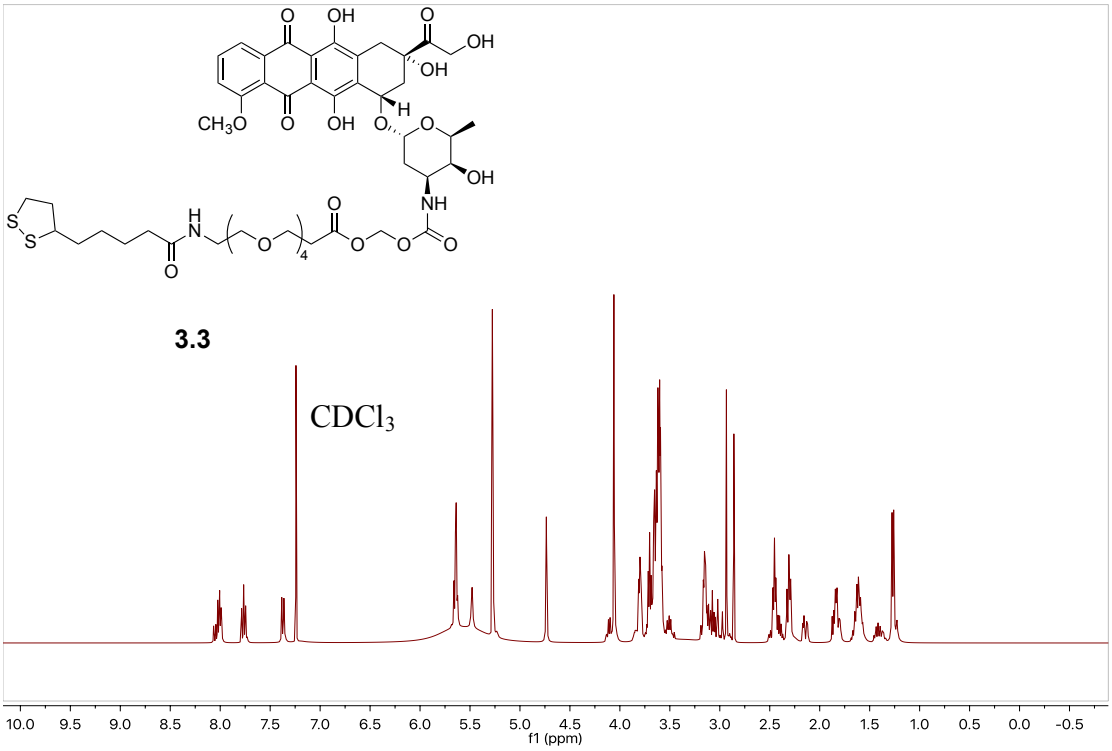

^{13}C NMR spectrum of **3.3** in $CDCl_3$ (125 MHz)

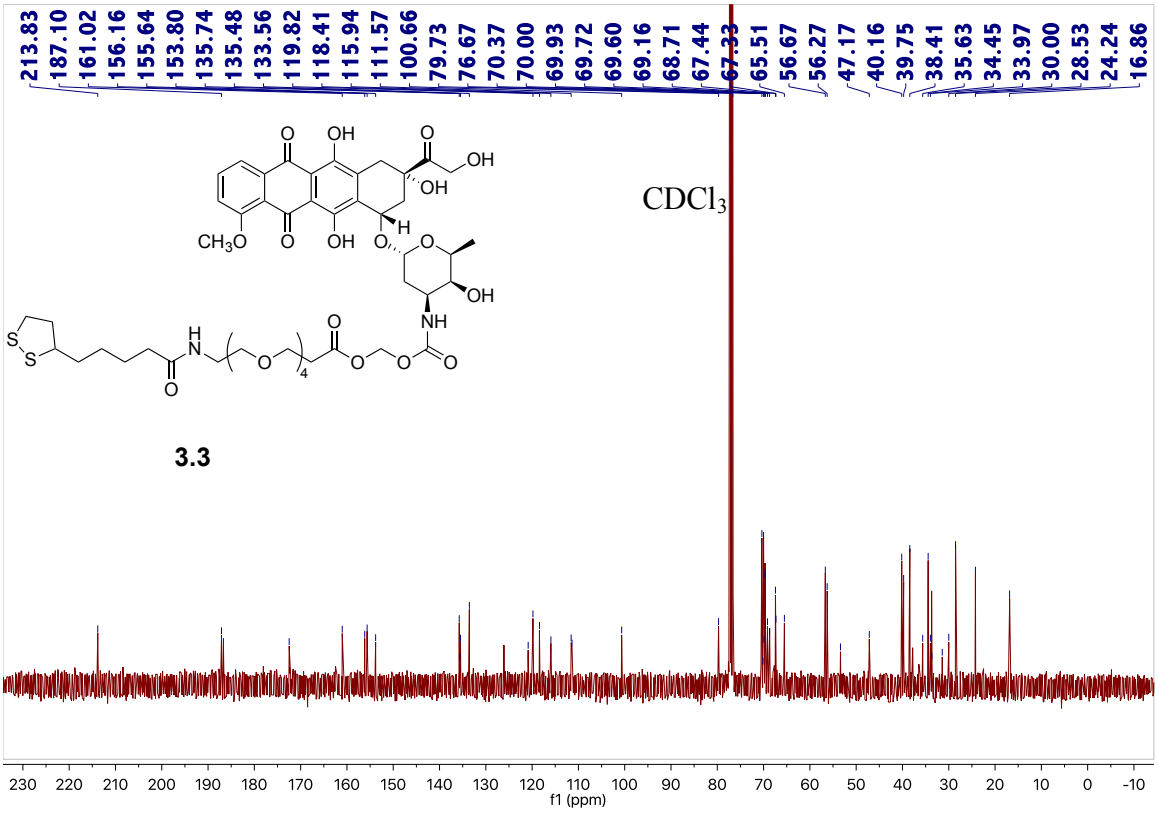

^{1}H NMR spectrum of **3.4** in $CDCl_3$ (500 MHz)

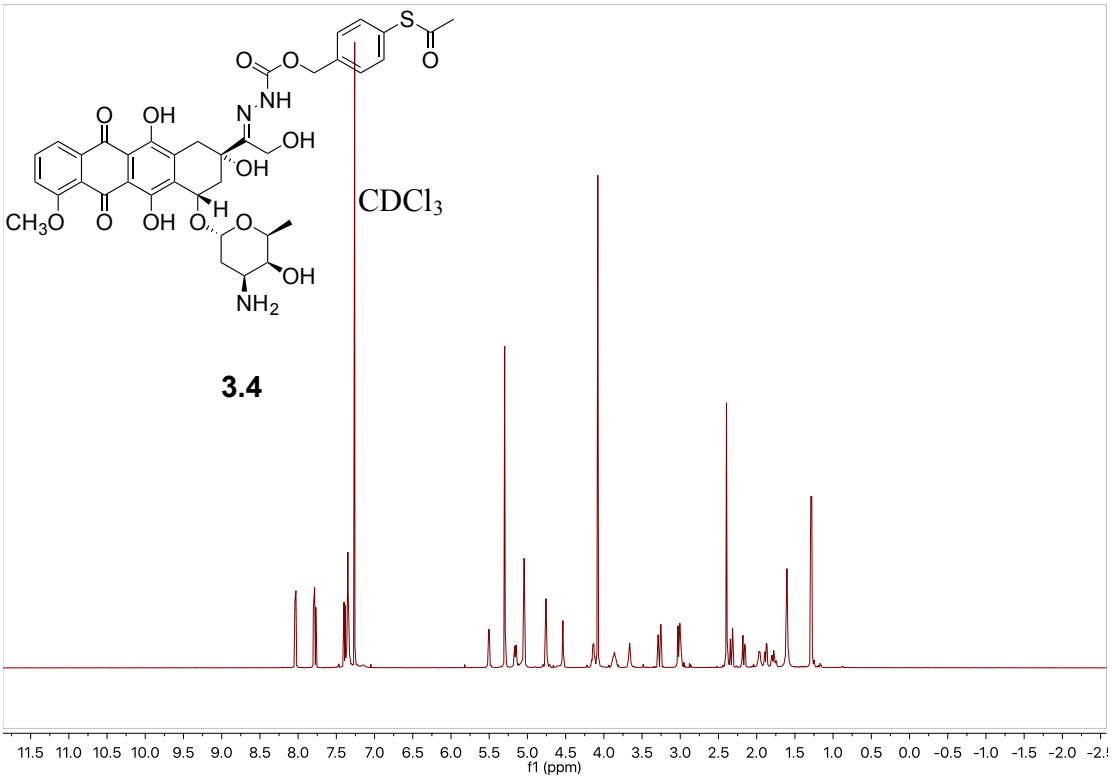

^{13}C NMR spectrum of **3.4** in $CDCl_3$ (125 MHz)

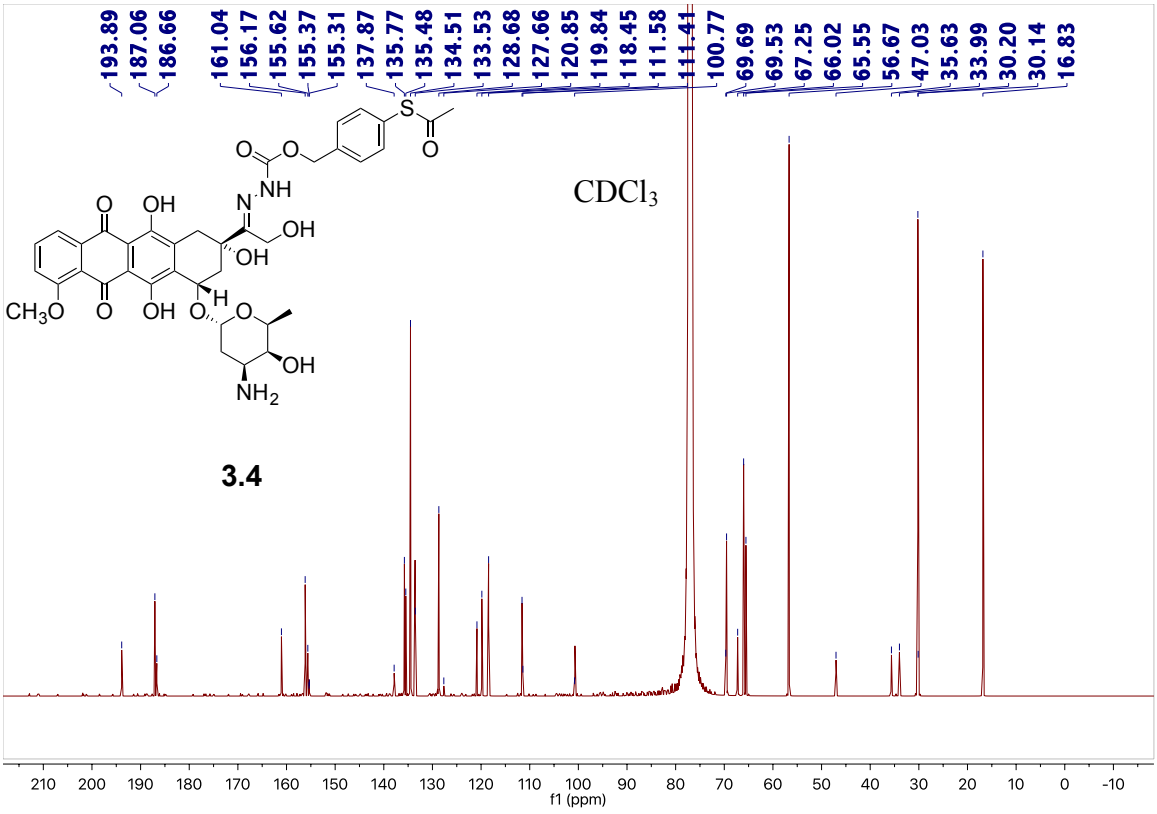

^{1}H NMR spectrum of **3.19** in $CDCl_3$ (500 MHz)

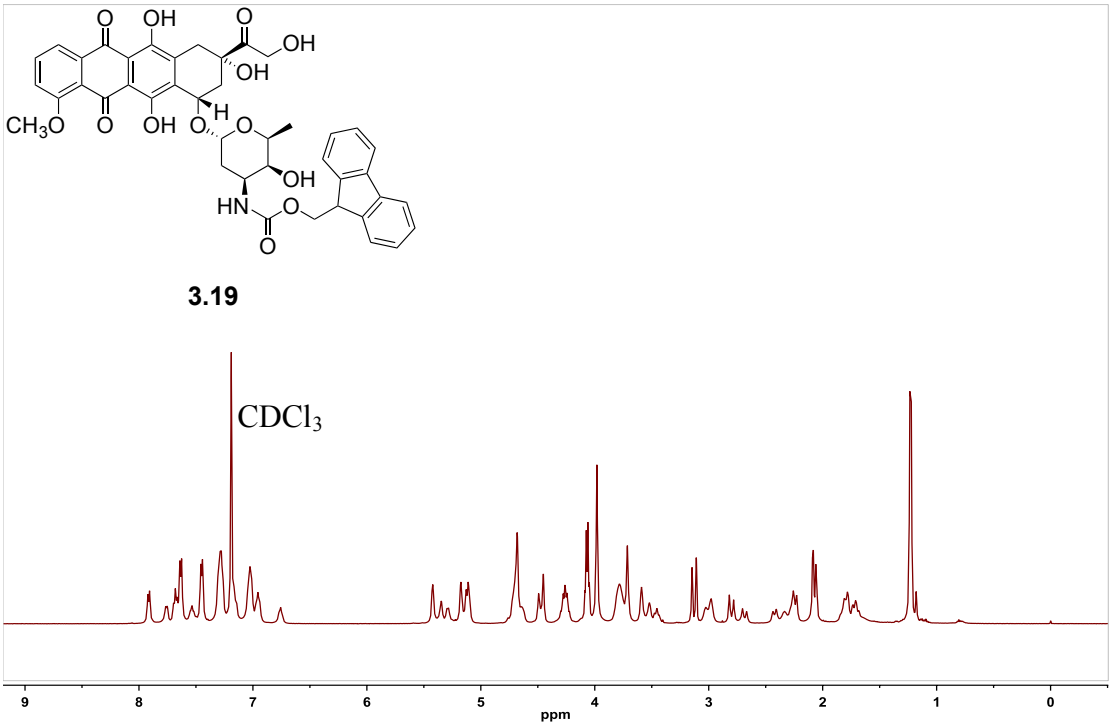

^{13}C NMR spectrum of **3.19** in $CDCl_3$ (125 MHz)

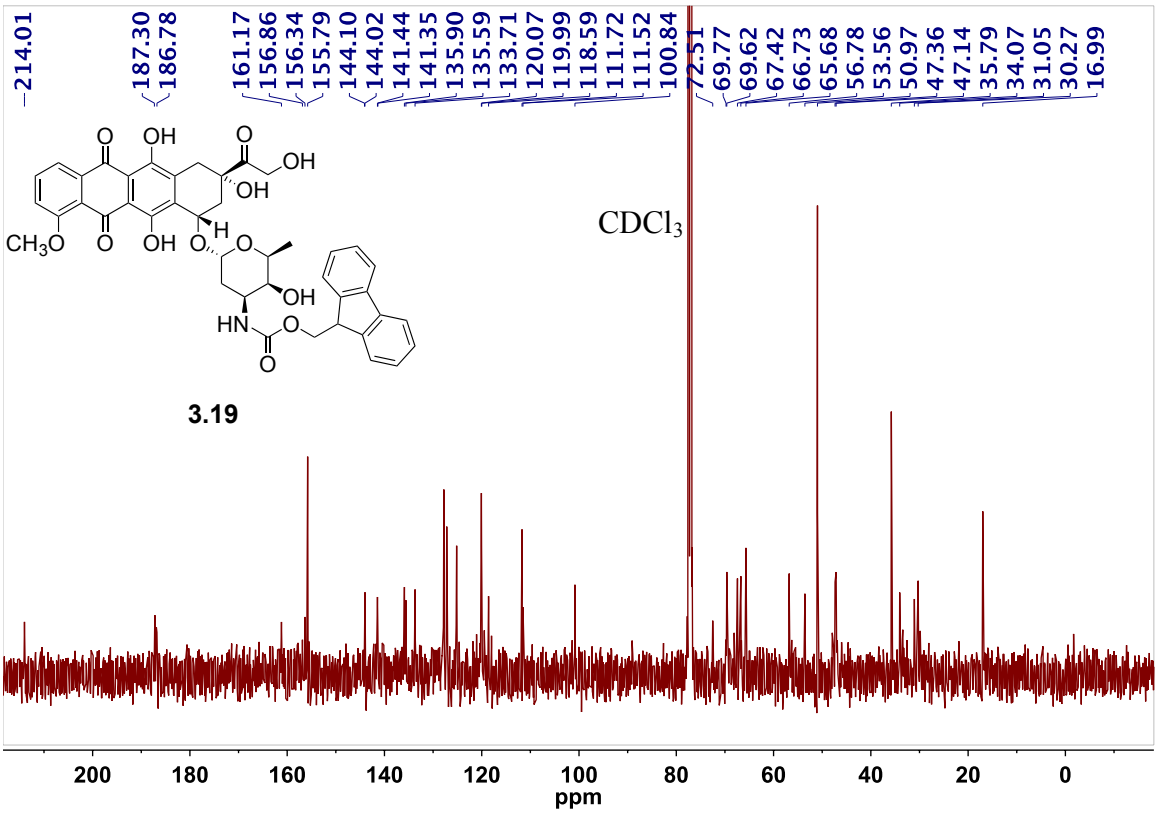

^{1}H NMR spectrum of **3.20** in $CDCl_3$ (500 MHz)

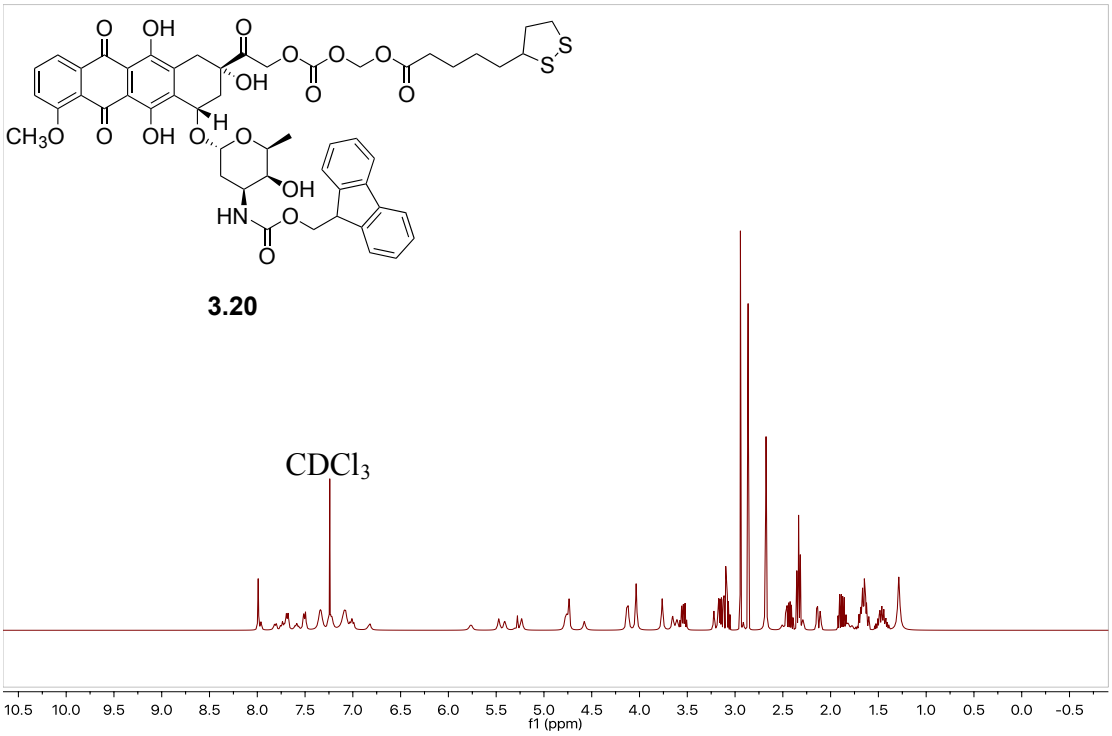

^{13}C NMR spectrum of **3.20** in $CDCl_3$ (125 MHz)

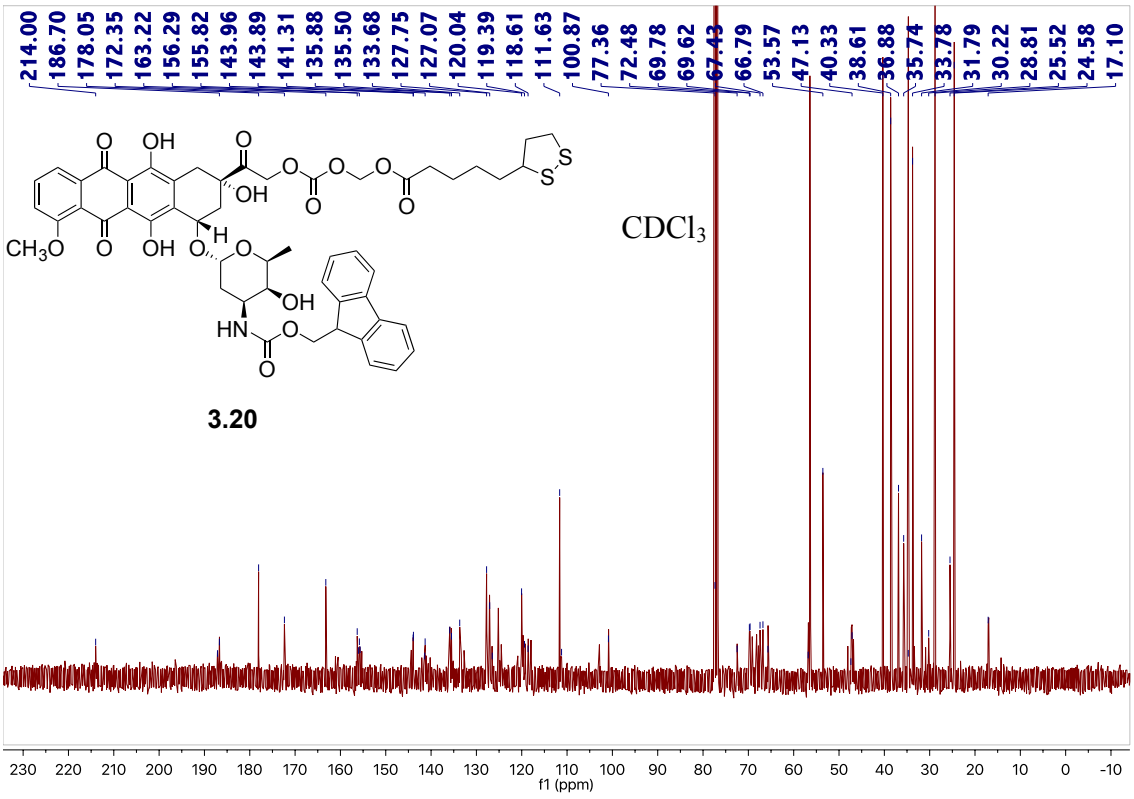

^{1}H NMR spectrum of **3.5** in $CDCl_3$ (500 MHz)

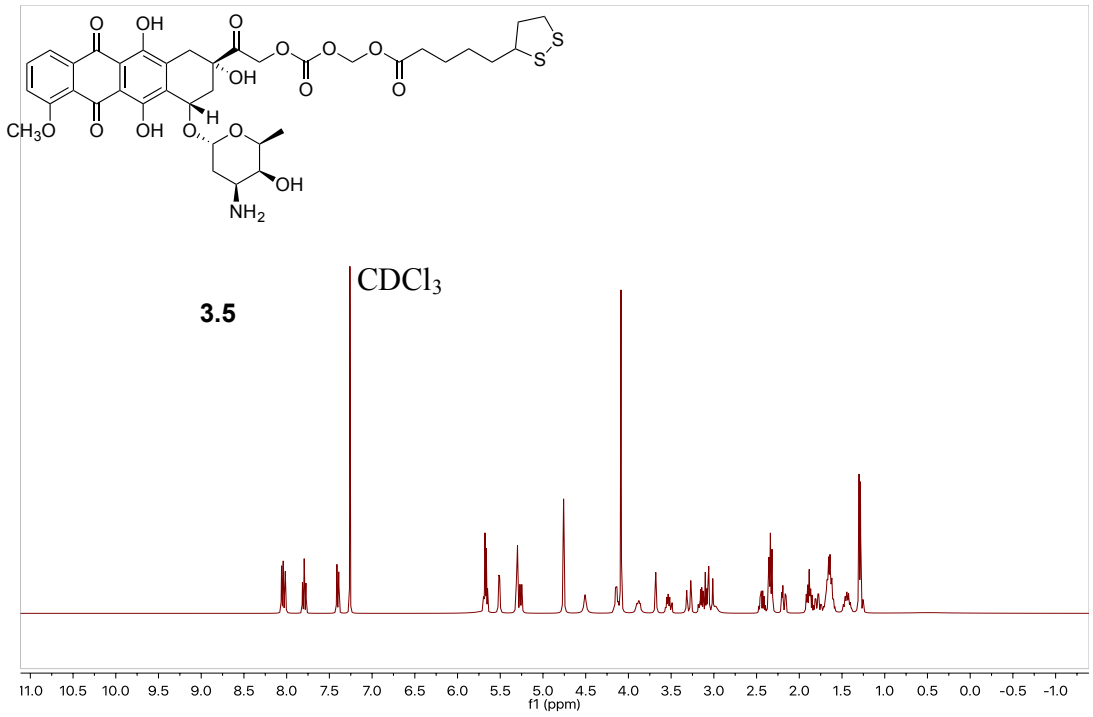

^{13}C NMR spectrum of **3.5** in $CDCl_3$ (125 MHz)